Stony Brook University

Assembly and Inhibition of Toxic Aβ42 Oligomers

A Dissertation Presented

by

Darryl Steven Aucoin

to

The Graduate School

in Partial Fulfillment of the

Requirements

for the Degree of

Doctor of Philosophy

in

Biochemistry and Structural Biology

Stony Brook University

August 2013

Stony Brook University

The Graduate School

Darryl Steven Aucoin

We, the dissertation committee for the above candidate for the

Doctor of Philosophy degree, hereby recommend

acceptance of this dissertation.

Steven O. Smith, Ph.D. – Dissertation Advisor
Professor, Department of Biochemistry and Cell Biology

Mark Bowen, Ph.D. - Chairperson of Defense
Assistant Professor, Department of Physiology and Biophysics

Erwin London, Ph.D.
Professor, Department of Biochemistry and Cell Biology

Lisa Miller, Ph.D.
Associate Division Director for Spectroscopy, Imaging, and Structural Biology,
Brookhaven National Laboratory

William Van Nostrand, Ph.D.
Professor, Department of Neurosurgery and Medicine

This dissertation is accepted by the Graduate School

Charles Taber
Interim Dean of the Graduate School

Abstract of the Dissertation

Assembly and Inhibition of Toxic Aβ42 Oligomers

by

Darryl Aucoin

Doctor of Philosophy

in

Biochemistry and Structural Biology

Stony Brook University

2013

The misfolding of the 42-residue amyloid beta protein has been strongly linked to Alzheimer's Disease. Prior to forming the amyloid fibrils typically associated with Alzheimer's Disease, the amyloid beta proteins associate to form a mixture of hexameric and dodecameric oligomers. This work investigates the process by which these proteins associate into oligomers and the mechanism by which different small molecule inhibitors prevent this assembly. NMR spectroscopy, atomic force microscopy and size exclusion chromatography were employed to determine the rate at which monomers assemble into hexamers, dodecamers and fibrils, and to correlate these changes in structure with changes in toxicity to neuronal cells. It was discovered that an increase in toxicity correlated with a population shift from hexamers to dodecamers, and that various inhibitors were able to block this conversion. By use of various biophysical techniques, this work demonstrates that these inhibitors bind to the monomeric peptide and prevent association of the hexameric oligomers into higher order dodecamers, thereby arresting

the formation of fibrils and blocking toxicity of the peptides. A common binding region was discovered for small molecule inhibitors such as curcumin and resveratrol. The largest changes in NMR chemical shift upon inhibitor binding to Aβ42 involve residues at the N-terminus and within the central portion of the peptide. Similar shifts upon inhibitor binding were observed in the NMR resonances for Arg5, Ser8, Tyr10, Gln15, Lys16, Leu17 and Phe20. Measurements of water accessibility indicate that the residues that interact with inhibitors are also solvent accessible. The structural insights into the mechanism of inhibition described here provide a basis for the design of improved inhibitors that specifically target Aβ42 dodecamers, which are emerging as the neurotoxic Aβ species.

Dedication Page

This work is dedicated to three people who will never get to read it:

Normand E. Aucoin (1924 – 2005) who showed me it was ok to take risks.

Alan A. Jones (1944 – 2006) who introduced me to NMR and academic research.

Paul W. Winston (1920 – 2013) who was the most knowledgeable person I ever met.

Table of Contents

List of Figures

List of Tables

List of Abbreviations

AD – Alzheimer's disease
AFM – Atomic force microscopy
ANS – Anilinonaphthalene-8-sulfonate
APP – Amyloid beta precursor protein
ATR–FTIR – Attenuated total reflection Fourier transform infrared spectroscopy
Aβ42 – 42 Amino acid length isoform of amyloid beta protein
CD – Circular dichroism
DARR – Dipole assisted rotational resonance
DMSO – Dimethyl sulfoxide
FTIR – Fourier transform infrared spectroscopy
GSM – Gamma secretase modulator
HCl – Hydrochloric acid
HFIP – 1,1,1,3,3,3, hexafluoroisopropanol
HSQC – Heteronuclear single quantum correlation
IR –Infrared spectroscopy
MTT – 3-(4,5-dimethylythiazol-2-yl)-2,5-diphenyltetrazolim bromide
NaOH – Sodium hydroxide
NMR – Nuclear magnetic resonance
SEC – Size exclusion chromatography
T1 – Spin–lattice relaxation time
T2 – Transverse relaxation time
Tc – Correlation time
TEM – Transmission electron microscopy

Acknowledgments

I would like to thank the following people:

Dr. Steven Smith for his assistance as an advisor.

Dr. Mark Bowen, Dr. Erwin London, Dr. Lisa Miller and Dr. William Van Nostrand, for serving on my dissertation committee and for their insight during those meetings.

Judianne Davis of the Van Nostrand laboratory for preparing the neuronal cultures used in the toxicity experiments and her assistance with the experimental design and discussions of the results.

Susan VanHorn for her assistance with troubleshooting the EM imaging.

The members of the Smith Lab for their assistance and companionship, with special thanks to Ian Brett for his assistance with the collecting of the solution NMR data and Martine Ziliox for assistance with the diffusion experiments.

Eric Steele and Hilary May for their assistance in editing this manuscript and presentations.

My family and friends for their continued support.

Chapter 1 – Introduction

The proper folding of proteins is essential for life. Each cell produces hundreds of proteins during its lifetime and each of these proteins must be properly folded in order to fulfill its function. When a protein does not fold properly (misfolds or adopts an alternative fold) the effects it has on the cell can be dire. Protein misfolding is associated with numerous diseases (1). The IAPP protein produced by the pancreas can misfold and aggregate into toxic proteins that lead to type II diabetes, misfolding of the immunoglobulin light chain proteins in bone marrow can cause problems ranging from kidney damage to multiple myeloma, a type of cancer (1). The crystallin proteins in eyes can misfold to cause Cataracts disease.

Many proteins in the brain can also misfold to cause neurodegenerative disease. Numerous misfolded proteins are associated with diseases of the brain, such as prion protein (transmissible spongiform encephalopathy – mad cow disease), alpha synuclein (Parkinson's Disease) and amyloid beta protein (Alzheimer's Disease). While many of these diseases have different symptoms and prognoses, they all have in common that a misfolded protein has aggregated and induced neuronal damage.

Alzheimer's Disease (AD) is a neurodegenerative disease whose incidence rate has greatly risen worldwide over the past decade. The typical onset age of the disease is 65 and it is estimated that 45% of all Americans over age 85 have at least some mild form of the disease (2). AD is characterized by a decline in cognitive abilities and memory with damage increasing as the disease progresses. Post-mortem analysis of the brains of AD patients revealed large amyloid plaques in the gray matter of the brain. These plaques were localized to areas affecting memory and cognition. In late stages of the disease damage extends to regions of the brain affecting

speech, motor skills and, in extreme cases, the autonomous nervous system, impacting the ability to breathe (3). However, due to the increasing damage to cognitive abilities most AD patients die from other factors before the disease has progressed to this stage.

AD is the 6th leading cause of death in the US, accounting for approximately 7% of the deaths of people aged 85 and over in the US (4th leading cause in this group) (2). However, of the top eight leading causes of death only AD (#6), cancer (#2) and chronic lung disease (#4) have seen an increase in the relative death rates since 2004, indicating that despite advances in medical technology more research is needed to understand and treat this disease.

While AD was first described over 100 years ago, the causative agents were only identified more recently. The amyloid plaques found in AD patients are composed mainly of the amyloid beta (Aβ) protein (4). This protein is the cleavage product of the larger Amyloid Precursor Protein (APP) found in both diseased and healthy brains. APP is cleaved at three different sites by two pathways (Figure 1.1) (5, 6). One pathway involves cleavage of the APP protein by α-secretase and γ-secretase and produces a short non- Aβ peptide (5). The other pathway cleaves APP with β- and γ-secretase to produce an Aβ peptide that is between 38 and 43 residues long (5). It is this second cleavage pathway that produces the Aβ peptides associated with AD. While mutations in the APP gene can change the length distribution of the Aβ peptides produced, typically Aβ peptides of 40 amino acid length (Aβ40) and 42 amino acid length (Aβ42) are the most common. Post mortem analysis of the composition of plaques of AD patients showed a high concentration of Aβ42 (compared to Aβ40) by both mass spectrometry (7) and by Aβ specific antibodies (8), which was surprising given that measurements of APP processing and Aβ levels in cerebral spinal fluid indicated that it was the Aβ40 that was

produced 90% of the time (9). This early observation led to other studies that determined that the Aβ42 peptide aggregates at a faster rate and is more toxic than the Aβ40 peptide (10, 11).

The presence of fibrillar plaques in AD patients led early researchers to believe that Aβ42 fibrils were the toxic agent causing AD. However, very little correlation was found between the plaque load in the brain and disease severity in AD patients (12-14). Subsequent studies into Aβ toxicity revealed that smaller oligomeric peptides produced before fibril deposition were more toxic than the fibrils and protofibrils. Later research has revealed many toxic species that form as the monomeric Aβ peptides convert into fibrils (Figure 1.2). Current research indicates that it is the oligomeric Aβ42 peptides that are the toxic species responsible for AD (6, 15-20). These species form rapidly from monomeric Aβ42, and assemble into disc-shaped pentamers/hexamers (referred to hereafter as hexamers) (21, 22). Over time these oligomers stack to form decameric/dodecameric oligomers (referred to hereafter as dodecamers) (21). The dodecamers transition into protofibrils, which have a distinct structure from the oligomers and fibrils (Figure 1.3). The protofibrils later convert into fibrils.

The mechanism by which Aβ42 oligomers become neurotoxic remains controversial. Aβ42 oligomers have been shown to interact with numerous membrane proteins as well as with the membrane itself, resulting in a range of toxic pathways from incorrect signaling to pore formation. When Aβ peptides were incubated with GM1 gangliosides, a common neuronal membrane component, large oligomers formed which then bound to nerve growth factor receptors, resulting in cell death (23). This interaction has been observed both in the lab (23) and AD brain samples (24). Other neuronal membrane receptors have also been shown to bind to Aβ42 oligomers, including the Frizzled receptor (25), and the NMDA receptor (26, 27). The Frizzled receptor is a component of the Wnt signaling pathway, which is involved in neuronal

formation, function and development (25). When Aβ42 oligomers bind to the Frizzled receptor, they inhibit Wnt signaling, which disrupts long–term potentiation responsible for learning and memory as well as neuronal development. Interestingly, disruption of Wnt also results in increased phosphorylation and aggregation of the tau protein (25). The Tau protein is another aggregating protein whose misfolding results in aggregation, neuronal loss and AD, so Aβ42 oligomers may be involved in this disease by increasing the amount of Tau phosphorylation. The NMDA receptor is one of the required receptors for calcium regulation in neuronal cells, and binding of Aβ42 oligomers to these receptors disrupts calcium levels, resulting in neuronal death from increased oxidative stress (26, 27). The NMDA pathway is also involved in memory and special learning, so disruption due to Aβ42 oligomer binding could also be a causative factor in AD (26). Another means by which Aβ42 oligomers can disrupt calcium levels in cells is by making pores in the membrane (28-30), which would allow unregulated ion flow in and out of the cell. Since neurons rely on calcium levels for signaling, unregulated flow of calcium can be detrimental to these cells. This variety of targets illustrates how the means by which Aβ42 oligomers induce neuronal toxicity are complex and most likely involve multiple pathways.

Due to their early implication as the toxic species in AD, much work was done to determine the structure of the fibrils. The fibrils formed by Aβ42 and Aβ40 are similar in structure and morphology (Figure 1.4). Structural studies using solid-state nuclear magnetic resonance (NMR) on Aβ40 (31-33) and mutational studies using Aβ42 (34) both concluded that the fibrils form a β strand-turn-β strand (β-turn-β) structure . In this structure, the side chains are oriented into or out of the U-shaped region of the peptide, with hydrogen bonding between neighboring peptides along the parallel-in-register β-sheets (Figure 1.4). Two β-sheets spanning residues 10-22 and 30-42 are separated by a turn (35). The N-terminal portion of the peptide was

found to be unstructured. The peptides were found to be aligned such that the strand with residues 15, 17, 19 and 21 is facing the strand with residues 30, 32, 34, 36 and 38 (33, 35). Solid-state NMR experiments in our lab determined that pre-fibrillar oligomers of Aβ42 also form this β-turn-β structure, but do not have parallel and in-register β-sheets (36).

Current medical treatment of AD often focuses on enhancing remaining cognitive ability and alleviating symptoms rather than halting progression or slowing onset of the disease. Previous attempts to prevent AD in high risk patients by either drug or vaccine have been unsuccessful. More recent means of preventing the disease follow two methods. The first approach inhibits β- or γ- secretase activity to prevent Aβ peptide production and the subsequent formation of amyloid fibrils and plaques. Drugs, such as Lilly Research LY450139 (37) and ibuprofen (38), follow this approach. The main problem with these β- and γ-secretase inhibitors is that they may interfere with other biological processes, such as Notch signaling, and increase the risk of cancer and other developmental defects (39, 40). Recent inhibitors have been developed which are specific for γ-secretase (41).

The alternative treatment is to target the Aβ peptides directly after they have been processed by γ-secretase, but before they can form amyloid oligomers or fibrils. Many compounds have been identified as inhibitors of Aβ aggregation. These compounds bind to Aβ and prevent its subsequent fibrillization, and in some cases dissolve aggregates that have already formed. The inhibitors that target Aβ fibrillization and toxicity are generally small natural products, such as curcumin (42, 43) (a compound found in Indian curries) and resveratrol (44-46) (a polyphenol found in wine (44-48)), or other wine derived polyphenols (47, 48). Other small designed peptides (49-56) and synthetic compounds (57-59) have been proposed based on

current structural models and have also been investigated. These compounds all have in common that they bind to Aβ to prevent its subsequent fibrillization.

While numerous studies have found and reported on compounds which inhibit Aβ aggregation and toxicity, these studies have generally focused on the effectiveness of the compounds and not on the mechanism by which these compounds inhibit Aβ oligomerization. While screening chemical libraries can produce useful inhibitory compounds, it is only by studying the mechanism through which these compounds act that we can get a true understanding of how these compounds interact. This information will be valuable for the generation of future treatments for AD. The objective of this thesis was to understand the mechanism by which two Aβ inhibitors, curcumin and resveratrol, bind to Aβ and block toxicity. This goal would be obtained in three phases. The first aim was to characterize the structural elements in the Aβ42 peptide as it transitioned from monomers, oligomers, protofibrils and fibrils. Secondly, once these transitions were characterized, the effect of inhibitors on the transitions would be analyzed in order to see at which step in the fibril formation pathway these inhibitors interact. The final aim was to investigate differences in specific structural elements between the oligomers, protofibrils and fibrils in order to better understand the process by which these three species interconvert during fibril formation.

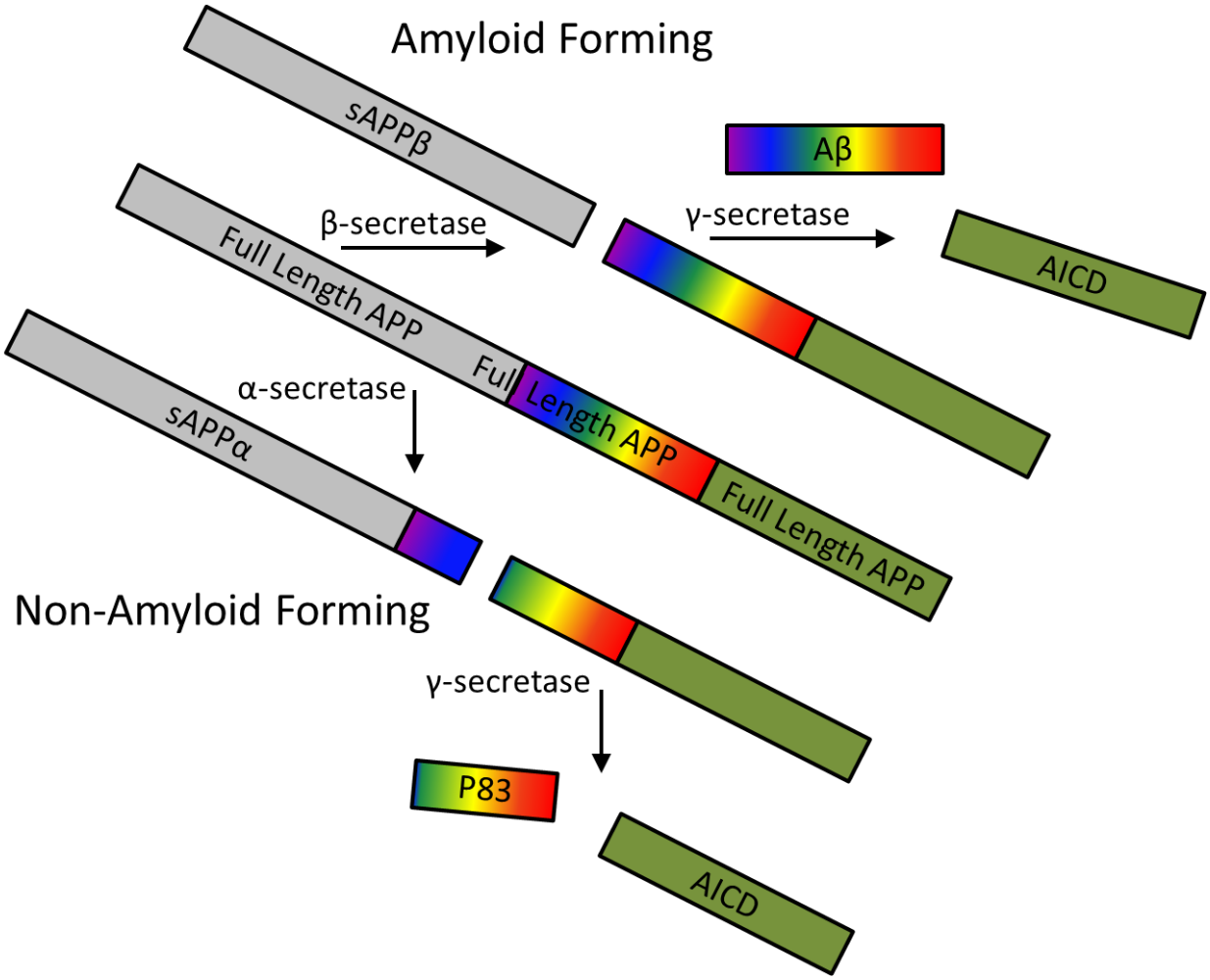

Figure 1.1 APP processing pathways.
APP is a single pass transmembrane protein that is processed by two different pathways. APP is first cleaved by either α-secretase or β-secretase. Subsequent cleavage of the membrane bound region by γ-secretase produces either a non- Aβ peptide (α-secretase pathway) or an Aβ peptide (β-secretase pathway) of variable length. The most common Aβ peptides produced are 40 (90%) and 42 (10%) amino acids long. Modified from (5).

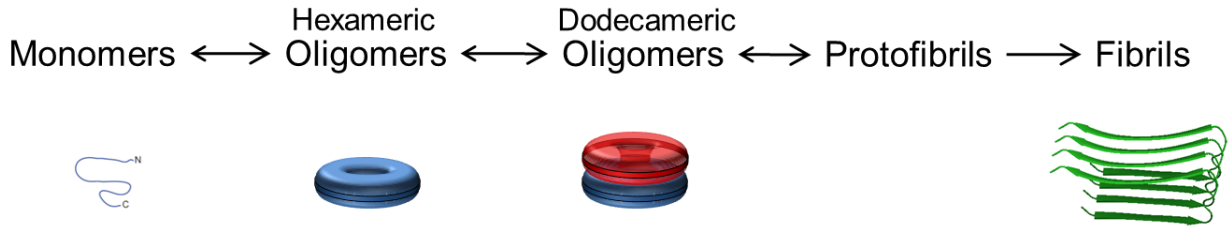

Figure 1.2 Pathway of fibril formation by Aβ42.
The monomeric Aβ42 peptides rapidly assemble into oligomers, which rearrange into protofibrils, which assemble into fibrils. The oligomers are believed to be the most toxic species.

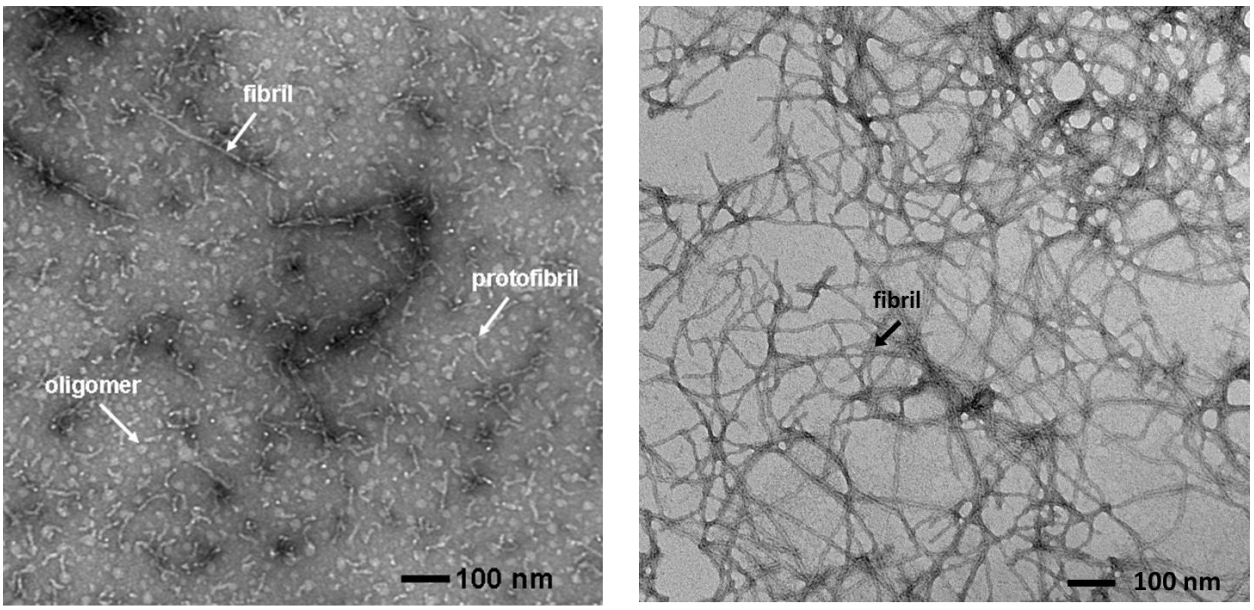

Figure 1.3 EM images showing oligomers, protofibrils and fibrils.
Images were obtained after 15 and 48 hours of incubation at 200 μM concentration at 37 °C. At early incubation times a mixture of small disk shaped oligomers, short curly protofibrils and short straight fibrils can is observed. At later times the sample becomes completely fibrillar.

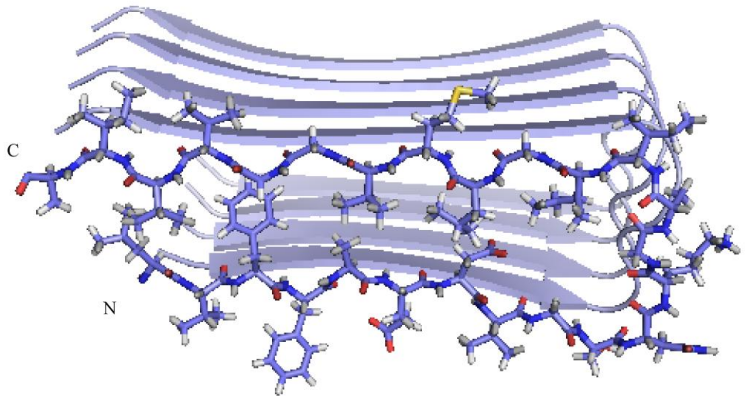

Figure 1.4 Cartoon representations of Aβ fibril structure.
Both Aβ40 and Aβ42 form fibrils with a β-turn-β structure where parallel and in-register β-sheets spanning residues 10-22 and 30-42 are separated by a turn. In this structure, residues 17 – 42 are shown in the foreground, subsequent fibril strands are shown as ribbons in the background. The figure shows four monomers of the fibril; the fibril axis is roughly oriented into the plane of the page. The hydrogen bonding between β sheets occurs into the plane of the page, while amino acid side chains are oriented along the page. Modified from (34).

Chapter 2 – Materials and methodology

Amyloid sample preparation

Aβ42 peptides were generated by solid-phase synthesis using t-BOC chemistry by James Elliot at Yale University. One benefit of this method over biosynthesis is that solid-phase synthesis allows for incorporation of site specific labels in the peptide for use by NMR. The peptides were cleaved from the resin and deprotected by addition of hydrofluoric acid and purified by HPLC using a water - acetonitrile gradient. The identity of the purified peptide was confirmed by mass spectrometry and the purity was assessed by analytical HPLC.

Purified peptides were dissolved in 1,1,1,3,3,3, hexafluoroisopropanol (HFIP), filtered with a 0.2 μm PTFE filter, frozen in liquid nitrogen, and lyophilized overnight on a Vertis lyophilizer to remove the organic solvent. The lyophilized peptides were stored at -20 ºC until use. Before each experiment the lyophilized peptides were dissolved in 100 uM NaOH (or in DMSO) to a concentration of 2,215 μM. These stocks were further diluted in phosphate buffer (10 mM phosphate 150 mM NaCl, pH 7.4) to a concentration of 200 μM, and when using NaOH stocks, titrated to pH 7.4 by addition of 300 mM HCl. The peptides were then incubated for times ranging from 0 - 72 hours while shaking at 37 °C. The small amount of DMSO (1-2%) slows the formation of stacked oligomers and protofibrils, but otherwise does not appear to influence the structure of the oligomers.

Fluorescence experiments (ANS and thioflavin T)

Fluorescence experiments of Aβ42 oligomers and protofibrils were performed in the presence of two different fluorescent dyes, anilinonaphthalene-8-sulfonate (ANS) or thioflavin T. At each time point, 2 μL (thioflavin T) or 6 μL (ANS) aliquots of the 200 μM Aβ42 samples

were diluted with 180 µL of 30 µM solutions of ANS or thioflavin T to yield an Aβ42 concentration of 2.2 µM (thioflavin T) or 6.45 µM (ANS). The samples were placed into a quartz cuvette with a path length of 5 mm and fluorescence was measured using a Horiba Jobin Yvon Fluorolog FL3-22 spectrofluorimeter.

Due to the different fluorescence properties of the two dyes, experiments were performed at different excitation wavelengths. For the ANS experiments, where a peptide-to-ANS molar ratio of 1 : 4.5 was used, the sample was excited at a wavelength of 349 nm and emission spectra were recorded from 400-600 nm. For thioflavin T experiments, a peptide-to-thioflavin T molar ratio of 1:20 was used. Samples were excited at a wavelength of 461 nm and emission was recorded from 475-550 nm.

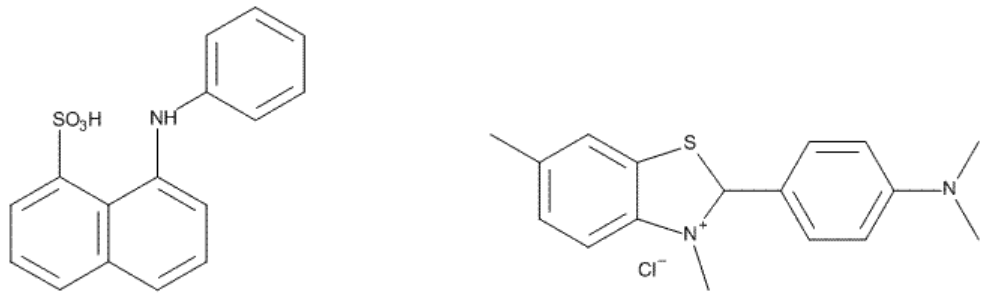

Figure 2.1 Structures of ANS and thioflavin T

Imaging experiments (EM and AFM)

Transmission electron microscopy images were obtained using a FEI Tecnai 12 BioTwin 85 kV transmission electron microscope. Samples were diluted to 20 µM using filtered water and 20 µL aliquots were deposited onto carbon coated copper mesh grids for 1 minute, then wicked off and negatively stained using a 2 weight percent solution of uranyl acetate for an additional

minute. Stain was removed and images of the samples were recorded at magnifications of 49,000 and 98,000 using an Advanced Microscopy Techniques camera.

Atomic force microscopy images were obtained using a Digital Instruments MultiMode microscope with a custom-built LifeAFM controller. Specially modified supersharp silicon probes with a 3 – 4 nm tip width were required for this machine. Samarium cobalt particles were attached to the probe to allow magnetic retraction of the probe upon contact with the surface. This modification to the instrument allows one low-force contact of the AFM tip to the sample surface per data point. This approach has previously been used to collect images of oligomer samples with less distortion than other AFM methods (36, 60). At each time point aliquots were diluted to 1 μM, adjusted to acidic pH by addition of 1% (w/v) HCl, and 20 μL of sample was adhered to freshly cleaved mica. Samples were dried under vacuum using a Virtis lyophilizer, and images were obtained under hydrated conditions. Height histograms were generated by measuring the height of non-overlapping particles from multiple fields and compiled using Microsoft Excel. The measured diameters of the oligomers were adjusted to account for size variations due to the width of the triangular probe (36).

Solution NMR experiments (^{1}H, T_1, T_2, diffusion and ^{1}H –^{15}N HSQC)

Sample preparation

Solution NMR experiments were performed on a Bruker AVANCE spectrometer with a TXI probe at a proton frequency of 700 MHz. Monomer experiments were conducted at a temperature of 4 °C to reduce peptide oligomerization. Kinetics experiments were conducted at 37 °C. HSQC and kinetics NMR measurements were made with standard 5 mm NMR tubes containing a Teflon tube liner (Norell, Inc.) to reduce fibrillization. T_1, T_2 and diffusion

experiments were performed in 5 mm Shigami tubes because of the higher magnetic field homogeneity required for these experiments. For all of the NMR experiments conducted (except for those measuring diffusion coefficients) Aβ42 was prepared from NaOH stocks and diluted to 200 μM in phosphate buffer containing 20% D_2O. Diffusion experiments were conducted with Aβ42 diluted with phosphate buffer containing 100% D_2O. Sample volume was approximately 400 μL (150 μL for diffusion experiments). Both relaxation measurements (T_1 and T_2), as well as the ^1H–^{15}N HSQC experiment required uniformly ^{15}N labeled Aβ42 peptide, while the other experiments were performed with unlabeled peptide. Standards for diffusion experiments were dissolved in phosphate buffer containing 100% D_2O diluted to 200 μM to ensure similar conditions as those of the Aβ42 diffusion experiments.

The stability of the peptide over long experiments was confirmed by comparing ^1H spectra before and after the diffusion experiments. Similarly, 2D ^1H-^{15}NHSQC spectra were obtained both before and after the T_1 and T_2 experiments to confirm sample stability.

Pulse sequences and calculations

^1H spectra were collected using the ZGPR Bruker pulse sequence. This pulse sequence includes a presaturation pulse to reduce the water signal which would otherwise dominate the spectra. In samples containing 100% D_2O, the ZG Bruker pulse sequence is used instead. Spectra are collected with between 16 and 256 scans depending on the signal intensity of the sample.

T_1 Spectra were collected with the HSQCT1etf3gpsi3d Bruker pulse sequence at 14 time points. 1024 points were collected in the direct dimension, with 128 indirect points, and 16 dummy scans. From this spectra, relaxation times for each of the NH protons in the Aβ42 sequence were measured by integrating individual Aβ42 resonances and plotting the loss of

integrated signal versus delay time. T_1 values were calculated by fitting these plots to the exponential decay curve, $I / I_o = exp\ (-t / t_1)$.

Spectra for T_2 relaxation times measurements were collected with the HSQCT2etf3gpsi3d Bruker pulse sequence using 8 time points with 1024 points in the direct dimension, 128 indirect points, and 16 dummy scans. Individual NH peaks were integrated, and the loss of integrated signal versus the delay time was plotted. T_2 values were calculated by fitting these plots to the exponential decay curve, $I / I_o = exp\ (-t / t_2)$.

2D ^{1}H-^{15}NHSQC spectra obtained before and after the T_1 and T_2 measurements were similar, indicating that the sample remained stable for the duration of these experiments.

The correlation time for each residue of Aβ42 was calculated from the T_1 and T_2 relaxation times using the equation (61):

$$\tau_c \approx \frac{1}{4\pi\nu_N}\sqrt{6\frac{T_1}{T_2} - 7}$$

where ν_N corresponds to the ^{15}N resonance frequency of 70.9 Hz.

Diffusion measurements were conducted using bipolar gradient pulse pairs in the longitudinal eddy current delay experiment with a stimulated echo (the Bruker LEDBPGP2S pulse sequence). For this experiment, 32 time points were acquired with between 32 and 512 scans per increment (depending on signal-to-noise). Delay times were adjusted to produce a signal attenuation that was ~ 90%. For the standards and the Aβ42 peptides this delay time varied between 2 and 5 ms. ^{1}H spectra were obtained before and after the PFG experiments to confirm the stability of the sample during the course of the experiment. Integrals of the amide

peak areas were recorded and plotted against the gradient strength squared. Diffusion coefficients were calculated by fitting the integrated amide intensity to the equation:

$$I/I_0 = exp(-D(2\pi * \gamma * Gradient * \delta)(2\pi * \gamma * Gradient * \delta)((\Delta - \delta/3) * 10{,}000)$$

where γ is the gyromagnetic ratio (4258 Hz/G), δ is the total gradient time the gradient is applied and Δ is the diffusion time (50 ms). δ was adjusted to achieve a 95% signal attenuation when the gradient was applied (δ varies with experiment but was generally between 2 and 10 ms) I_0 and D (m/s^2) values were adjusted until differences between the calculated and experimentally observed values were minimized using a custom curve fit module in Graphpad Prism software. In experiments conducted at 37 °C, where Aβ42 signal strength decreased over time, the I/I_0 values were adjusted to compensate for loss due to temperature based aggregation by replacing I/I_0 with I/I_{0t} where $I_{0t} = I_0 * (\text{total signal loss over experiment} * (1 - t/t_{total})$. This correction ensures that the only signal decrease is due to diffusion and not aggregation. This calculation assumes that the temperature based signal loss follows a linear dependence, which it was shown to do during <3 hour experiments.

$^1H - ^{15}N$ HSQC spectra were acquired using pulse field gradient water suppression and GARP decoupling with the transmitter offset placed at the water frequency in order to reduce the contribution of the ^1H signal from water. The HSQCetfpf3gpsi Bruker pulse sequence was used for data collection. 128 time increments were acquired in the indirect dimension with 16 scans per increment. Assignments of the $^1H - ^{15}N$ HSQC spectra were made based on reference (62).

FTIR experiments

Attenuated total reflection Fourier transform infrared spectroscopy (ATR–FTIR) spectra were obtained on a Bruker IFS 66V/S spectrometer. After each time increment, 90 μL of a 200

μM Aβ42 solution was deposited onto the germanium ATR plate and dried under vacuum using a Virtis lyophilizer. Spectra were obtained from 400-4000 cm^{-1}. A background containing spectra of the plate alone was subtracted from each spectra prior to analysis.

Circular dichroism experiments

Circular dichroism spectra were obtained on an Olis RSM 1000 CD spectrophotometer. Spectra of Aβ42 samples incubated at 200 μM were obtained at 200 μM or diluted to 75 μM at each time point. The path length of the quartz cuvette used was 1 mm, and the volume was 200 μL. CD spectra were acquired from 260 to 190 nm, with a variable scan rate which was adjusted to maintain constant signal intensity throughout the experiment. Three scans were collected and averaged using Olis software. Individual scans were compared and it was found that the spectra did not change significantly between the first and final scan, indicating no changes in Aβ42 aggregation state occurred during the spectra collection, and that the scans could be averaged.

Size exclusion chromatography experiments

Size exclusion chromatography (SEC) was undertaken using a Superdex 200 column which has a 3 – 600 kDa MW range on a GE Healthcare ÄKTA Purifier 10 FPLC. Samples were prepared at 4 °C and incubated for various times at 37 °C then injected into the Superdex 200 column and eluted at a rate of 0.4 mL/min.150 μL of sample was injected into a 100 μL loop. The loop was flushed with 400 μL of buffer to ensure that the entire sample entered the column. The FPLC instrument, column and buffers were maintained at 4 °C, which decreases further aggregation of the Aβ sample during the hour long SEC separation.

Samples for SEC were incubated at 200 μM, and injected into the column at their initial concentration of 200 μM or after dilution to 50 μM or 15 μM. Loading a larger sample volume

into the loop ensures that a similar amount of sample is present in each experiment. To ensure the absence of large aggregates which would clog the pores of the column, samples were filtered through a 0.45-micron cellulose acetate filter or spun in a centrifuge for 6 seconds to remove any large aggregates prior to injection. It should be noted that no large aggregates were observed by EM during the initial times (0 – 4 hours).

The radius and volumes of Aβ42 oligomers and protofibrils were compared with SEC profiles of standards of a known molecular weight and size. A standard calibration curve was constructed by measuring elution times of ferritin (440 kDa), alcohol dehydrogenase (150 kDa), bovine serum albumin (66 kDa), ovalbumin (44 kDa), carbonic anhydrase (29 kDa), soybean trypsin inhibitor (20 kDa), lysozyme (14 kDa) and aprotinin (6.5 kDa).

Cell toxicity experiments

Preparation and treatment of neurons

Rat cortical neuronal cultures from the brains of E17 pups were prepared by Judianne Davis of the Van Nostrand Laboratory. Neonatal rat cortical neuronal cultures were grown under sterile conditions in 48-well plates incubated at 37 °C. Experiments were performed 4-6 days after initial preparation, while the cells were in G2 Neurobasal medium without araC.

Two different Aβ42 preparations were used for the neuronal toxicity experiments, employing either NaOH or DMSO treated Aβ42. DMSO stocks of Aβ42 peptide were prepared in a similar manner as NaOH stocks replacing NaOH with DMSO and omitting the HCl titration. For samples involving inhibitors, an Aβ:inhibitor ratios of 1:1 was used. Aβ42 peptides were incubated from lyophilized stocks at 200 μM at 37 °C in low salt phosphate buffer for 0 - 72

hours, then diluted into neuronal cultures for a final concentration of 12 μM and incubated an additional 48 hours after which viability was assayed by one of the following two methods:

MTT assay

MTT assay measures the amount of viable cells by assessing mitochondrial activity after treatment with 3-(4,5-dimethylythiazol-2-yl)-2,5-diphenyltetrazolim bromide (MTT). In living cells, yellow MTT is metabolized in the mitochondria into insoluble formazan which is blue (Figure 2.2)(63, 64). The absorbance at 570 nm (blue light) can therefore be used to assess the relative amounts of live cells compared to a control of untreated cells.

Cell viability was determined using an MTT assay kit from Sigma. MTT solution was added to the neuronal cells at a concentration of 12 mM, and incubated for 4 hours, after which an ethanol detergent mixture was added. This mixture both lyses the cells and solubilizes the blue formazan reaction product. Plates were shaken 5 minutes, and viable cells were quantified using a Molecular Devices SpectraMax M2 plate reading spectrophotometer at a wavelength of 570 nm. The percent viability was determined by dividing absorbance of MTT for each sample by the absorbance of buffer alone (which serves as the 100% viable control).

A modified procedure was used with experiments in which samples contained inhibitors, which may interfere with the assay. Because the traditional method of MTT assay leaves the original cell mixture in the final solution, any curcumin added to the cell will remain present, where the yellow color could interfere with the assay. As in the above procedure, MTT was added to cells and incubated for 4 hours. However, instead of adding an ethanol detergent mixture to the cells, the cell buffer solutions were removed completely. Since formazan is

insoluble, it remained in the wells after the solution was removed. 100 µL of DMSO was added to dissolve the formazan. This ensured that each sample contained no interfering molecules.

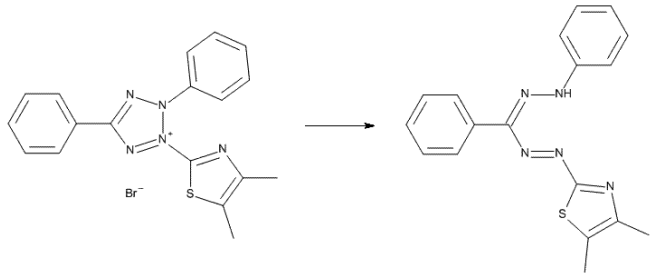

Figure 2.2 MTT reaction
In living cells, yellow MTT is metabolized in the mitochondria into blue formazan.

Live dead assay

A second assay of cell viability and toxicity was employed which uses two fluorescent compounds to measure the number of live and dead cells. Acetomethoxy calcein (calcein-AM) is not fluorescent, but can be transported across the cell membrane where it is metabolized into calcein which fluoresces green (64). Calcein cannot permeate the membrane and remains in the live cells (64). Since dead cells lack the esterase activity required to metabolize calcein-AM, only live cells fluoresces green (64). The second compound, ethidium homodimer-1, is unable to permeate the plasma membranes of live cells, but can cross the weakened membranes of dead cells (64). Once inside a cell, ethidium binds to DNA and fluoresces red. Both acetomethoxy calcein and ethidium homodimer-1 are not fluorescent outside of cells, ensuring that the background signal is low.

By counting and measuring the ratio of live (green) to dead (red) cells, a viability rate can be determined for the total number of cells observed. The main drawback of this method over the MTT assay is that each sample must be counted, while for MTT a quick absorbance reading will suffice.

Cell viability was measured using a Live/Dead assay kit from Invitrogen. After 24/48 hours of incubation with the Aβ42 solutions, cells were stained with calcein-AM and ethidium homodimer-1. 5 µL of each component was dissolved in 10 mL of G2 Neurobasal medium with AraC. 100 µL of media was removed from each well and replaced with 100 µL of this staining media. Cells were incubated for 15 minutes at 37 °C and then fluorescence images under red and green filters were taken using an Olympus DP72 camera attached to an Olympus IX70 microscope. Images were taken at 100X magnification. Cell counts were performed using the counting feature of Photoshop C4 (Adobe), and counts from multiple fields were compiled using Microsoft Excel. The viability of each sample was determined by dividing the number of live cells by the total number of live and dead cells. Viabilities were compared to that of a sample treated with buffer alone.

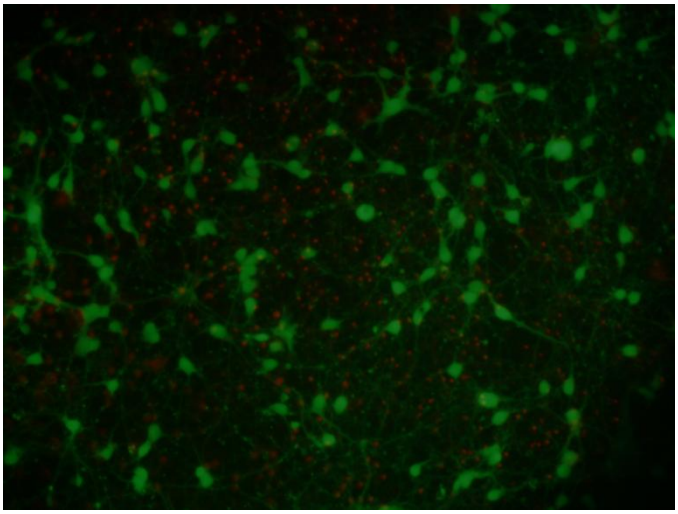

Figure 2.3 Example composite image of live (green) and dead (red) cells.
Aβ42 oligomers incubated 2 hours before addition to neuronal cells.

Preparation of seeded fibrils

Seeded fibrils were grown following the procedure devised by Tycko (65, 66). The Aβ42 fibrils were incubated at room temperature under stagnant conditions. 200 µM Aβ42 was prepared from NaOH stocks, and allowed to aggregate under stagnant conditions for 9 days.

During the 9 day period, the sample was sonicated in a Branson 1515 bath sonicator for 30 seconds every hour controlled by a timer. This sample (200 μL) was sonicated for 10 minutes, and 5% of the volume was added to a fresh 200 μM Aβ42 solution. This sample was allowed to aggregate for 7 days with 30 seconds of sonication every hour to produce generation 2 fibrils. Fibril generations 3-11 were produced by sonicating the previous generation for 10 minutes then adding a 5% volume of these seeds to a freshly prepared 200 μM Aβ42 solution. The samples were allowed to aggregate for 1 hour, after which the process was repeated for the next generation. The 12^{th} generation, which was used for the NMR experiments, was seeded with a 5% volume of generation 11 after generation 11 had been sonicated for 10 minutes. These fibrils were then allowed to aggregate under stagnant conditions for 1 week with a 60 second sonication after 2 hours of incubation. (Note, that this sample contained 10 mg of Aβ42 at a concentration of 200 μM in order to obtain enough material for NMR experiments. The previous 11 generations contained 200 μL a of 200 μM peptide). The sample was aliquoted into 1.5 mL Eppendorf tubes, spun at 14,000 RPM for 30 minutes, and the supernatant was discarded. Fibrils were then resuspended in water, and pooled into 2 tubes and the process was repeated twice. After the supernatant was removed from the triple washed fibrils the sample was frozen and lyophilized to remove any excess water. The dried samples were packed into the center of a 4 mm NMR rotor.

Solid-state NMR experiments (^{1}H ^{13}C DARR)

Solid-state NMR investigations of seeded Aβ42 fibrils were conducted on a 600 MHz Bruker AVANCE spectrometer, equipped with a 4 mm magic angle spinning (MAS) probe. MAS allows elimination of chemical shift anisotropic and dipolar interactions, both of which broaden the lines observed in the spectra of a solid sample. The suppression of these effects

narrows the width of the individual resonances allowing the signals from each of the individual amino acids to be distinguished. Samples were spun at rates of 9,000 to 12,000 KHz, the spinning rate was adjusted for each experiment in order to prevent MAS sidebands from overlapping with the peaks in the spectra.

$^{1}H - ^{13}C$ dipolar assisted rotational resonance (DARR) spectra were acquired with two-pulse phase-modulated decoupling (67-69). The CPDARR Bruker pulse sequence was used for data collection. 256 time increments were acquired in the indirect dimension with 64 scans per increment. The strength of the ^{1}H pulse during mixing time for the determined spinning speed (typically between 10 and 13dB for 9.5 and 11 KHz spinning) and decoupling field strength (typically between 22 and 24 dB) were optimized on ^{13}C labeled glycine prior to sample acquisition. Multiple spectra were acquired and the signals were summed to produce final spectra. Little variation was observed between individual spectra, indicating no changes in the state of the peptide during the experiment. Spectra were processed using Bruker Topspin software without line broadening.

Chapter 3 – Oligomers

Aβ42 is monomeric at 4 °C

The classical aggregation pathway of Aβ42 involves monomeric Aβ42 assembling into oligomers which then convert into protofibrils, and later into fibrils. EM images of Aβ42 when the peptides are incubated at 37 °C reveal a mixture of oligomers, protofibrils and fibrils. When incubated for longer periods of time (~ 1 week) the mixture is entirely fibrillar (Figure 1.3).

Previous experimental evidence indicates that initially solubilized Aβ42 is monomeric. NMR studies suggest that Aβ42 is monomeric at concentrations up to 50 μM (70), while single molecule fluorescence experiments imply that monomers are only stable at concentrations below 3 μM (71). Diffusion measurement, AUC and light scattering indicate that Aβ42 is monomeric at concentrations of 150 μM and 5 °C (72). Other groups have reported using ion mobility, time of flight mass spectrometry (73) and crosslinking (22) that at 30 μM, Aβ42 monomers exists in equilibrium with higher order oligomers (pentamers – hexamers) (Figure 1.2).

While the Aβ peptides aggregate at high temperatures, previous work has shown that at low temperatures, low concentration, or in low salt conditions, the Aβ40 and Aβ42 peptides remain stable and do not associate into larger aggregates (36, 74). We have previously used low salt and low temperature conditions to investigate Aβ42 peptides (36). Under these conditions, the peptide was observed to remain unchanged for up to 48 hours.

There are many biophysical techniques used to study the aggregation of Aβ42 *in vitro*. Fluorescence is a relatively simple technique that allows for observations of changes in the accessible structure in peptides over time. These measurements involve changes in the spectra of a fluorescent dye that is added to the Aβ42 peptides. Thioflavin T is one dye that has been used

extensively to monitor Aβ40 and Aβ42 aggregation (42, 75, 76). Thioflavin T is reported to only bind to species with a high β-sheet content (76, 77), so it should only bind to protofibrils and fibrils, and not to monomers or oligomers. Since it does not bind to oligomeric Aβ42, it does not inhibit the aggregation process (78). When Aβ42 aggregation is monitored at 4 °C, there is no change in thioflavin T fluorescence, indicating that no changes in secondary structure occur at this temperature (Figure 3.1).

NMR relaxation experiments provide evidence for monomeric Aβ42

NMR can provide information on the molecular structure of small proteins in solution. The integrated signal intensity is proportional to the amount of peptide in solution. If a species becomes too large, it will tumble too slowly to be observable by NMR. By monitoring the loss of signal over time, the rate at which the Aβ42 peptides convert from a small, solution visible, into a larger, solution invisible, state can be determined. At 4 °C the signal intensity remains constant, indicating that the Aβ42 peptides remain in a stable state which is visible by NMR and which does not increase in size or aggregation state over the course of the experiments (48 hours) (Figure 3.2).

Once it had been established that Aβ42 peptides can be stabilized at 4 °C, the question arose as to what species was stable. Various reports have been made as to the concentration at which monomers of Aβ42 cease to exist in solution (22, 70-73, 79). In order to determine the oligomeric state of the Aβ42 peptides at 4 °C, solution NMR was employed to measure the correlation time and diffusion coefficient of the Aβ42 peptides, which would provide information on the size of the species in solution.

The correlation time of a molecule in solution is proportional to its hydrated radius, with smaller proteins tumbling at a faster rate and therefore having a smaller correlation time. The correlation time (T_c) can be calculated by measuring two other relaxation rates by NMR, longitudinal relaxation (T_1 relaxation) and transverse relaxation (T_2 relaxation). T_1 corresponds to the rate at which the z – axis magnetization returns to equilibrium, while T_2 relates the rate at which the magnetization in the xy – plane loses coherence. In a high magnetic field, the correlation time of a protein is related to T_1 and T_2 by the equation (61):

$$T_c = \frac{\sqrt{\frac{6T_1}{T_2} - 7}}{4\pi * 70.9}$$

ν_N corresponds to the ^{15}N resonance frequency of 70.9 MHz.

The calculated T_1, T_2 and T_c times for each observable residue in the ^{15}N spectra of the Aβ42 peptide is shown in Figure 3.3. Overall the entire peptide experiences similar relaxation times at each residue. In order to make a qualitative estimate of the size of the NMR visible Aβ42 species, the average correlation time of the Aβ42 species was compared to that of ubiquitin, an 8 kDa protein used as a standard in NMR, under similar conditions (Table 3.1). The average T_c value for Aβ42 was 3.33 ns, while ubiquitin had a value of 3.15 ns. The similarity in T_c values indicates that the NMR visible Aβ42 species at 4 °C is close in size to a monomer or dimer.

NMR diffusion experiments provide evidence for monomeric Aβ42

The size of a molecule will also affect the rate at which it diffuses in solution. In order to confirm the size assessment from correlation times, the diffusion coefficient of Aβ42 peptides at 4 °C was calculated and compared to standard samples under similar conditions (Table 3.2). A

benefit of measuring the diffusion coefficient over measuring correlation times is that diffusion experiments can be performed without the use of expensive ^{15}N labeled peptides, allowing more standards to be measured. Standard curves for diffusion coefficient versus molecular weight at 4 °C are shown in Figure 3.4. The diffusion coefficient value for Aβ42 falls between aprotinin (6.5 kDa) and α-Chymotrypsinogen A (25.7 kDa), indicating that the Aβ42 species is close in size to a monomer. Our finding that the diffusion coefficient is close to that of monomeric Aβ42 is consistent with the results of other diffusion experiments (62, 72, 80).

Both the correlation time and diffusion experiments indicate that the Aβ42 peptides are monomeric at 4 °C. A final control experiment involved the measurement of the diffusion coefficient at high pH. Aβ42 peptides are typically resuspended in high concentration stock solutions (2000 μM) at high pH before being diluted and titrated to lower concentration at physiological pH (7.4). Despite the high concentration of these stocks, the Aβ42 peptide does not aggregate, indicating that the stocks remain monomeric at this pH. If the Aβ42 peptides remain monomeric at pH 10, the observed diffusion coefficient should remain similar to monomeric Aβ42 peptides at pH 7.4. At pH 10, the diffusion coefficient was calculated to be smaller than the peptides at neutral pH, indicating at high pH the peptide diffuses at a *slower* rate than at pH 7.4 (Table 3.3). The molecular weight which corresponds to this value is ~ 20 kDa. However at pH 10 the sample should consist solely of monomeric Aβ42 peptides. Therefore, this decrease in diffusion coefficient is most likely due to unfolding of the monomeric Aβ42 proteins at high pH. For proteins of the same MW, random coil structures will have a slower diffusion rate (smaller diffusion coefficients) than globular, folded proteins. This result indicates that despite the Aβ42 proteins being monomeric, they still have a folded structure at pH 7.4. This is consistent with water accessibility measurements of the Aβ42 protein at 4 °C which reveal regions of the protein

that are protected from solvent exchange and are therefore likely in a folded structure (Figure 3.5).

The solvent exchange data presented in Figure 3.5 are in agreement with previous measurements of the water accessibility of Aβ42 peptides (36). In this experiment amide protons exchange magnetization with water molecules, and a signal is observed depending on the amount of exchange. The experiments were conducted at three separate mixing times in order to observe the rate of exchange. The residues which showed least exchange with water were 10-12, 17-19 and 39-42. While these residues exhibited little exchange with water neighboring residues 15 and 16 were greatly exposed, which could indicate a turn in the N-terminus at residues 15/16. Such a turn would result in a small hydrophobic region of the monomer. Since residues 1-9 are mostly exposed to solvent, they may be structured in a way that shields the protected region.

Aβ42 oligomerizes at 37 °C

NMR evidence for Aβ42 oligomerization

It has been previously observed that Aβ42 monomers associate into larger oligomers and fibrils when incubated at temperatures above 4 °C (36, 74). In order to measure the kinetics of the conversion of monomeric Aβ42 into oligomers, ^{1}H NMR spectra were obtained of a solution of Aβ42 monomers incubated at 37 °C. Within 15 minutes of heating the sample, there was a rapid loss of signal (Figure 3.6). This loss of signal continued over time, but was greatest over the first two hours of heating, after which it proceeded at a slower rate (Figure 3.7). A previous rapid loss of NMR signal in high concentration Aβ42 samples was attributed to a conversion of monomers into protofibrils (70, 79), based on measurements of NMR relaxation time. It was shown that 50 μM Aβ42 remained over 90% monomeric for 1 week, while 160 μM Aβ42 aggregated quickly and reached an equilibrium that was 22% monomeric after 2 days (70, 79).

While these samples were conducted at 10 °C opposed to our 37 °C experiments, similar behavior can be expected. As decreases in NMR signal often correspond to an increase in molecular radius or molecular weight, we attributed this loss of signal to the conversion of monomers into larger order species.

The signal loss observed after heating the Aβ42 sample to 37 °C was not reverted when the sample was cooled back to 4 °C. This lack of an increase in signal after cooling the sample indicates that the assembly of the Aβ42 monomers into an NMR invisible species is not simply a temperature dependent association which can be reversed by cooling. This result is in contrast with NMR experiments on Aβ40 conducted by Yamaguchi *et al.* who observed a loss of NMR signal at high temperatures which could be recovered by cooling the sample back to 37 °C (81).

Fluorescence evidence for Aβ42 oligomerization

Previous NMR experiments by Clore and coworkers implied that the loss of NMR signal is due to direct assembly of monomeric Aβ42 into protofibrils (70, 79). In order to monitor the rate of protofibril formation by a second method, thioflavin T fluorescence was measured. Thioflavin T is a dye which undergoes a red shift upon binding to regions of high β-sheet content, such as Aβ42 protofibrils (75). By monitoring the level of thioflavin T fluorescence over time, a rate of protofibril formation can be determined. This plot is shown in Figure 3.8 along with the plot of NMR decay from Figure 3.7. There was a noticeable lag period in which the NMR signal decays while the thioflavin T fluorescence remains constant. It was not until after 6 hours of incubation at 37 °C that the thioflavin T fluorescence began to increase, long after the NMR signal from the Aβ42 monomers has reached its equilibrium value.

Evidence of large molecular weight intermediates in Aβ42 oligomerization

SEC evidence for multiple Aβ42 species

The gap in time between monomer assembly (as seen by NMR) and protofibril formation (as observed by thioflavin T fluorescence) implies that there is an intermediate species into which the monomers assemble before forming protofibrils. Many such oligomeric intermediates have been proposed ranging in size from dimers to 20mers (9, 21, 22, 74). In order to further investigate and characterize this oligomeric species, size exclusion chromatography (SEC) was employed. SEC has been used previously to separate oligomeric and protofibrillar Aβ42 (82, 83). Our SEC profiles of Aβ42 peptides look similar to previously reported profiles, containing two bands (74, 82).

Figure 3.9 shows an SEC profile of freshly solubilized Aβ42 peptides prepared at 4 °C. The chromatogram shows a single peak eluting at 17 mL. When the peptide is incubated at 37 °C prior to injection, this peak decreases in intensity, and a peak at 8 mL begins to elute (Figure 3.10). A table of integrated peak intensities is shown in Table 3.4 and a combined figure showing the changes in peak-shapes over 12 hours of incubation at 37 °C is shown in Figure 3.10. Together these data indicate that the initially monomeric Aβ42 peptides (according to NMR data) rearrange to form a larger species within the first 3 hours of incubation that is visible by SEC but not by NMR. As seen with the NMR signal decay experiments, the increase in molecular weight observed by SEC is not reversible by decreasing temperature, since the SEC experiments are conducted at 4 °C (after the sample has been incubated at 37 °C).

In order to determine the identity of the Aβ42 species observed in the SEC chromatograms, the elution times of the Aβ42 peptides were compared to those of standards. SEC columns are typically calibrated to standard curves based on the elution times of compact,

folded proteins of known structure and mass. However since proteins elute through a column based on their hydrodynamic radius, such a curve of molecular weight versus elution time, will be incorrect for less tightly folded proteins such as Aβ42 monomers and oligomers. If instead a standard curve of hydrodynamic radius (based on published crystal structures) versus elution volume is employed, it is seen that the Aβ42 species that elutes at 17 mL is more likely a loosely folded monomer with a radius of 1.5 nm opposed to a pentamer/hexamer with a mass of 20 kDa (Table 3.5 & Figure 3.11). This also means that the Aβ42 species that elutes at 10 mL is more likely a loosely folded oligomer with a radius of 5 nm opposed to a protofibril with a mass of 300 kDa. Larger oligomers and protofibrils will all elute at 8 mL (the void volume of the column at which species larger than 300 kDa elute).

Since both the oligomeric and protofibrillar Aβ42 species will elute at similar times, we sought to determine if the two species could be differentiated by other means. Since protofibrils consist of multiple Aβ42 molecules in an extended beta sheet structure, these species should be more stable than the oligomeric Aβ42. This stability could manifest as a species that can be dissociated by dilution. The ^{1}H NMR signal from the Aβ42 monomers never falls below ~30% even after 12 hours, which indicates that the monomer concentration in the sample remains at about 50 μM. This implies that there is a critical concentration of approximately 50 μM which the peptide must exceed before oligomers begin to form. Below this concentration the sample should remain monomeric. Therefore, if the sample is diluted from 200 μM to a 50 μM or 15 μM concentration before injection into the SEC column, the oligomeric Aβ42 may return to a monomeric state, while the protofibrillar Aβ42 will remain as protofibrils. The protofibrils have undergone a change in conformation and are stabilized by multiple β – sheets, so they are expected to remain stable even at low concentrations. Aβ42 peptides were incubated at 37 °C for

2, 4 or 6 hours, diluted to 50 and 15 μM concentrations and injected for SEC fractionation (Figure 3.12). When diluted, the 2 hour sample shifted from a 39% monomeric mixture to one containing 76% monomeric Aβ42 (Table 3.6). Dilution was less effective with the sample incubated for 4 hours, and the 6 hour sample showed little reversion back to monomeric Aβ42, indicating that the species forming after 6 hours of incubation was in a stable state not easily broken up into its components.

AFM evidence of two Aβ42 oligomer species

With the data that the Aβ42 peptides observed by both NMR and SEC are initially monomeric with an initial rapid conversion to oligomers over time at 37 °C, we sought to further characterize the changes in oligomeric structure over time. Imaging the samples with electron microscopy (EM) provides a useful means of obtaining images of the peptides at a resolution capable of distinguishing oligomers, protofibrils and fibrils. However, EM is typically unable to measure the height of the peptides or provide any three dimensional information. Atomic force microscopy (AFM) provides a similar image scale of Aβ42 peptides, but is also able to measure heights with little distortions to the samples. However AFM imaging is dependent on sample adherence to the mica or graphite surface used in the imaging experiments. Therefore a combination of EM and AFM provides a thorough means of visualizing the changes in Aβ42 peptides as they transition from monomers to oligomers to protofibrils and fibrils.

Samples of Aβ42 incubated at 37 °C were taken every two hours for AFM analysis where the height of each Aβ42 species present in the field was counted. From this data histograms of height distribution were made and compared over 10 hours. Based on the image seen in Figure 3.13A there are two distinct Aβ42 species, with similar area but different heights. Analysis of multiple datasets indicates that there are two Aβ42 oligomers one with an average height of 2 nm

and one with an average height of 4 nm. A two tailed students t-test comparing these two peaks found their differences to be significantly different (p values for distinct species were below 0.01). At early times (0 – 4 hours), the sample consists mostly of these short oligomers, with the larger species becoming the dominant species after 8 hours (Figure 3.14). No taller species are observed in any of these images. Based on these observations it would appear that the Aβ42 oligomers are stacking over time which results in the taller species which are approximately twice the height of the smaller species (Figure 3.13B). This is consistent with a model of Aβ42 oligomerization proposed by Teplow and coworkers on the basis of mass spec data where hexamers of Aβ42 were observed to stack to form Aβ42 dodecamers (21, 22) (Figure 3.13B).

The combination of NMR and AFM data indicates that the Aβ42 monomers rapidly assemble into hexameric oligomers with a radius of ~ 5 nm, and a height of ~ 2 nm. This association of monomers results in the loss of NMR signal as the Aβ42 peptides become too large to remain visible by NMR. Over time, these hexamers stack to form dodecameric oligomers that are ~ 4 nm in height. Since both hexamers and dodecamers have a similar radius (~ 5 nm) they elute at the same time on the SEC column. Despite the rapid rate of hexamer formation (most of the peptide has formed hexamers within the first 2 hours), the initial association of hexamers is slow; however after 6 hours, the dodecamers are more abundant than hexamers. Based on the times where these species are most abundant it would seem that the hexamers can be diluted back into monomers while the dodecamers cannot.

Secondary structure changes during Aβ42 oligomerization

The dodecamers become the major oligomeric species at a time similar to the initial rise in thioflavin T fluorescence (Figure 3.8), indicating that the dodecamers may be an intermediate between oligomer and protofibril formation. Protofibrils are not visible via AFM due to poor

binding to the mica surface employed. EM images of Aβ42 samples after 6 hours of incubation reveal the presence of very short protofibrillar species along with oligomers (height cannot be distinguished by EM) (Figure 3.15).

Since Aβ42 protofibrils have been reported to contain a high beta sheet content, spectroscopic methods were used to monitor changes in secondary structure of the Aβ42 peptides over time. Fourier transform infrared and circular dichroism spectroscopy (FTIR and CD) are biophysical tools for measuring the secondary structure of a protein. Both methods were employed to monitor the changes in the secondary structure of the Aβ42 monomers as they transitioned from monomers to protofibrils. FTIR and CD spectra of freshly solubilized Aβ42 monomers at 4 °C are shown in Figure 3.16 and Figure 3.17. The IR spectra display two peaks corresponding to structural features: a broad peak at 1680 cm^{-1} indicative of random coil, and a sharper peak at 1640 cm^{-1}which corresponds to β – strand. A peak at 1695 cm^{-1}which could be due to antiparallel β – sheet is also sometimes observed. The random coil nature of the initially solubilized Aβ42 peptide is less apparent in the CD spectra, where the initial spectrum at 0H is a relatively featureless flat line. As the sample is heated and time elapses, a peak at 215 nm appears, and becomes more intense as time passes. This indicates the formation of β – sheets over time. The random coil nature of the initially solubilized Aβ42 peptide is also observed in the CD spectra. The peak at 195 nm in the CD spectra is assigned to random coil. When the sample is heated, the peak position shifts from 195 nm to 215 nm indicating the formation of β – sheets (Figure 3.17). This transition from random coil to β – sheet occurred over a 2 hour period. After 2 hours, the sample consisted mostly of β – sheets which increase in intensity. Since the sample already consists of β – sheets this increase in intensity must be due to a further ordering of the β – sheets to produce a stronger signal. After 24 hours the sample remains unchanged,

indicating that the transition from protofibril to fibril is not observable by CD. As is the case with thioflavin T measurements (Figure 3.8) there is no distinction between protofibrils and fibrils; both contain ordered β – sheets and despite physiological differences in the two structures (Figure 1.3), both contain similar secondary structures and thus appear the same by these methods. Chapter 5 explores structural differences between protofibrils and fibrils.

In a similar fashion as seen with the CD spectra, IR spectra of Aβ42 peptides incubated at 37 °C over time show a gradual conversion from random coil and β – strand to ordered β – sheets (Figure 3.18). The β – strand peak at 1640 cm^{-1} in the spectra at 0 hours shifts to a β – sheet peak at 1630 cm^{-1}, with a coincidental loss of intensity in the broad random coil peak at 1680 cm^{-1}. Like in the CD spectra this shift occurs around 6 hours after the start of incubation, at a similar time as the increase in thioflavin T fluorescence. Taken together the CD, IR and Thioflavin T fluorescence data all show a transition from random coil and β – strand to ordered β – sheets occurring after 6 hours of incubation at 37 °C. Importantly these three methods show few changes in the overall secondary Aβ42 structure over the two hours of incubation during which the loss of NMR signal is greatest, indicating that the monomers and small hexameric oligomers share a similar secondary structure.

If the hexameric oligomers are stacking to form dodecamers, then it is possible that this stacking will change the hydrophobic accessibility of the peptide. 1-anilinonaphthalene-8-sulfonate (ANS) is a fluorescent dye which binds to hydrophobic surfaces, and has been previously shown to interact with Aβ42 oligomers (84). In a similar fashion as with the Thioflavin T experiments, ANS was added to aliquots of Aβ42 over the course of 24 hours of incubation at 37 °C. While early time points showed similar spectra, later times revealed a shift in the intensity and position of the spectra with a maximum intensity occurring after 6 hours of

incubation (Figure 3.19). This 6 hour time is around the same point as the shift in the IR spectra, and the increase in β – sheet content by thioflavin T. However since this intensity drops after 6 hours, while the IR and Thioflavin T results continue to increase, it would seem that the species causing the increase in ANS fluorescence is an intermediate. The timing of this intermediate is similar to that of the increase in dodecamer population by AFM (Figure 3.14). The AFM data indicates that the dodecamer population begins to increase after 4 hours of incubation, and should be at a maximum around 6-8 hours. Previous studies by Bolognesi *et al.* did not determine if the ANS was binding to low or high MW oligomers, but they did show a rise and fall of ANS fluorescence that correlated with increased toxicity (84). The toxicity data presented later in this chapter indicates that the increase in ANS fluorescence and the increase in toxicity occur at similar times.

Figure 3.20 illustrates the kinetics of Aβ42 fibrillization by combining the data presented in Figure 3.8, Figure 3.10, Figure 3.14 and Figure 3.19 as a single plot. The transition from oligomers to protofibrils as monitored by thioflavin T (Figure 3.8) and IR (Figure 3.18) was observed to occur after 6 – 8 hours of incubation. The initial conversion of monomers to oligomers was determined by NMR (Figure 3.8) to occur rapidly over the first hour. During the intermediate times between monomer assembly and protofibril formation, the AFM data shows a stacking of oligomers (Figure 3.14). The SEC data (Figure 3.10) also shows a rapid association of monomers and assembly into larger species over time. Since the AFM data can only give information on the relative amounts of each type of oligomers, the NMR and thioflavin T fluorescence data were used to determine that a maximum dodecamer population exists between 5 and 7 hours, and that once the protofibrils begin to form, these dodecamers are quickly lost. This time coincides with the increase in ANS fluorescence (Figure 3.19).

Large molecular weight Aβ42 oligomers are the toxic species in AD

Many different Aβ42 conformations have been implicated as the toxic species responsible for AD (6, 15-20, 85). The collection of structural data above provides a timeline across which we can monitor the progression of Aβ42 monomers to fibrils over time. Therefore, we monitored changes in neuronal toxicity exhibited by Aβ42 after different incubation times. By comparing this toxicity data to our other structural data we could determine which Aβ42 species is most toxic. Previous experiments measuring the aggregation and toxicity of Aβ42 peptides have been conducted at different peptide concentrations, temperature, and buffer conditions, so a full comparison between the structural data and toxicity was not possible. Aβ42 peptides were incubated at 200 μM at 37 °C in low salt buffer for 0-72 hours and then added to cultured rat neuronal cells for 2 days after which viability was measured. Cell viability was measured by MTT assay. This is a relatively quick method of determining viability of neuronal cells. MTT is a dye which is metabolized by mitochondria. If a cell is alive the mitochondria will metabolize the MTT, which is yellow, into formazan which is blue (63). After the reaction is allowed to proceed for 4 hours, all of the cells are lysed with detergent and the insoluble formazan is solubilized with ethanol and the absorbance is measured to determine the amount of live cells.

A plot of cell viability versus Aβ42 incubation time is shown in Figure 3.21A. The 0, 24 and 72 hour incubated Aβ42 peptides exhibit the least neuronal toxicity, while peptides incubated for 6 – 8 hours show the greatest toxicity. The decrease in cell viability over the first 2 hours correlates with the decrease in NMR signal, which we attribute to assembly of monomers into hexamers. This decreased toxicity of Aβ42 monomers is consistent with other reports indicating that monomers are non-toxic and may even be neuroprotective (27, 86). As the

hexamers assemble into dodecamers (as seen by AFM to occur over the 2 – 8 hour period), the toxicity to neurons increases, reaching a maximum at a similar time as both the change in ANS fluorescence (Figure 3.19) and the shift in height population from 2 nm to 4 nm, as seen by AFM (Figure 3.14).

This observation that Aβ42 dodecamers are more toxic than Aβ42 hexamers is in agreement with several other studies investing Aβ42 toxicity. Lensé and coworkers, working with transgenic mice which overexpress APP, found that an Aβ42 species with a molecular weight of 56 kDa was the neurotoxic agent responsible for memory loss in these mice (85). The 56 kDa species they observed is most likely the Aβ42 dodecamers formed by stacked hexamers that we (36) and others (21) have observed. A neurotoxic species with a weight corresponding to a dodecamer was also observed *in vivo* and *in vitro* by Bargorn *et al.* (18). They found that Aβ42 dodecamers bound to cultured neuronal cells and blocked long–term potentiation in rat hippocampal slices while not affecting basic synaptic transmission (18). Since long–term potentiation is believed to be responsible for learning and memory (87), these dodecamers are potentially responsible for memory loss in AD. In addition to observing toxic dodecamers in animal studies, they have also been observed in the brains of AD patients (18). Fukumoto and coworkers observed an increase in the level of large Aβ42 oligomers (10-20 mers) in cerebral spinal fluid of AD patients compared to age matched, non-AD controls (9). The presence of these large oligomers in AD patients indicates that a larger oligomer species may be responsible for the neurological damage. Together, the mass spectrometry (21) and AFM results suggest that disc-shaped hexamers can associate to form neurotoxic dodecamers both in vitro and in AD brains.

Typically, onset of AD does not usually begin until late in life. This late onset could be the result of a lifetime accumulation of Aβ, or it could be that as we age normal processes became abnormal and Aβ accumulates as a result. Aβ levels in the brain are very low, and a recent study found that brain Aβ40 and Aβ42 levels in cerebral spinal fluid to be 2 nm and 0.2 nM, respectively, in both AD patients and control brains (9). The concentrations used in this study are significantly (~ 10,000 – 100,000 X) higher than those found in the brains of both healthy and AD adults. However, there is some evidence that the Aβ species that are formed in the lab and in the AD brain are the same. A recent analysis of brain tissue found that levels of 56 kDa Aβ42 (likely the dodecamers observed here) accumulates in the brains of people after age 40 prior to onset of AD symptoms (88). The levels of this species drop after the disease begins to manifest, while the level of dimeric Aβ is elevated in the brains of AD patients (88). Additionally through use of specific antibodies, Bargorn *et al.* saw dodecamer binding in both rat neuronal cultures and in samples from AD brains (18).

The differences in toxicity of the Aβ42 peptides incubated for different times despite the long incubation time is indicative of a fast interaction between the Aβ42 peptide and the neurons. The 0 – 15 hour incubation outside the cells is much less than the 48 hour incubation on the cells, so if the Aβ42 peptides continued to aggregate in the cell buffer both of these samples should exhibit similar toxicity.

Additional measurements of cell toxicity were performed using an alternate assay, the Live/Dead from Invitrogen. This method involves addition of two fluorescent dyes to the cells. One dye, calcein-AM, crosses the plasma membrane and is metabolized by live cells where it fluoresces green, while the other, ethidium homodimer-1, binds to the exposed nucleus of dead

cells where it fluoresces red (64). By counting and measuring the ratio of live (green) to dead (red) cells, a viability rate can be determined for the total number of cells observed. The main drawback of this method is that it requires counting of each sample, which is less accurate than measuring the absorbance of a dye as is done with MTT. Neuronal cells were treated with Aβ42 in a similar manner as in the MTT assays and the results are shown in Figure 3.21B. As with the results from MTT, a decrease in neuronal viability is seen over 8 hours, indicating that the Aβ42 species present at later times is more toxic than the hexamers found at early times.

In the MTT assay, the viability of the neurons treated with Aβ42 is significantly lower than that of untreated neurons, or of neurons treated with buffer controls. There were two factors that separated the buffer control cells from the other cells: addition of Aβ42 and adjustment of pH with NaOH. The lower viability of the Aβ42 neurons compared to the buffer controls could be due to either of these factors. To confirm that the viability differences were not being affected by some difference in pH buffer, controls containing NaOH without Aβ42 were incubated and added to neuronal cells. These controls exhibited neuronal toxicity, but to a lesser extent than the Aβ42 peptides did. This indicates that the lower viability in the Aβ42 containing samples (especially in the non-toxic 0 hour and 72 hour samples) is partly due to the pH of the samples. In order to observe the toxicity of Aβ42 without differences in pH, Aβ42 peptides were dissolved in DMSO, an organic solvent with neutral pH. When DMSO dissolved Aβ42 peptides were incubated in a similar experiment, a comparable profile of toxicity versus time, with higher toxicity occurring between 6 and 10 hours, was again observed (Figure 3.22). A delay in the onset of maximum toxicity with the DMSO solubilized peptides compared to the NaOH Aβ42 was also observed.

In order to determine if the delay in onset of toxicity in the DMSO solubilized Aβ42 was due to a slower rate of oligomer formation the ANS, NMR, SEC and thioflavin T experiments discussed previously were repeated using DMSO solubilized Aβ42 (Figure 3.23). Measurements of thioflavin T fluorescence over time showed a delay in the transition from oligomers to protofibrils increased from ~7 hours to ~ 9 hours, indicating that the conversion of oligomers into protofibrils was slower in the presence of DMSO. In order to determine if this delay in protofibril formation was due to a slower conversion of oligomers or due to a lower oligomer concentration, the decay of ^{1}H NMR signals over time at 37 °C was recorded as it was for NaOH solubilized Aβ42. If the monomers associate to form oligomers at the same rate in both samples, then this would indicate that it is the conversion of oligomers into protofibrils which is slowed, perhaps because the oligomers are stabilized under these conditions. The decay of the NMR signal is similar to that of the NaOH treated sample, indicating that DMSO stabilizes the oligomers, slowing their conversion into protofibrils (Figure 3.24). The NMR spectra of the DMSO solubilized Aβ42 contains a new peak which is not present in the NaOH treated peptides. Strangely, while the rest of the peaks loose signal, this peak increases in intensity over time. Normally Aβ42 oligomers are not seen in the NMR spectra, however it would seem that small amounts (2% of the total volume) of DMSO are able to stabilize Aβ42 oligomers in an NMR visible state.

Attempts were made to characterize this new state by comparing the diffusion coefficient of this peak with that of the other Aβ42 peaks. At 4 °C, this peak is less intense than the other peaks and like the rest of the spectra, does not change over time. At 4 °C, the diffusion coefficient of this peak is faster than that of the peptide indicating it is a smaller species. This peak is not due to DMSO. This if for two reasons, one, the DMSO is deuterated so most of it will

not show in the spectra. Secondly the DMSO peak is assigned to show at 2.5 ppm, which is outside the aliphatic region. To further rule out that this peak was from DMSO, the calculated diffusion coefficient of the DMSO peak and of this peak were compared. The significantly shorter diffusion coefficient for this peak compared to that of the other Aβ42 peaks indicated that this data was flawed in some way. Attempts to measure the diffusion coefficient of the DMSO sample at 20 °C were unsuccessful because the sample changed aggregation state too quickly to make an accurate measurement of the diffusion coefficient. The increase in peak intensity coupled with the decrease from the diffusion experiment resulted in a poor value.

The ANS, thioflavin T, SEC and cell toxicity data (Figure 3.23) all indicate a slower time course for hexamer stacking to form dodecamers in the presence of DMSO. The NMR data (Figure 3.24) shows that monomers assemble to hexamers under these conditions at a similar rate as with the NaOH stocks. Therefore the delayed onset of toxicity with the DMSO solubilized peptides is due to the slower rate of dodecamer formation with these stocks.

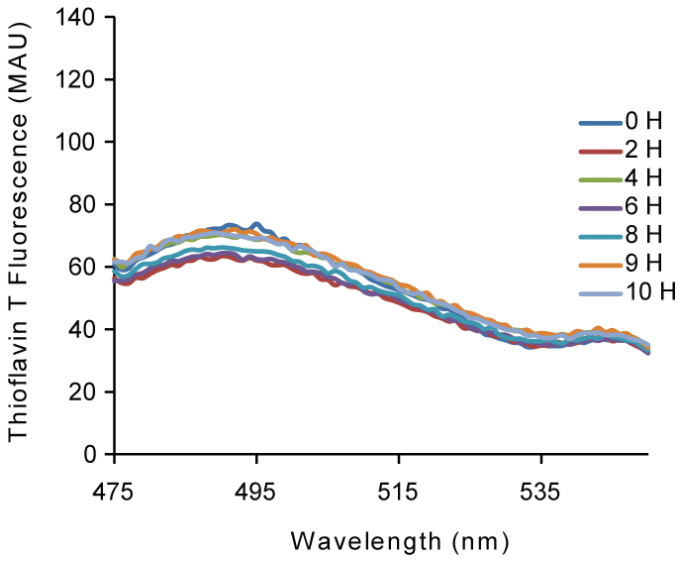

Figure 3.1 Thioflavin T fluorescence of Aβ42 at 4 °C.
Aβ42 peptides were prepared on ice at 200 μM and maintained at 4 °C throughout the experiment. At each time point, an aliquot of sample was removed, thioflavin T was added and a fluorescence spectra was collected. The spectra collected after 0 hours and 10 hours remain similar, indicating that little aggregation occurs during this time period at low temperature.

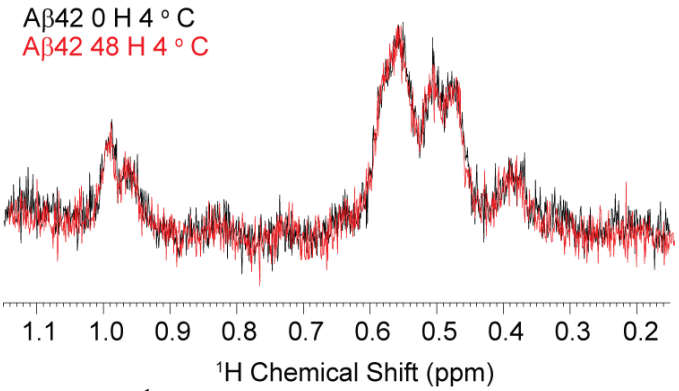

Figure 3.2 ^{1}H NMR spectra of Aβ42 at 4 °C.

^{1}H NMR spectra of a 200 µM Aβ42 solution maintained at 4 °C. Spectra were collected every 15 minutes. The region of the spectra spanning 0.15 to 1.15 ppm is shown. Two spectra collected at 0 (black) and 48 (red) hours show no differences in signal intensity, indicating that no changes in structure occured at this temperature.

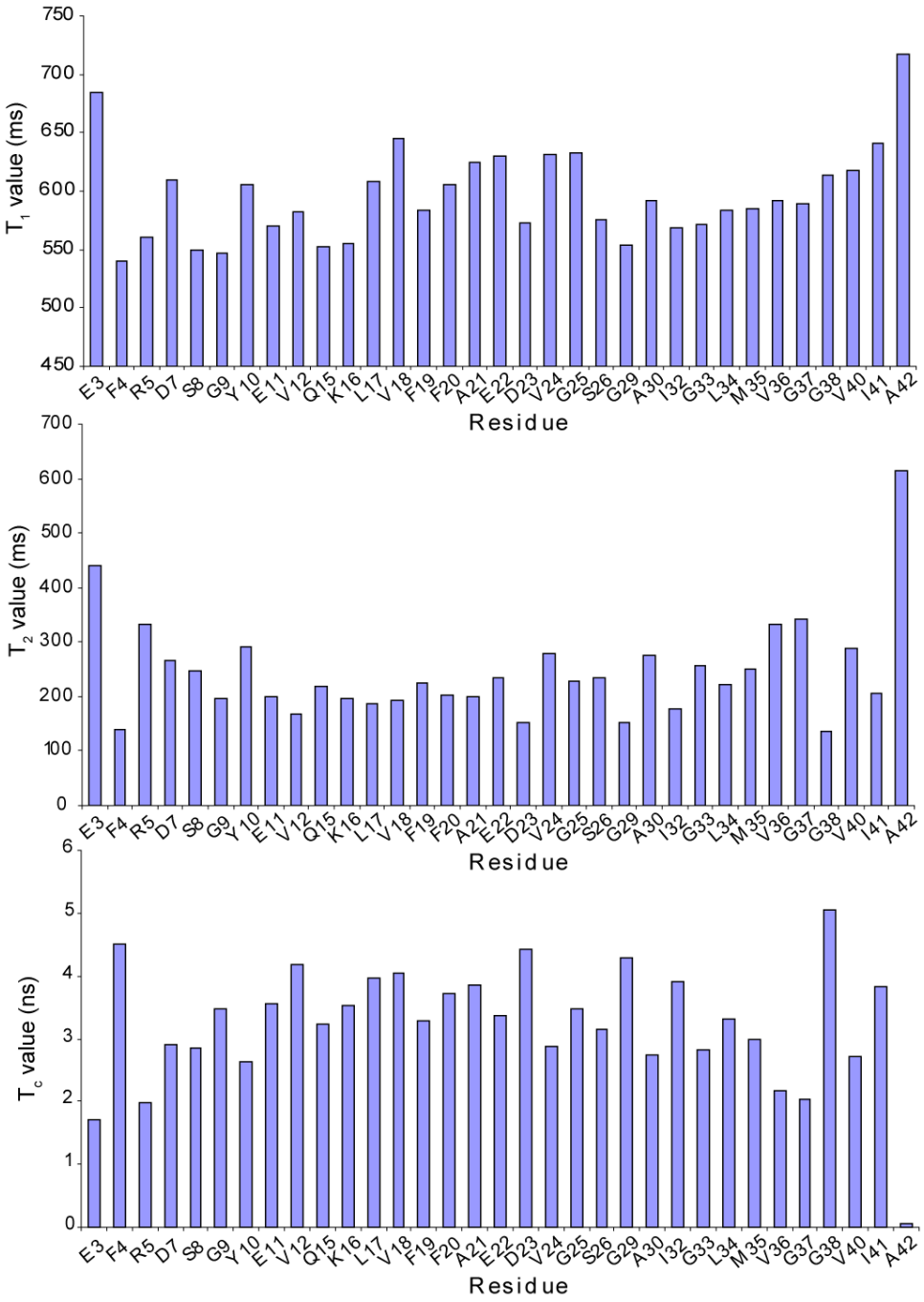

Figure 3.3 Calculated T_1, T_2 and T_c times for amide protons of the Aβ42 peptide.
The x-axis lists the peptide sequence from N to C - terminus. Little variation is observed for the values across the peptide.

	T_1 (ms)	T_2 (ms)	Tc (ns)
Aβ42	592	233	3.33
ubiquitin	847	345	3.15

Table 3.1 The average calculated T_1, T_2 and T_c times for the Aβ42 peptide and ubiquitin.

Water	200 uM α-Chymotrypsinogen A (25.7 kDa)	200 uM Aprotinin (6.5 kDa)	200 uM Aβ42
87.6 $X10^{-11}$	4.53 $X10^{-11}$	5.92 $X10^{-11}$	5.28 $X10^{-11}$

Table 3.2 Diffusion coefficient of Aβ42 and standard samples at 4 °C.
All diffusion coefficients are recorded in cm^2/s.

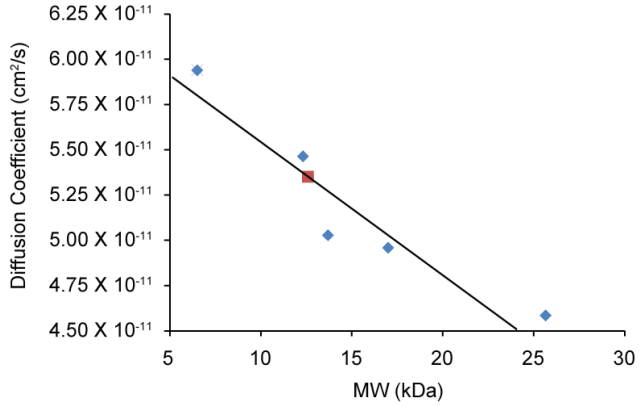

Figure 3.4 Diffusion coefficient of standard samples at 4 °C.
Diffusion coefficients for each standard were measured under the same conditions and are plotted verses molecular weight as blue diamonds. The average diffusion coefficient for Aβ42 is shown as a red square.

	4 °C pH 10			4 °C pH 7.4	
	Water	Aβ42		Water	Aβ42
Diffusion Coefficient (cm^2/s)	87.6 $X10^{-11}$	4.63 X 10^{-11}		87.6 $X10^{-11}$	5.24 X 10^{-11}

Table 3.3 Diffusion coefficient of Aβ42 at 4 °C at pH 7.4 and pH 10.
The calculated diffusion coeficient for the pH 10 sample was smaller than that observed at pH 7.4. This smaller diffusion coeficent indicates a slower rate of diffusion, which could only occur if the sample is larger at pH 10, which could be the result of unfolding at high pH.

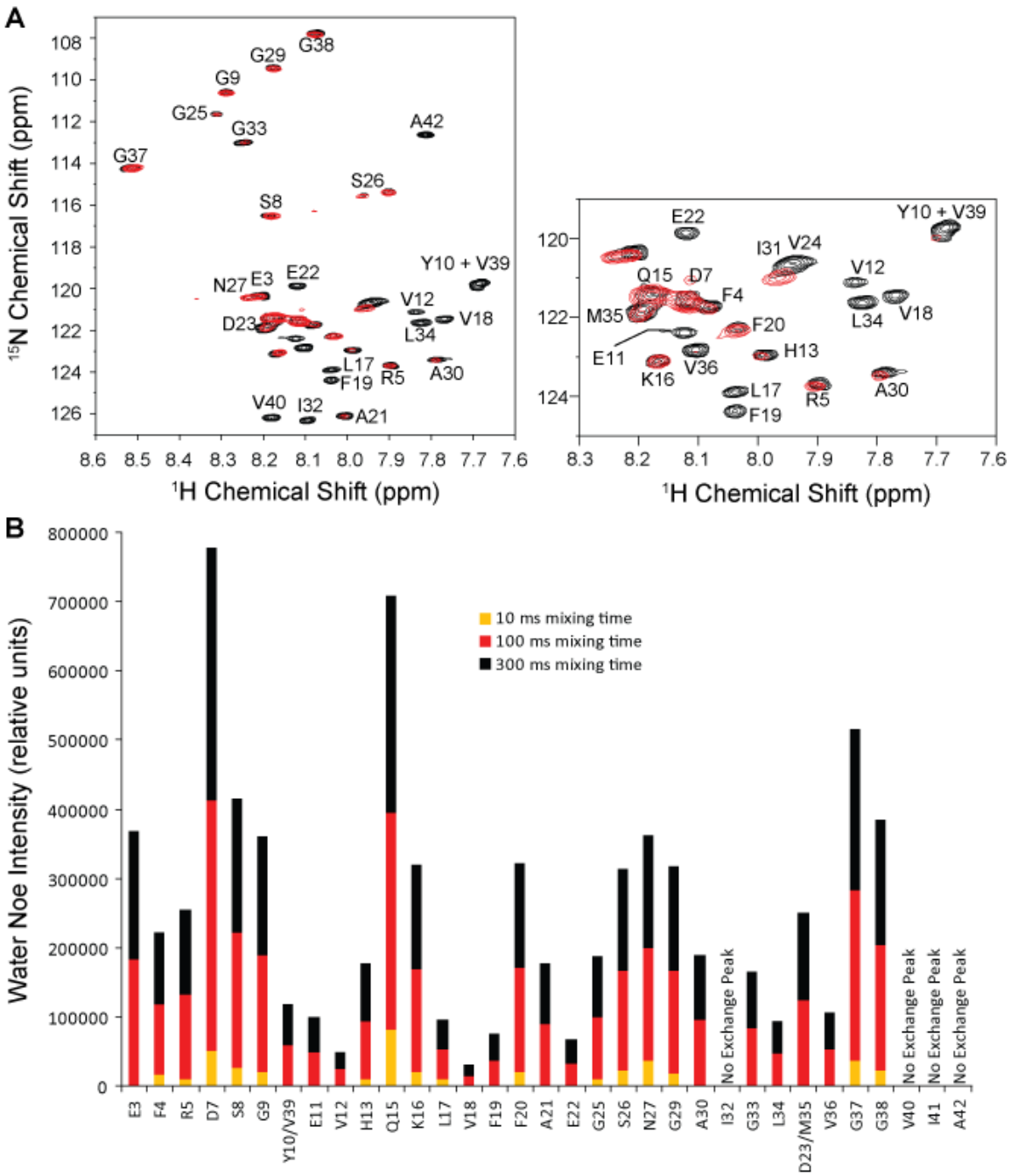

Figure 3.5 Water accessibility of Aβ42 at 4 °C.
A) Overlay of ^{1}H-^{15}NHSQC spectra (black) and ^{1}H-^{15}N CLEANEX-PM spectrum (red). Water accessible amide protons will show in both spectra, while inaccessible protons will only show in the black (HSQC) spectra.
B) Peak intensities of ^{1}H-^{15}N CLEANEX-PM spectrum at three mixing times. Longer mixing times will produce greater signal intensity, and are used to confirm the results. The rate at which the signal increases over mixing times can indicate the accessibility of a residue. The most protected residues are Y10, E11, V12, V18, F19, E22, L34, V36, V39, V40, A41 and A42.

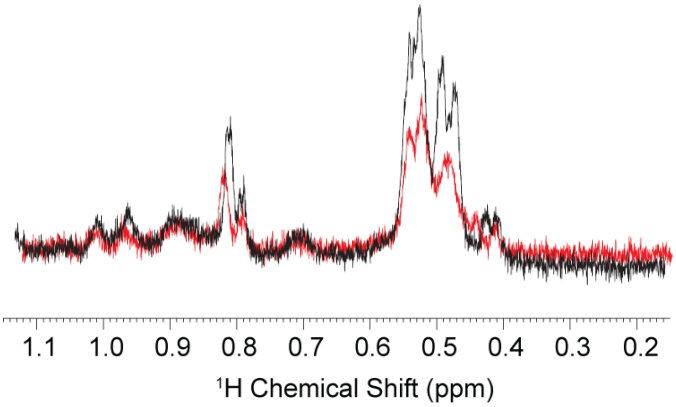

Figure 3.6 NMR signal loss upon heating Aβ42 from 4 °C to 37 °C.
^{1}H NMR spectra of a 200 µM Aβ42 solution were collected at 4 °C and 37 °C, then at every 15 minutes at 37 °C. The region of the spectra spanning 0.15 to 1.15 ppm is shown. The spectra collected at 37 °C (red) shows a decrease in signal intensity compared to the spectra collected at 4 °C (black), indicating a change in structure occured upon heating. Further signal loss at 37 °C was observed in subsequent spectra indicating that this signal loss continues at high temperatures.

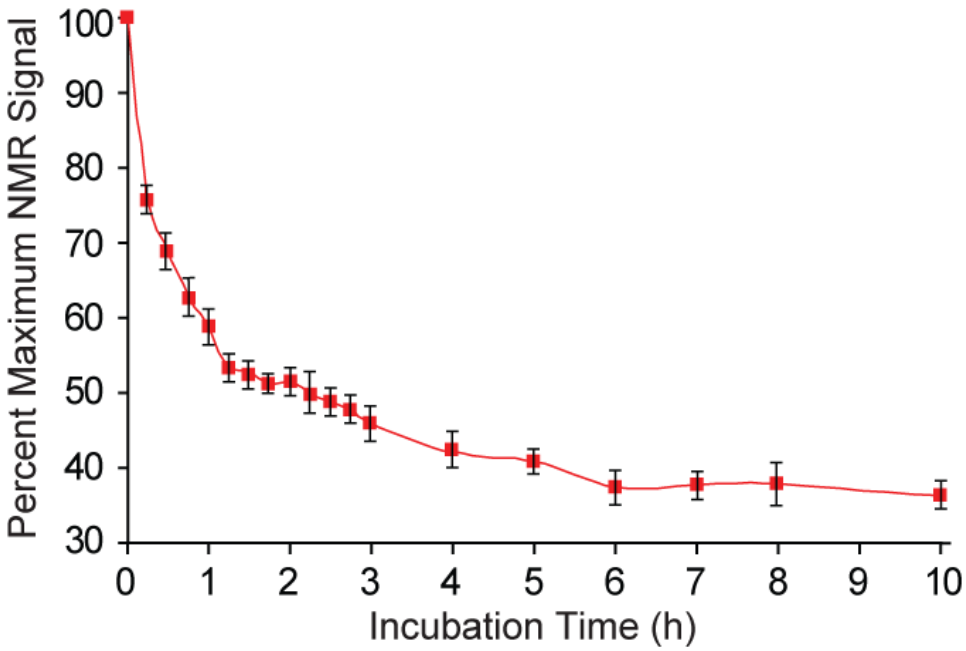

Figure 3.7 Measurement of NMR signal of Aβ42 at 37 °C over 10 H.
Integrated signal intensity from the 0.15 to 1.15 ppm region of the ^{1}H NMR spectra of a 200 µM Aβ42 solution collected every 15 minutes at 37 °C. The sharpest decrease in signal intensity occurs over the first 2 hours of incubation. Error bars are the result of triplicate experiments.

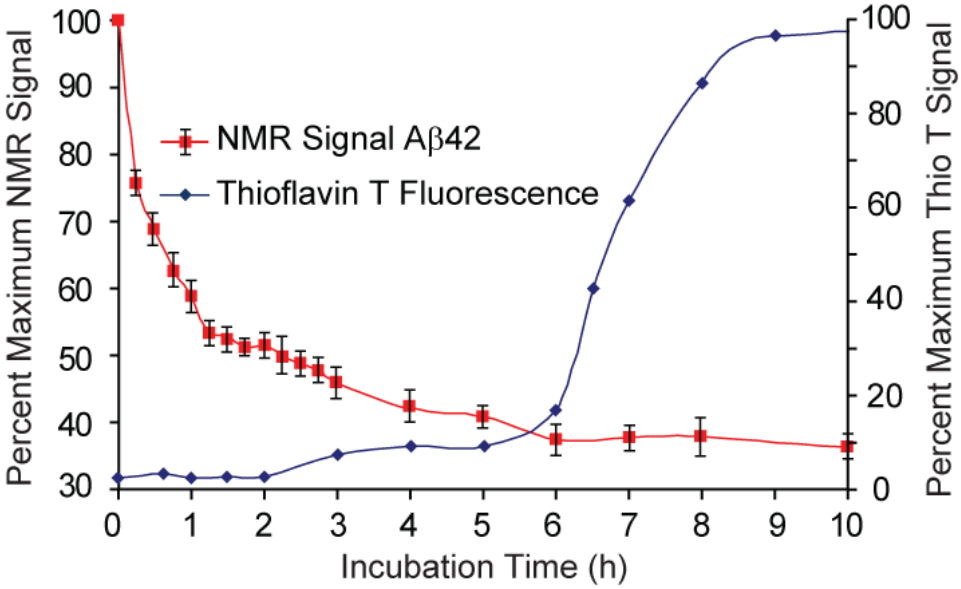

Figure 3.8 Overlay of thioflavin T and NMR signal of Aβ42 at 37 °C over 10 H. Thioflavin T experiments were conducted on Aβ42 peptides prepared at 200 μM and incubated at 37 °C. At each time point, an aliquot of sample was removed, thioflavin T was added and a fluorescence spectra was collected. The spectra show a lag time of approximately 6 hours before fluorescence begins to increase. The lag between the NMR decay and the increase in thioflavin T fluorescence implies that the loss of NMR signal is not due to protofibril formation.

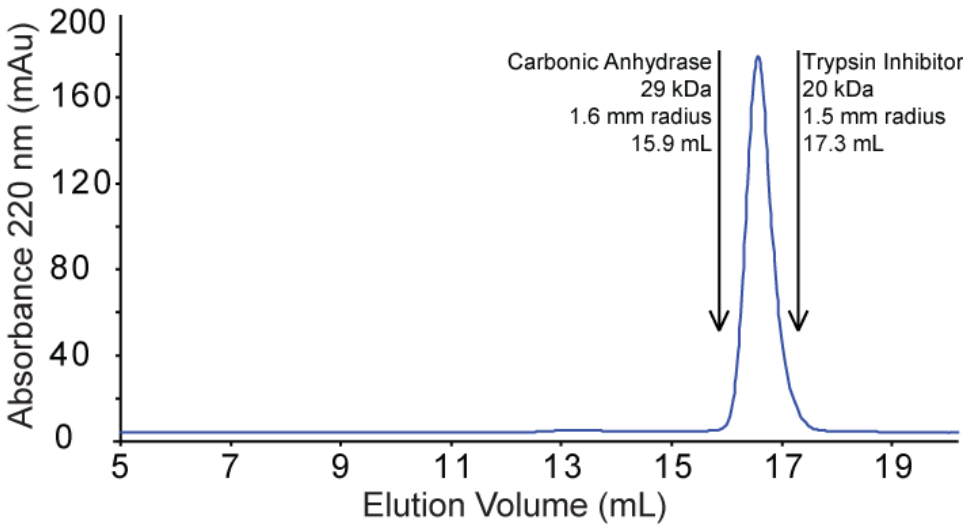

Figure 3.9 SEC profile of freshly solubilized Aβ42 peptides prepared at 4 °C.
Aβ42 peptides were prepared on ice at 200 μM, and SEC fractionation was conducted at 4 °C. The elution times of standards under similar conditions are shown as arrows. The Aβ42 elutes as a single peak with a mass of 20 kDa or a radius of 1.5 nm.

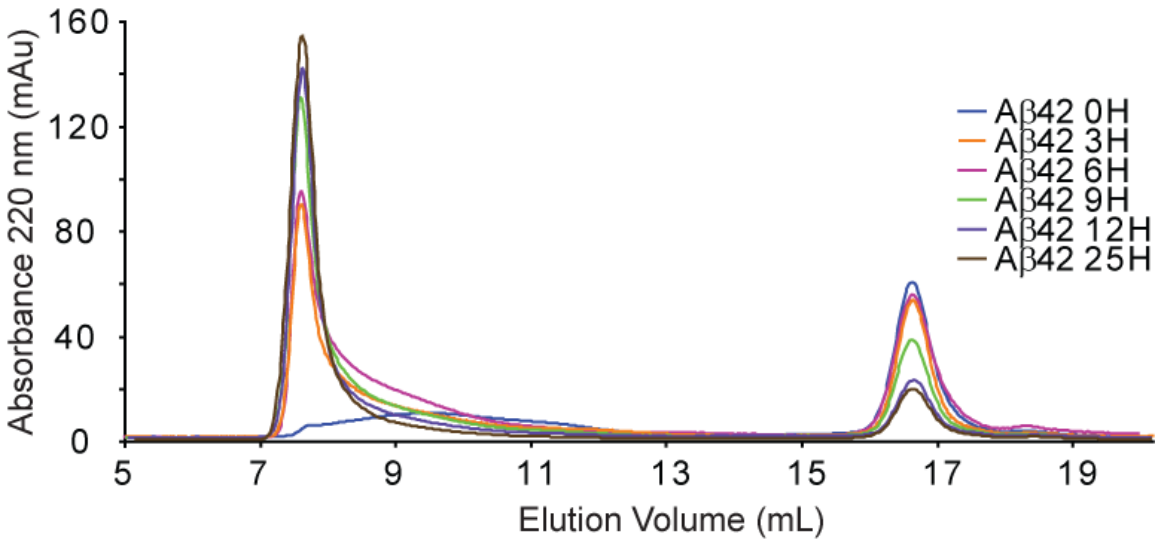

Figure 3.10 SEC profile of Aβ42 peptides incubated at 37 °C.
After each incubation time, 200 μM Aβ42 samples were injected into an SEC column for fractionation at 4 °C. The samples were integrated and signal intensity was normalized between samples. Integration values for each time point are listed in Table 3.4.

	0 H	3 H	6 H	9 H	12 H	15 H
8 mL peak	40 %	66 %	67 %	78 %	85 %	88 %
17 mL peak	60 %	34 %	33 %	22 %	15 %	12 %

Table 3.4 Table of peak integrations.

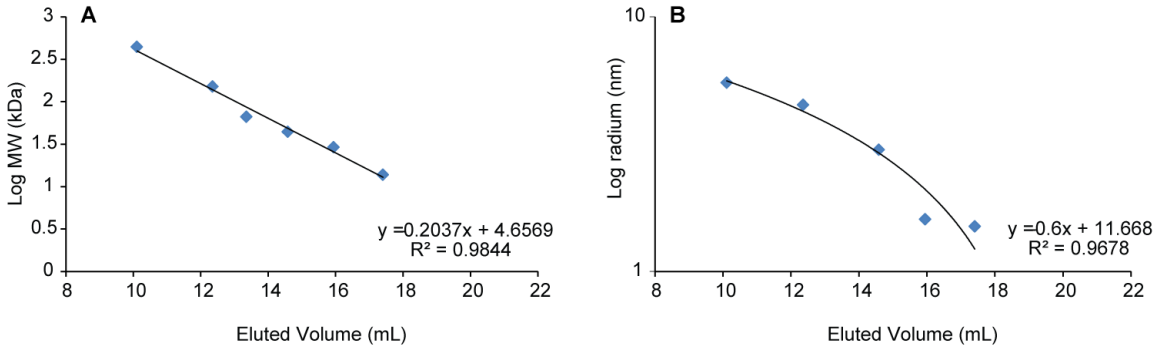

Figure 3.11 Standard curves for SEC experiments.
A) Plot of molecular weight value verses elution volume for the standards.
B) Plot of radius versus elution volume for the standards.
200 µM standard samples were injected into an SEC column for fractionation at 4 °C. The elution times of these standards were plotted verses molecular weight or radius. Measured values are listed in Table 3.5.

Protein	Elution volume (mL)	Molecular weight (kDa)	Radius (nm)	PDB
Carbonic Anhydrase	15.9	29	1.6	1CA2
Alcohol Dehydrogenase	12.4	150	4.5	1AGN
Kunitz Trypsin Inhibitor	17.3	20	1.5	1TIE
Feratin	10.1	440	5.5	Ferratin
Ovalbumin	14.6	44	3.0	1OVA

Table 3.5 Table of elution times of standard samples.
The radius for each protein was determined by measurements of the structure in the PDB.

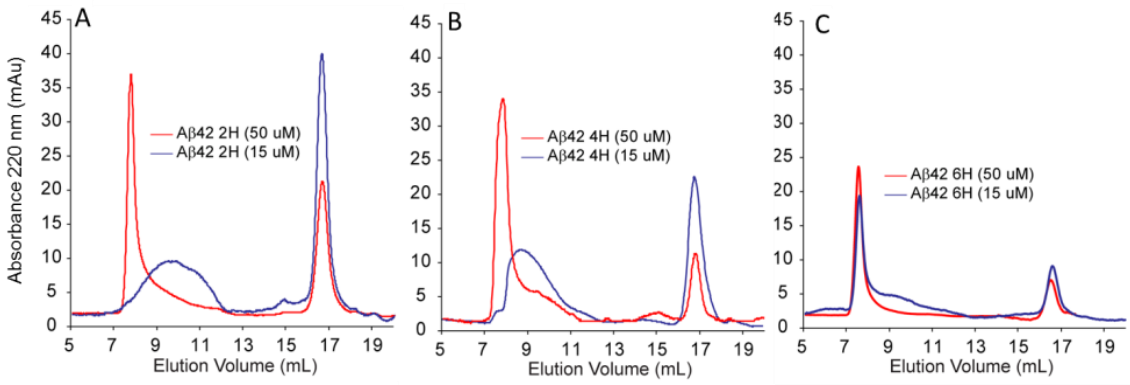

Figure 3.12 SEC dilution experiments.
A) Aβ42 oligomers incubated at µM for 2 hours at 37 °C then diluted to 50 or 15 µM.
B) Aβ42 oligomers incubated at µM for 4 hours at 37 °C then diluted to 50 or 15 µM.
C) Aβ42 oligomers incubated at µM for 6 hours at 37 °C then diluted to 50 or 15 µM.
After each incubation time, 200 µM Aβ42 samples were diluted and injected into an SEC column for fractionation at 4 °C. The samples were integrated and signal intensity was normalized between samples in order to compare the lower inteisty 15 µM data. Integration values for the two peaks in each time point are listed in Table 3.6.

	2 H	Diluted 2H	4 H	Diluted 4H	6 H	Diluted 6H
8 mL peak	61 %	24 %	54 %	36 %	62 %	77 %
17 mL peak	39 %	76 %	46 %	64 %	38 %	23 %

Table 3.6 Integrated intensities of peaks in dilution experiments.

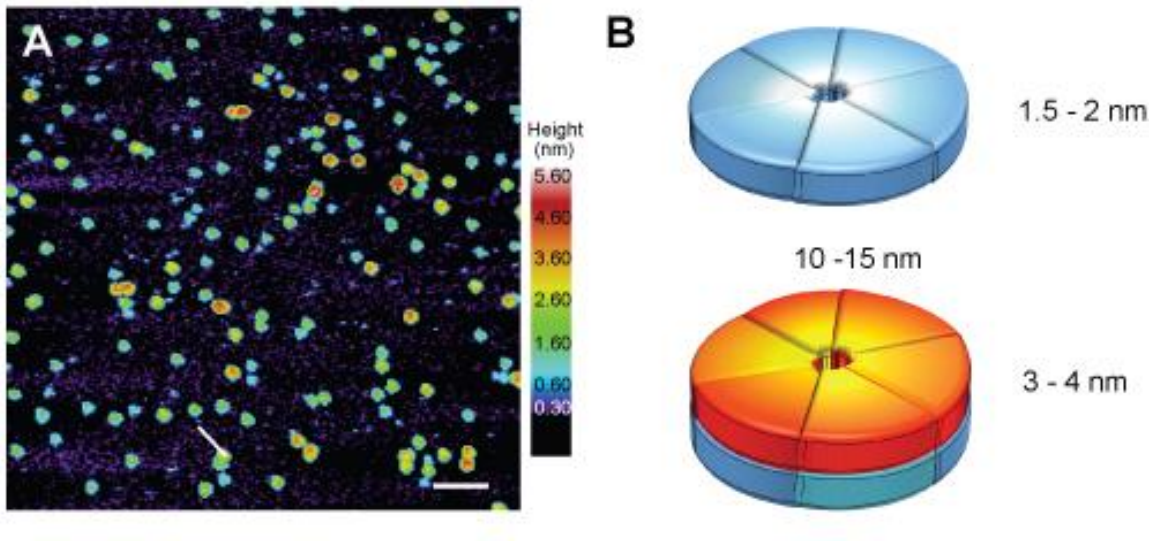

Figure 3.13 AFM image showing two heights.
A) AFM images of Aβ42 oligomers incubated 6 hours at 37 °C.
B) Cartoon representation of hexamer stacking to form dodecamers.
Aβ42 peptides were prepared at 200 µM, incubated for 6 h at 37 °C, then diluted to 1 µM for AFM imaging. The image field is 1,000 X 1,000 nm with the scale bar (white) corresponding to 100 nm. The Aβ42 observed typically have diameters between 10 and 20 nm.

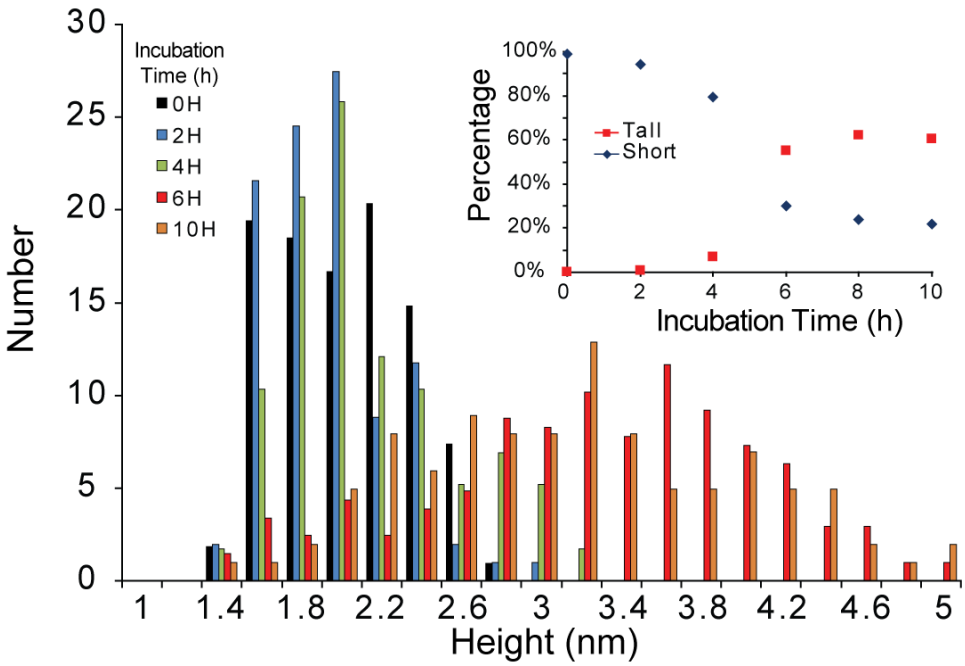

Figure 3.14 Histogram of AFM height data.
Aβ42 peptides were prepared at 200 µM and incubated between 0 and 10 h at 37 °C. At each time point, samples were diluted to 1 µM for AFM imaging. Histograms were generated from 3 – 5 AFM images of different 1,000 X 1,000 nm fields. Oligomers ranging in size from 1.5 – 2.5 nm were categorized as short, while those with sizes from 3.0 – 5 nm were categorized as tall.

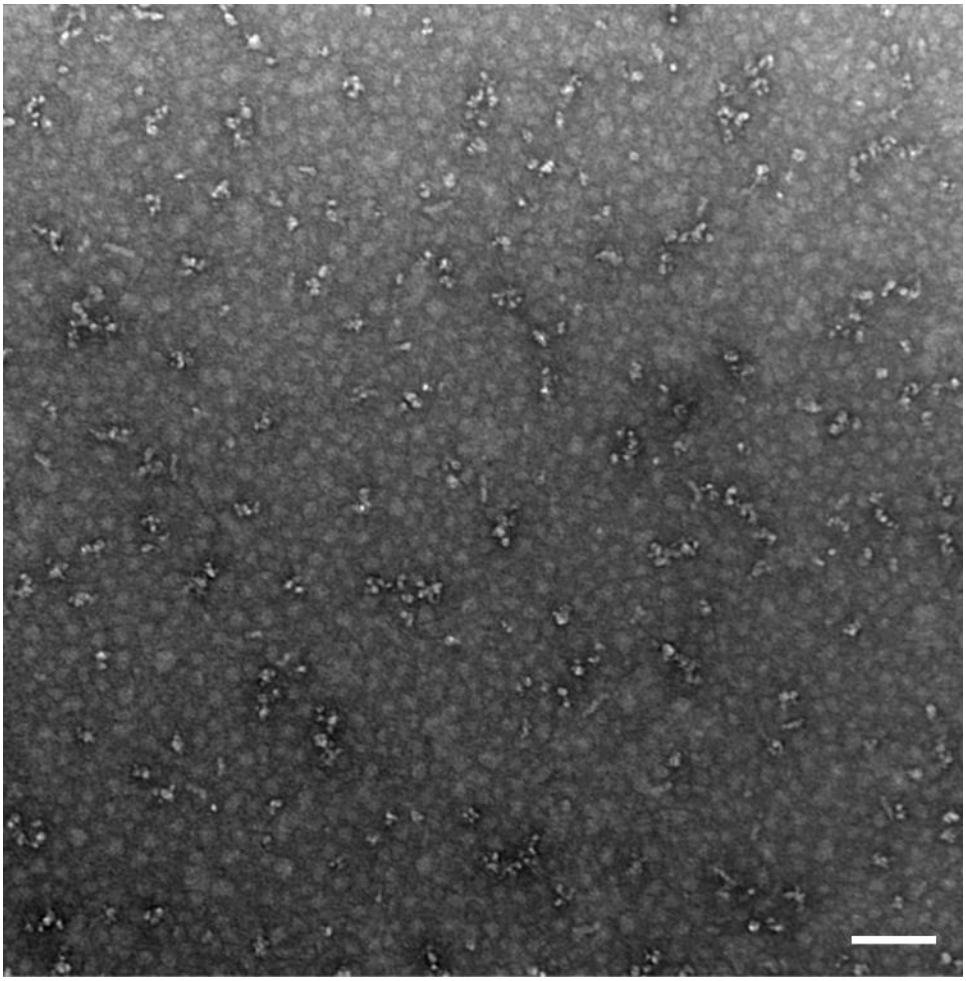

Figure 3.15 EM image of Aβ42 at 6 H.
Aβ42 peptides were prepared at 200 μM, incubated for 6 h at 37 °C, diluted to 15 μM, deposited on a copper grid, and stained with uranyl acetate. The image field is 1,000 X 1,000 nm with the scale bar (white) corresponding to 100 nm. The image background is mostly composed of Aβ42 oligomers. Of note are the small protofibril species with sizes roughly corresponding to the diameter of an oligomer, which could indicate that the protofibrils are first generated from an internal re-arrangement of the oligomers before subsequent elongation.

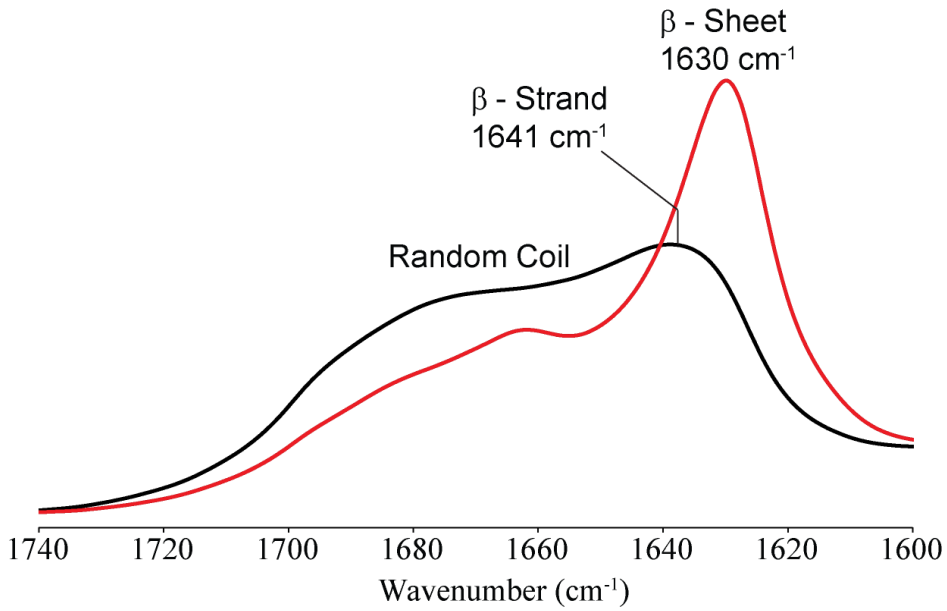

Figure 3.16 Labeled FTIR spectra.
FTIR spectra of a 200 μM Aβ42 solution prepared at 4 °C (black) and then incubated at 37 °C for 10 hours (red). The region of the spectra spanning 1740 to 1600 cm^{-1} is shown. The spectra collected at 37 °C (red) shows an increase in β – sheet character compared to the mostly random coil and β – strand spectra of the initially solubilized peptide (black), indicating a change in structure occurs over time at 37 °C.

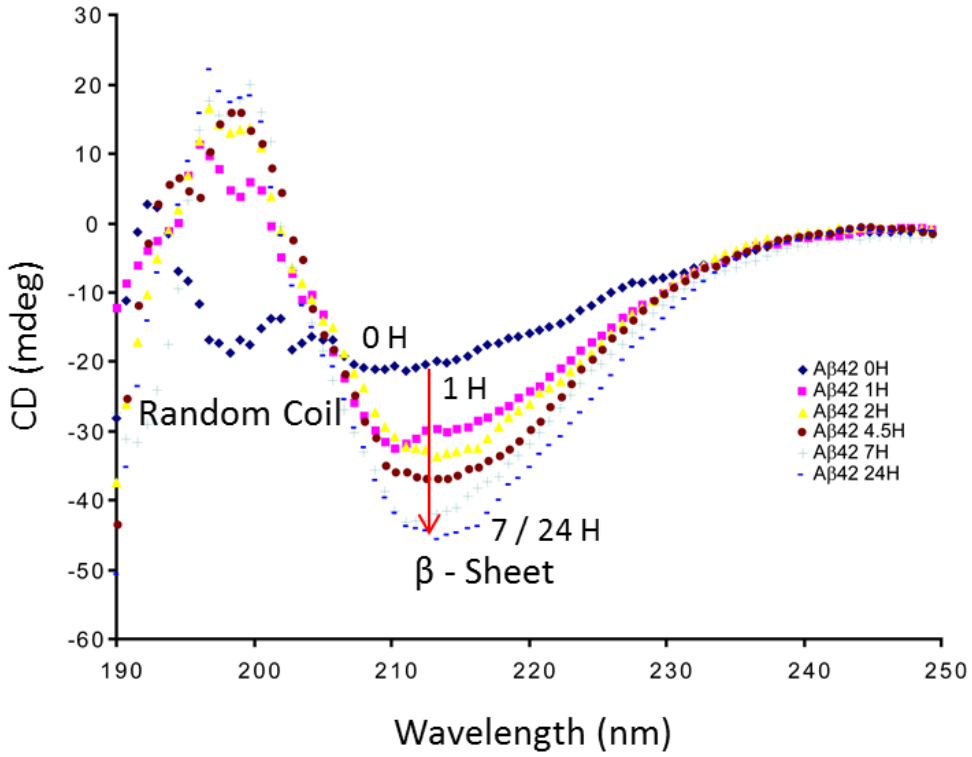

Figure 3.17 CD spectra of Aβ42 as a function of time.
CD spectra of a 200 µM Aβ42 solution prepared at 4 °C (blue diamonds) and then incubated at 37 °C. The region of the spectra spanning 190 to 250 nm is shown. The spectra display an increasing β – sheet character (peak at 215 nm) over time at 37 °C.

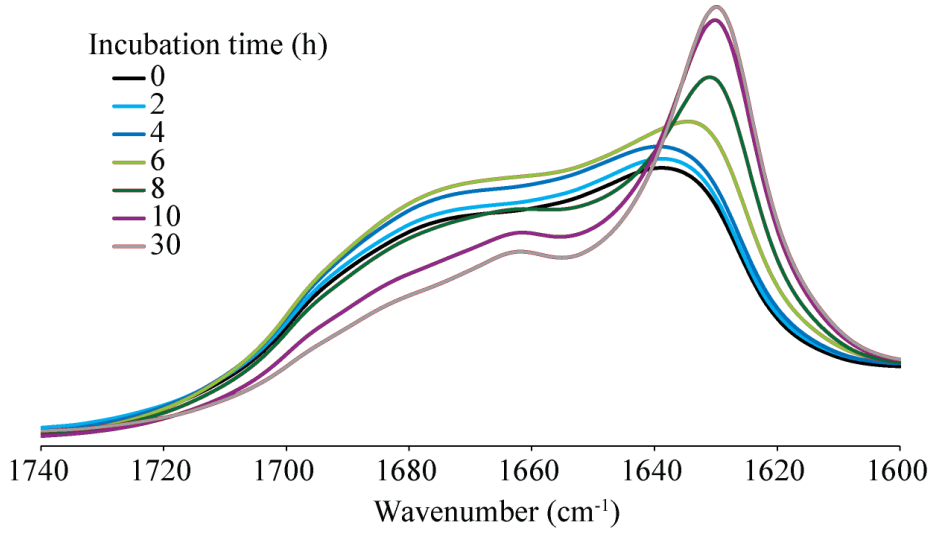

Figure 3.18 FTIR spectra as a function of time.
FTIR spectra of a 200 µM Aβ42 solution prepared at 4 °C (black) and then incubated at 37 °C. The region of the spectra spanning 1740 to 1600 cm^{-1} is shown. There is little change in the spectra over the first 4 hours. Between 6 and 8 hours an increase in β – sheet content is observed which reaches a maximum after 10 hours of incubation at 37 °C. Both the protofibril rich sample (10 hours purple line) and the fibil sample (30 hours pink line) have a similar lineshape and intensity, indicating that both of these two species are composed mostly of β – sheet that are indisinguishable by IR.

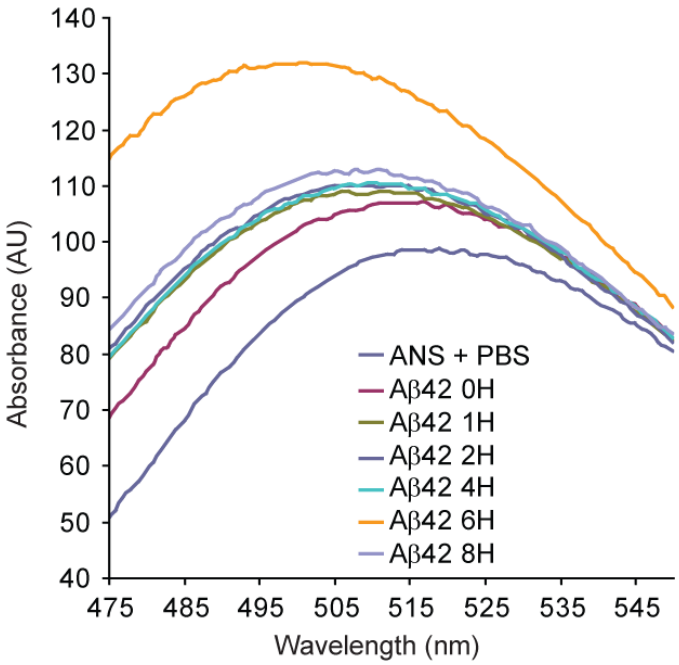

Figure 3.19 ANS fluorescence spectra of Aβ42 at 37 °C.
Fluorescence spectra of Aβ42 mixed with ANS. 200 μM Aβ42 was incubated at 37 °C for 0 – 8 hours, then mixed with ANS for a final ratio of 4.5 :1 ANS : peptide. The samples were excited at 349 nm and emisson spectra from 475 to 550 nm were collected. After a slight increase in flouerscene after the first hour, there is little change in the spectra until 6 hours. At 6 hours an increase in flouresence is observed. After 8 hours the fluoresence has returned to the 4 hour level, indicating that the fluorescent species is transient.

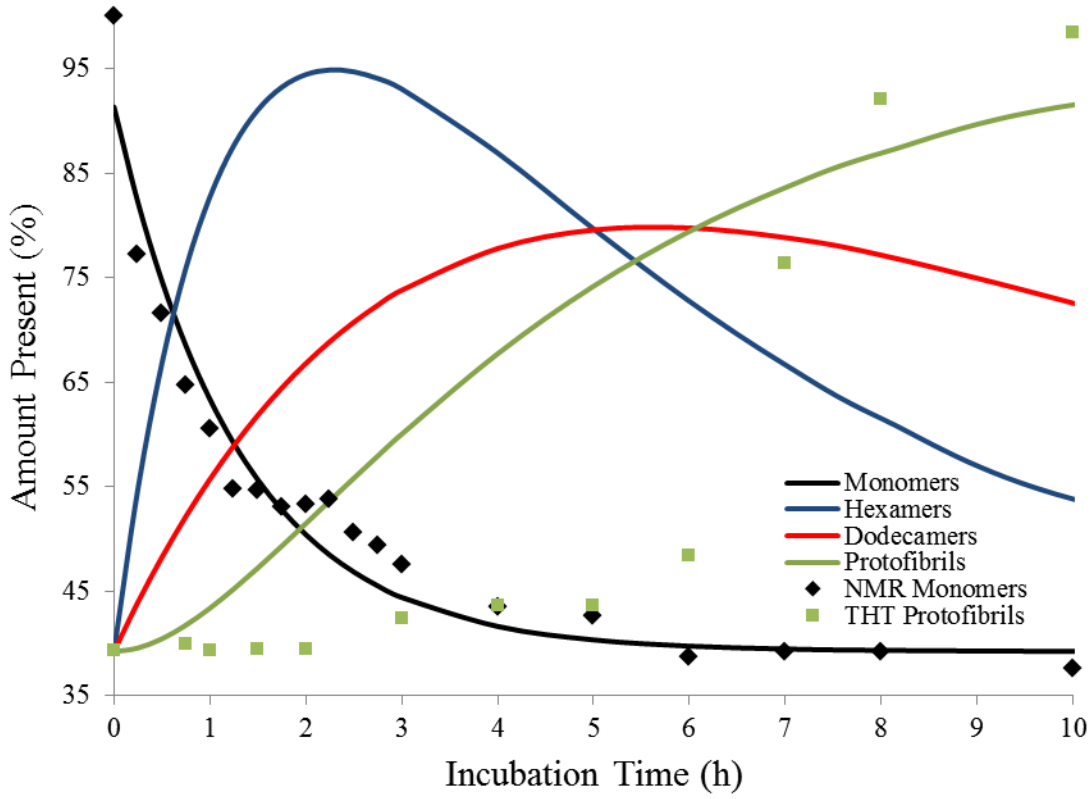

Figure 3.20 Kinetics of Aβ42 oligomer formation.
The NMR decay (black diamonds) and thioflavin T flourescence (green squares) data presented in Figure 3.8 was fit to kinetics equations to produce a model showing the correlation between loss of monomers (black) and formation of hexamers (blue), dodecamers (red), and protofibrils (green). As monomers convert into hexamers, the monomer population decreases. Hexamers are most concentrated around 2 hours, after which dodecamers begin to increase. After a maximum dodecamer population occurs around 6 hours, the protofibrils become the dominant species.

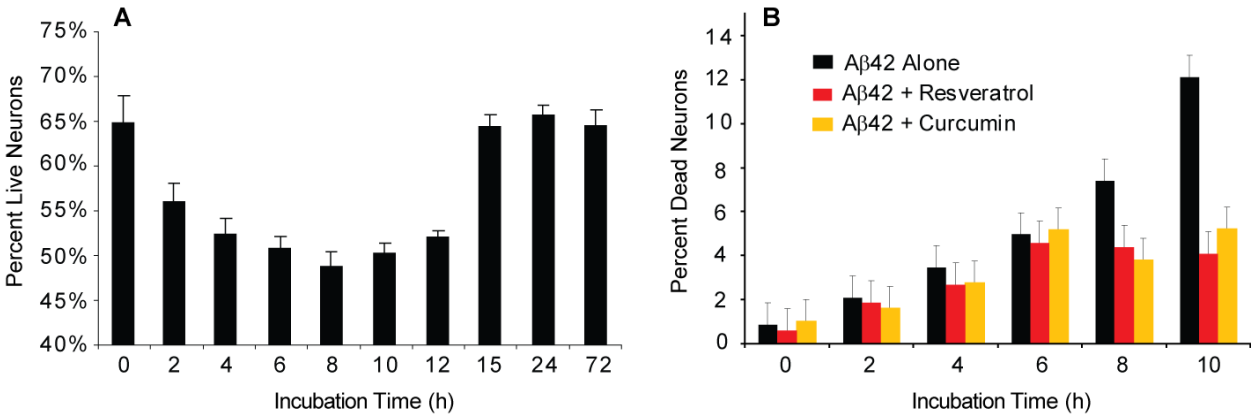

Figure 3.21 Neuronal toxicity over time.
A) MTT and B) Live/dead assay results for NaOH stock Aβ42.
Influence of Aβ42 oligomers on the cell viability of rat neurons was assayed by two methods. 200 μM Aβ42 was incubated at 37 °C for 0 – 72 hours with or without inhibitors (Aβ: inhibitor ratio of 1:1). The Aβ42 peptides were diluted into neuronal cultures (12 μM final concentration) and incubated an additional 48 hours before viability was assayed. The toxicity of the Aβ samples increased with time with a maximum around 8 hours. These results indicate that the small oligomeric Aβ species are more toxic than the monomeric or fibrillar Aβ. When incubated with inhibitors, toxicity did not increase after 4 hours, indicating that the inhibitors prevented the formation of the toxic species normally present at later times.

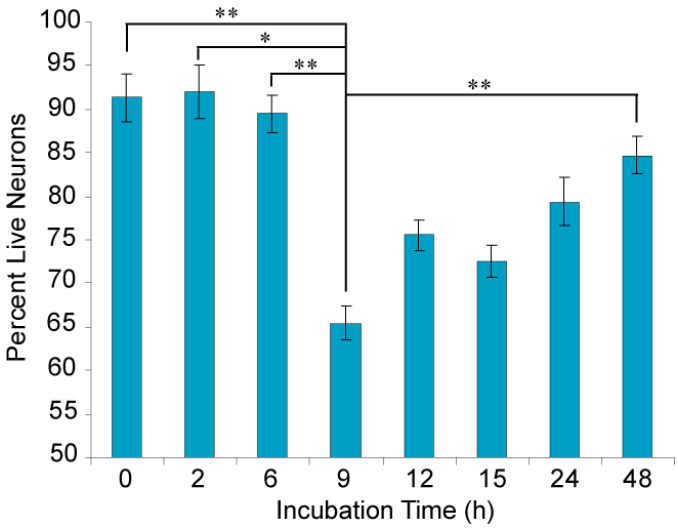

Figure 3.22 Neuronal toxicity over time with DMSO stock.
200 μM Aβ42 was incubated at 37 °C for 0 – 48 hours. The Aβ42 peptides were diluted into neuronal cultures (12 μM final concentration) and incubated an additional 48 hours before viability was assayed. The toxicity of the Aβ samples increased with time with a maximum around 9 hours. Results of statistical analysis are indicated by stars. * indicates that the results of a two tailed students t-test are >0.05 and ** indicates a result > 0.01. The sample incubated for 9 hours prior to addition to the neurons was found to be significantly more toxic than the samples incubated for 0, 2, 6, or 48 hours, indicating that the oligomeric Aβ species present at 9 hours is more toxic than the monomeric or fibrillar Aβ present earlier or later. These Aβ42 samples were generated from a DMSO stock, while those in Figure 3.21 were made using NaOH solubilized Aβ42. The two methods each produce a similar Aβ42 oligomer, but the kinetics using DMSO are slower (see Figure 3.23 below).

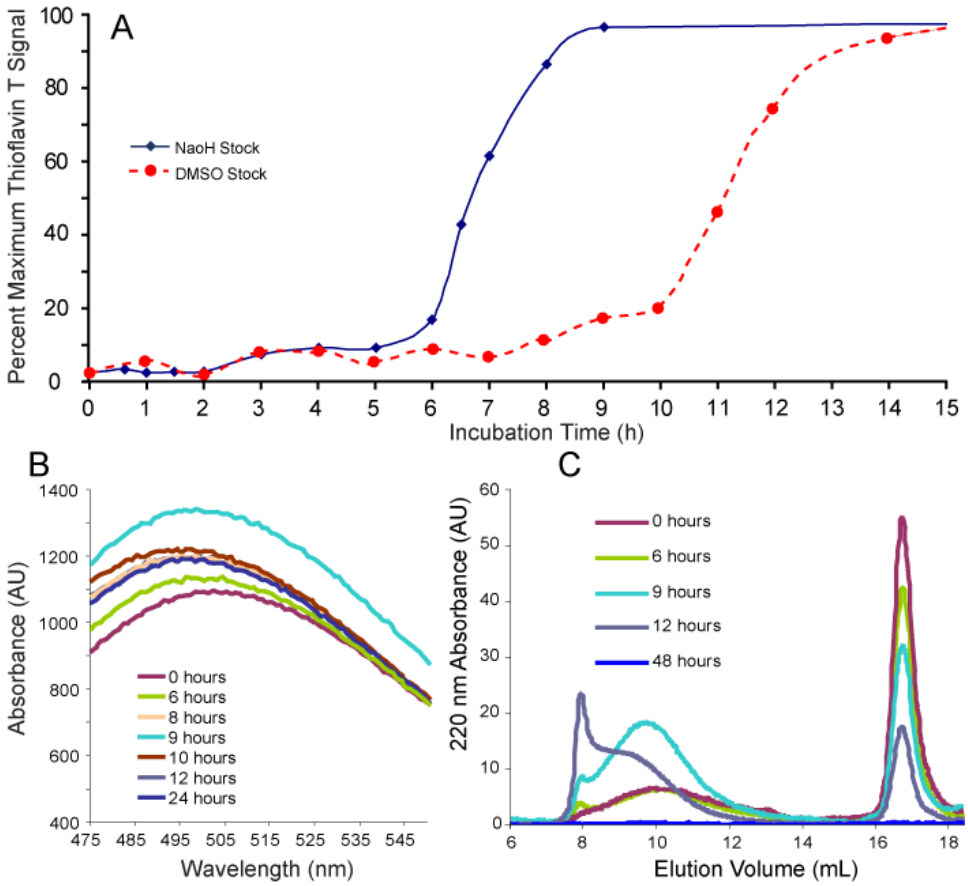

Figure 3.23 DMSO stocks delayed Aβ42 aggregation.
A) Thioflavin T fluorescence with Aβ42 from NaOH (blue) and DMSO (red) stocks.
B) ANS fluorescence spectra of Aβ42 at 37 °C from DMSO stock.
C) SEC profiles of Aβ42 incubated at 37 °C from DMSO stock.
Aβ42 samples generated from DMSO stock produce similar Aβ42 oligomers as those made with NaOH, but with slower kinetics. The thioflavin T fluorescence (Figure 3.8), ANS fluorescence (Figure 3.19) and SEC experiments (Figure 3.10) were repeated with DMSO stocks.

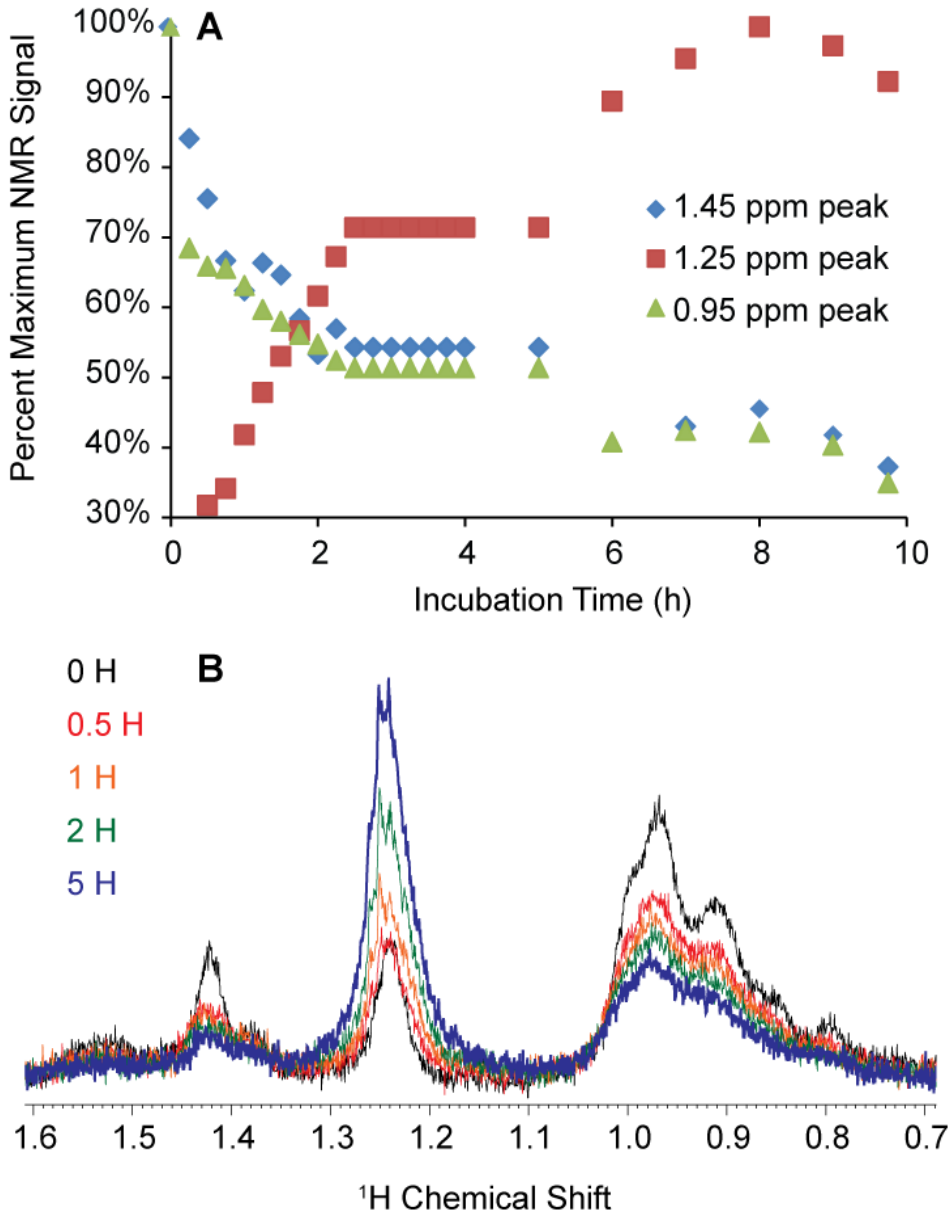

Figure 3.24 Measurement of NMR signal from DMSO stocks.
A) NMR signal of three peaks in the spectra of Aβ42 at 37 °C made from DMSO stocks.
B) ^{1}H spectra showing that the peak at 1.25 ppm increases while the others decrease.
The 0.7 to 1.6 ppm region of the ^{1}H NMR spectra of a 200 μM Aβ42 solution samples generated from DMSO stocks contain an extra peak around 1.25 ppm not observed in the NaOH stock. Unlike the peaks at 1.45 and 0.95 ppm, this peak increases in intensity when the sample is incubated 37 °C. As with the NaOH samples, the sharpest decrease in signal intensity occurs over the first 2 hours of incubation.

Chapter 4 – Interaction between oligomers and inhibitors

In recent years, many different natural and synthetic compounds have been identified as inhibitors of Aβ aggregation. These compounds have a variety of targets, some bind to and stabilize monomeric Aβ and prevent further aggregation, while others bind to the fibrils in the plaques and assist in their removal.

Small molecules can interact with Aβ in one of three different ways: by inhibiting oligomerization, by inhibiting fibrillization, or both (57). Small molecules such as resveratrol (89), curcumin (57) and indomethacin (57) fall into the first category, while compounds such as apigenin (57) fall into the second category. Other compounds such as RI-OR2 recently developed by Taylor *et al.* inhibit both oligomer and fibril formation (58). Inhibiting oligomer formation is the most advantageous strategy because current data indicates that small Aβ oligomers are the neurotoxic species (6, 15-17, 19, 20), while Aβ monomers are neuroprotective (86). Recent work by Teplow and coworkers indicates that Aβ42 oligomers are composed of a mixture of dimer, tetramer, hexamer and dodecamers (21). In a crosslinking study with Aβ40, toxicity increased as oligomer order increases, further demonstrating the need for inhibitors of oligomerization (90). These results demonstrate the importance of stabilizing Aβ oligomers in a small, non-toxic conformation.

Of the various natural product inhibitors that target Aβ fibrillization and toxicity, curcumin (42, 43) (a compound found in Indian curries) and resveratrol (44-46) (a polyphenol found in wine (44-48)) were chosen for further investigation due to their similar structures (Figure 4.1) and their abundance in certain human food which would allow for dietary intake.

Curcumin is the yellow pigmenting agent in the spice turmeric, but curcumin has no taste. Since it has some anti-oxidant properties, curcumin has been suggested as a potential therapeutic agent for numerous diseases ranging from arthritis to cancer to AD (91). The low incidence of AD in India and the high intake of curcumin in their diets led to an investigation into the anti-amyloidogenic properties of curcumin (92). Early studies have shown that curcumin may have anti-aggregation properties that can be exploited for treatment and prevention of AD (42, 43). Transgenic AD mice given a daily diet of curcumin had lower plaque levels compared to control mice (43). Problems with curcumin treatment stem from its relatively poor solubility, and fairly rapid breakdown. In addition to its low solubility, it is not able to readily cross the blood brain barrier, so a very large dietary intake is needed to obtain any in the brain.

Subsequent studies have looked at the use of curcumin as an inhibitor of Aβ42 fibril formation (42, 43, 92, 93) for review see (47, 91). Other studies have looked at the role of the structure of the curcumin molecule in inhibition. A study by Gestwicki and Reinke investigated the structural requirements for inhibition of fibril formation by curcumin (94). They found that the length and flexibility of the chain linking the two rings, as well as the substitution of the rings affected the inhibition as detected by thioflavin T fluorescence. Another study by Yan investigated the importance of the enol form of curcumin in fibril binding (95). Curcumin has also been shown to bind to Aβ40 fibrils with high affinity (96). While previous studies have noted that curcumin has anti-aggregation effects on the Aβ peptides both *in vitro* and *in vivo,* little research has been done to investigate how these compounds prevent aggregation. By conducting the experiments from Chapter 3 in the presence of curcumin, we can determine at which step in the fibril formation pathway curcumin interferes, and how it blocks toxicity.

Resveratrol, a polyphenol found in red wine, has been recently been shown to have potent anti-cancer and anti-Alzheimer's properties (45, 46, 48, 89, 97-99). Recent studies using antibodies specific to toxic oligomers and to fibrils have shown that resveratrol selectively remodels toxic Aβ42 oligomers into a nontoxic aggregate, and converts Aβ42 fibrils into nontoxic aggregates, while not affecting non-toxic monomers (97). Based on this combination of effects, and its increased affinity for Aβ42 resveratrol may be more inhibitory than curcumin (46).

Inhibitors reduce toxicity of Aβ42 oligomers

Figure 4.2 shows the effect curcumin and resveratrol have on reducing Aβ42 toxicity. When incubated with Aβ42, both of these compounds lower the toxicity of Aβ42 oligomers to rat cortical neurons. Neuronal toxicity levels for Aβ42 coincubated with a 1:1 peptide: inhibitor ratio are close to that of both monomeric or fibrillar Aβ42. When incubated without inhibitors, Aβ42 showed a high level of toxicity after 6 – 10 hours. When incubated with inhibitors the levels of toxicity were significantly higher (two tailed students t-test values comparing the 6, 8 and 10 hour incubations returned p values less than 0.01).

Inhibitors prevent formation of large Aβ42 oligomers

<u>AFM shows that inhibitors prevent Aβ42 oligomer stacking</u>

In order to determine how the inhibitors affect assembly, and to determine which species they are stabilizing, AFM experiments were performed in the presence of inhibitors. AFM images of uninhibited Aβ42 show that after 6 hours the sample contains mostly (over 60% of the population) the taller dodecameric species (Figure 3.13, Figure 3.14). However when incubated for 6 hours with curcumin (in a 1:1 ratio) the sample contains mostly (over 90% of the

population) the shorter hexamers (Figure 4.3, Figure 4.4). The AFM and toxicity data presented in chapter 3 showed a correlation between the rise in the tall oligomer population and the increase in neuronal toxicity. Here we see that the inhibitor containing samples are stabilized as short oligomers, and exhibit lower toxicity to neurons. This indicates that the taller oligomers (or a species that forms from them) are the toxic species, and stabilizing the shorter oligomers is a means of attenuating toxicity. A two tailed students t-test comparing the height distributions of the samples with and without inhibitors found the differences in peak distribution to be significant (p values below 0.01).

SEC shows that inhibitors prevent Aβ42 oligomer association

In order to confirm that no larger species were forming in the presence of the inhibitors, samples were analyzed by SEC after incubation for 6 hours with or without inhibitors. The SEC profiles are shown in Figure 4.5. The sample incubated for 6 hours shows two peaks, eluting at 8 mL and 16 mL. We assigned these peaks to protofibrils and associated oligomers (8 mL) and monomers (16 mL) (see chapter 3). When incubated for 6 hours with curcumin, the component eluting at 8 mL was not observed. We attribute this to the loss of protofibrils and a decrease in oligomer association in the presence of curcumin.

Inhibitors prevent β – sheet formation

Changes in accessible hydrophobic regions and in β – sheet composition in the presence of curcumin were measured via ANS and thioflavin T fluorescence. As shown previously, ANS undergoes a shift in fluorescence after 6 hours of incubation with Aβ42 (Figure 3.19). When the Aβ42 samples are co–incubated with curcumin, this shift is not observed (Figure 4.6A). This lack of binding is not due to curcumin occupying the ANS binding site, since NMR experiments conducted with Aβ42 and bis-ANS, an ANS derivative containing two ANS molecules, showed

little interaction. Likewise, no changes in thioflavin T fluorescence were observed for curcumin coincubated Aβ42 samples, indicating that the accumulation of β – sheets in the Aβ42 peptides was halted in the presence of curcumin. The lack of shift in ANS fluorescence and absence of thioflavin T binding in the presence of curcumin are in agreement with the AFM data showing that curcumin caps the short oligomers and prevents their transition to the larger oligomers which seem responsible for ANS fluorescence and then go on to form protofibrils which bind thioflavin T.

To confirm that this sample remains stable in the presence of curcumin without any changes in secondary structure, IR measurements were made in the presence of curcumin over a 9 hour period (Figure 4.7). The sample remained unchanged over this time course, indicating that the secondary structure remained the same throughout the experiment. Additionally no changes in secondary structure were observed by ANS or IR when the sample was analyzed at 4 °C in the absence of curcumin, as would be expected for stable monomers (Figure 4.6B). This similarity of spectra under these two conditions indicates that the monomeric and early oligomeric Aβ42 have similar secondary structure compositions, and therefore appear similar by FTIR (Figure 3.18). It is only at later time points when larger oligomers and protofibrils have accumulated that changes in the spectra are observed.

Inhibitors do not dissolve Aβ42 oligomer into monomers

The similar structural features and fluorescence properties of Aβ42 co–incubated with curcumin and Aβ42 monomers stabilized at 4 °C suggested the possibility that the curcumin may stabilize monomeric Aβ42. This would prevent hexamer formation, and there would be no hexamers to stack to form dodecamers or protofibrils. The monomers and hexamers would look very similar by structural methods such as IR, and since neither should bind to the fluorescent

dyes, thioflavin T and ANS would not distinguish the two either. We therefore used NMR to measure the diffusion coefficient to the Aβ42 peptides coincubated with curcumin. If the curcumin stabilizes Aβ42 as a monomer, we should observe a monomeric diffusion coefficient at temperatures above 4 °C.

Diffusion coefficients were similar with and without curcumin when measured at 4 °C as expected. However when this sample was heated in order to begin aggregation (at 20 °C), there was a decrease in the ^{1}H NMR signal as seen with the uninhibited Aβ42 samples at 37 °C (Figure 4.8). Despite this loss in signal intensity, diffusion coefficients were still able to be measured (Table 4.1). Analysis of the diffusion coefficient reveals a gradual increase in the size of the NMR visible Aβ42 species over time (Table 4.2). The diffusion coefficient of Aβ42 is initially close to that of aprotinin, after 24 hours at 20 °C it has moved to midway between the 6 kDa and the 26 kDa standard. This and the loss of signal intensity indicate that curcumin does not arrest the assembly of monomers into a larger species.

Temperature	Water	200 uM α-Chymotrypsinogen A (25.7 kDa)	200 uM Aprotinin (6.5 kDa)	200 uM Aβ42 + curcumin
277	87.6 X10^{-11}	4.53 X10^{-11}	5.92 X10^{-11}	5.28 X10^{-11}
293	150 X10^{-11}	7.73 X10^{-11}	11.92 X10^{-11}	10–13 X10^{-11}
310	235 X10^{-11}	13.52 X10^{-11}	18.41 X10^{-11}	– – – – – –

Table 4.1 Diffusion coefficients for 200 μM Aβ42 + curcumin at 4 °C.
All diffusion coefficients are recorded in cm^2/s.

Hours at 20 ºC (start – end)	0:25 – 2:45	2:45 – 5:15	5:15 – 8:00	20:40 – 23:10
Diffusion Coefficient	12.6 X10^{-11}	10.8 X10^{-11}	10.5 X10^{-11}	9.96 X10^{-11}

Table 4.2 Diffusion coefficients for 200 μM Aβ42 + curcumin at 20 °C.
All diffusion coefficients are recorded in cm^2/s.

In order to fully determine if the curcumin stabilized the monomeric or hexameric oligomer state, the diffusion experiments were conducted at 37 °C. At this temperature the ^{1}H

NMR signal decreased at a rate too rapid for the diffusion coefficient to be measured. The ^{1}H signal loss was less than that of the uninhibited Aβ42 samples at 37 °C.

The loss of NMR signal in the presence of curcumin indicates that the curcumin is not stabilizing the monomeric Aβ42 peptides, because they are still assembling into a larger NMR invisible species. However, SEC profiles of Aβ42 samples incubated with curcumin at 37 °C show very little of the sample elutes as the larger 8 mL peak (4% of the total area or less) (Figure 4.5). This would imply that the larger NMR invisible species (presumably a hexamer) is eluting in the 17 mL peak of the SEC column, despite radius estimates based on standards predicting it would elute at 8 mL. The coelution of monomers and small oligomers in the same SEC peak has previously been observed by Chromy *et al*. (74). In their experiments the later eluting peak contained both monomers and tetramers when analyzed by native gels (74). The species in the later eluting peak did not bind to neurons, suggesting they were in a non-toxic conformation (74).

Harmeier *et al.* (100) recently presented a similar analysis of SEC fractions of Aβ42. Their SEC results for wild type Aβ42 showed two peaks, one corresponding to hexamers and one corresponding to larger oligomeric species. By mutating Gly33 to alanine they were able to shift the chromatographic band containing oligomers to longer elution times corresponding to monomers. Other mutations encouraged the formation of larger species as shown by an increase in the earlier eluting peak. Like the wild type spectra observed by Harmeier *et al.*, *w*e do not see a separate peak for monomers, indicative that the monomers and hexamers coelute. We also do not see a separate monomer peak even upon the addition of curcumin that indicates that curcumin shifts the high MW oligomers into low MW oligomers, but not into monomers.

NMR reveals a common region of inhibitor binding to Aβ42

In order to investigate the region where the inhibitors bind to the Aβ42, $^{1}H - ^{15}N$ HSQC experiments were carried out on ^{15}N labeled Aβ42 peptides. Each amide proton in the Aβ42 peptide will have a unique peak. If the chemical environment around a proton changes, such as binding to an inhibitor, the peak will shift to a new resonance in the spectra. By observing any changes between the spectra of the Aβ42 peptide alone, and of the peptide with inhibitors, we can determine the binding region of the inhibitor. The assigned spectra of the monomeric Aβ42 is based on assignments in reference (62). When curcumin is added to the peptide, changes in peaks at the N–terminal and central regions of the peptide are observed (Figure 4.9). The other peaks in the spectra do not shift, indicating that the binding is only to certain regions of the peptide, which implies that the binding is localized to these regions. A lack of changes in the C–terminal region is consistent with other data collected by our lab and others that show the last 5 residues of the Aβ42 sequence have very little accessibility (Figure 3.5). Specific residues for which large chemical shift changes were observed are Glu3, Arg5, Ser8, Tyr10, Gln15, Lys16, Leu17 and Phe20. When resveratrol is added to the Aβ42, similar changes in chemical shift are observed, with a strong shift at Arg5, Gln15, Leu17 and Phe20 being common in both (Figure 4.10 and Figure 4.12).

In order to confirm that the observed spectral changes were not simply due to the addition of any compound to the Aβ42 sample, thioflavin T was employed as a negative control. We have previously shown (Figure 3.8) that thioflavin T spectra show no increases in fluorescence when added to Aβ42 monomers, or low molecular weight oligomers. This data is consistent with reports that thioflavin T only binds to protofibrils and fibrils (76, 77). Thioflavin T has been used as a negative control for aggregation studies in the past, and has been shown to have no

inhibitory effect on Aβ42 aggregation (78). As expected, when thioflavin T is added to Aβ42 monomers, there are no changes in the HSQC spectra (Figure 4.11).

Since the NMR visible form of Aβ42 has been shown to be monomeric, this implies that the inhibitors are binding to monomeric Aβ42. The diffusion data for Aβ42 incubated with curcumin shows that, at temperatures above 4 °C, in the presence of the inhibitors, monomeric Aβ42 is still able to assemble into NMR invisible, large molecular weight species. This indicates that while the inhibitors are binding to Aβ42 monomers, they are not stabilizing Aβ42 in a monomeric state. The other experimental data presented here shows that these inhibitors block the formation of large oligomers and protofibrils, but cannot say if they do this by stabilizing monomers or hexamers. Through analysis of the NMR data we can show that there still is a monomer to hexamer transition in the presence of curcumin. By showing this transition still occurs, and showing the lack of dodecamers and toxicity, we can make a stronger point that the inhibitors are blocking the hexamer to dodecamer transition.

The AFM, SEC and NMR data indicate that these inhibitors seem to cap the Aβ42 oligomers as hexamers, by binding and preventing the stacking of hexamers into dodecamers. In the presence of these inhibitors, monomers are still able to associate into hexamers. This stabilizing of hexamers correlates with the decrease in neuronal toxicity, which we previously associated with an increase in dodecamer population. These results are in agreement with those of Li *et al.* (101), who observed reduced toxicity when they stabilized small oligomers (with a hydrodynamic radius of 8-12 nm) reduced toxicity, compared to increased toxicity in the presence of larger oligomers with a radius of 20-60 nm. The ability to inhibit dodecamer assembly but not the formation of smaller oligomers was also observed by Gazit and coworkers

whose peptide inhibitors abolished the 56 kDa Aβ42 species but had no effect on the 18 kDa Aβ42 species (102). These sizes roughly correspond to the low MW and high MW oligomers described above.

Binding of GSM inhibitors to Aβ42

In order to see if the results obtained for the inhibitors curcumin and resveratrol applied to other inhibitors of Aβ42 aggregation, we looked at the HSQC spectra of Aβ42 with other inhibitors. The peptide inhibitor I21 is a second generation of inhibitors that were designed by our lab on the basis of structural studies of Aβ42. These peptide inhibitors were designed to bind in the grooves created by a GxxxG motif in the C–terminus of fibrillar Aβ42 once the fibrils have assembled into a parallel and in–register orientation (50). We found that these peptide inhibitors bound to oligomeric Aβ42 and prevented the conversion of oligomers to fibrils (50, 60). I21 is a modification of the original I1 peptide where the two phenylalanines were replaced with tryptophan, and the two glycines replaced with serine in order to increase solubility. When added to Aβ42 monomers at 4 °C the HSQC spectra shows similar shifts as with curcumin and resveratrol, namely at Arg5, Gln15, and Phe20 (Figure 4.12). This similarity in binding is consistent with their similar mechanisms of inhibition, as I21 has also been shown to cap Aβ42 as small oligomers (60). The common mechanism of binding to Aβ42 observed between these compounds could be the result of their similar structures. All three compounds contain phenol rings, and furthermore the ring separation of I21 and curcumin is similar. Previous work by Gestwicki and Reinke determined that the ring separation in curcumin was at the optimum distance for most effective inhibition of aggregation (94). The existence of a second compound with similar ring spacing which also inhibits Aβ42 validates this observation.

Several studies have investigated the interaction of small molecule inhibitors with Aβ40 and Aβ42. Galanakis *et al.* noted a possible binding region between His13 and Phe20 of Aβ40 when looking at interactions between Aβ40 and two antioxidants (oleuropein and melatonin) (103). Gazit and coworkers also noted changes in chemical shifts for Phe20 upon addition of inhibitor to an Aβ12-28 fragment which also blocks dodecamer formation (102). The common targeting of the aromatic core of Aβ42 by inhibitors could explain their mechanism of action. It has been suggested that π-stacking involving Phe19 and Phe20 could mediate the assembly of Aβ42 peptides into oligomers and fibrils (104, 105). The aromatic groups of small molecule and peptide inhibitors may disrupt these aromatic π-stacking interactions and block assembly (for review see refs. (47, 104)). In our experiments, the large changes in the chemical shifts of Arg5 and Phe20, but not at Phe19, upon inhibitor binding suggest that cation-π, rather than the π-π, interactions mentioned above, mediate the formation of Aβ42 oligomers and are disrupted by inhibitor binding.

We also looked at the interaction of Aβ42 with gamma secretase modulating compounds which have also been shown to interact with Aβ42. Sulindac sulfide is a gamma secretase modulator that has been shown to bind to Aβ and inhibit fibrillization (106). In addition to its anti-aggregation properties, it also affects cleavage of APP resulting in reduced Aβ production (107). Previous work by Richter showed changes in the C–terminus of Aβ42 when bound to sulindac sulfide (107). They also looked at the effect of indomethacin, another GSM, with similar results as sulindac sulfide. Under our conditions, when either of these compounds is mixed with Aβ42 the resulting HSQC spectra here showed little binding to the peptide. Some minor binding was observed at the C–terminus (Figure 4.13A,B). This could be due to the

different concentrations used in our experiments. Since these compounds showed little activity for Aβ42, their ability to cap the oligomers by AFM was investigated. When incubated for 6 hours with Aβ42, these drugs showed little capping ability (Figure 4.13C,D). This lack of capping and lack of N–terminal binding indicates that it is the ability to bind to the central portion of the Aβ42 monomers that is important for capping the oligomers as 2 nm tall hexamers. Conversely, inhibitors that bind at the C–terminus, such as indomethacin and sulindac sulfide, have a different mechanism of reducing Aβ42 toxicity, such as by modulating the production of Aβ42 from APP.

The strong chemical shift changes at Arg5 and Phe20 in the presence of inhibitors such as curcumin and resveratrol is noteworthy when looked at in the context of mutations in the Aβ42 sequence. Mutations to residues 6, 7, 22, and 23 all increase the rate of fibril formation. H6R and D7N are familial mutations which increase the positive charge of the N-terminus, and accelerate fibril formation (108, 109). Since these mutations do not seem to increase the amount of protofibrils, indicating that they instead drive the conversion of protofibrils into fibrils (108). The random coil to β-sheet transition was also faster in these mutants (109). If the typical lag in fibril formation is due to conversion of oligomers into protofibrils, this would indicate that a weakly charged N-terminus is important for oligomer stability. As the N-terminus becomes more positive (by H6R or D7N mutations), the stability of the oligomers decreases (or protofibril stability increases). Our NMR data shows that curcumin interacts with this region, which means that it probably stabilizes the charges and keeps the Aβ peptides in an oligomeric state. The other mutations which increase Aβ aggregation also affect the charge of the peptide. The Dutch (E22Q) and Iowa (D23N) mutations both replace a negative charge with a neutral residue. Since

this loss of charge increases the rate at which fibrils form, the negative charges must stabilize the monomers and oligomers.

In addition to strong shifts at the N-terminus of the peptide, Phe20 also shows large changes in chemical shift upon inhibitor binding. A F20A substituted Aβ42 peptide was found to aggregate at a slower rate, remaining in the protofibril stage while the wild type had formed extensive fibrils (110). Since little differences were seen in secondary structure by CD or toxicity by MTT, this mutation may reduce oligomer stability which slows monomer association, reducing toxicity and aggregation. Alanine scans by Williams *et al.* also showed a strong destabilization of fibrils by F20A (111).

A recent solution NMR structure of Aβ40 monomers contains an α-helix spanning residues 13 to 23 (112). The residues which show strong changes in chemical shift upon addition of curcumin or resveratrol are in proximity in this structure (Figure 4.14), so it is consistent with our NMR data of Aβ42 monomers. This region is also important for fibril stability, as alanine substitutions at residues 15-21 (especially at 18-20) all destabilize fibrils (111).

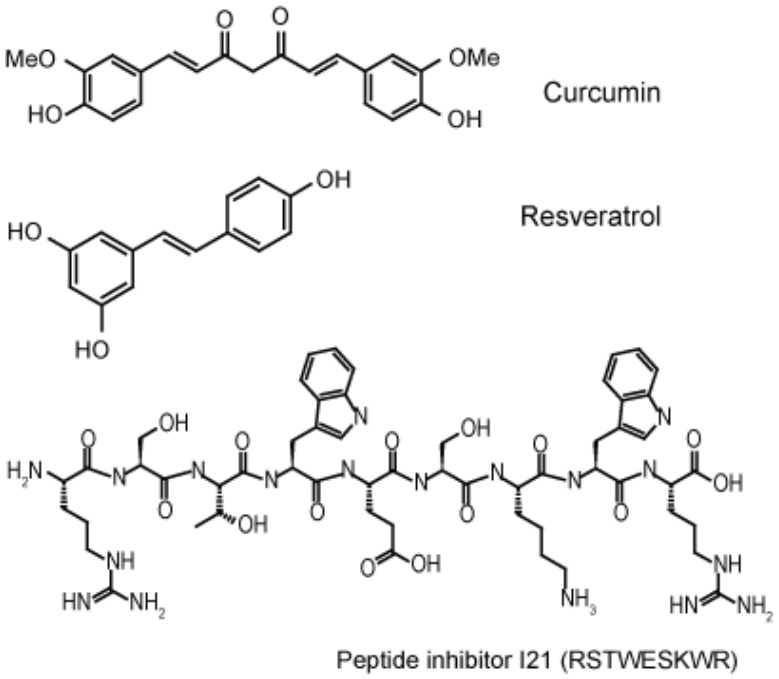

Figure 4.1 Chemical structures of the investigated inhibitors.

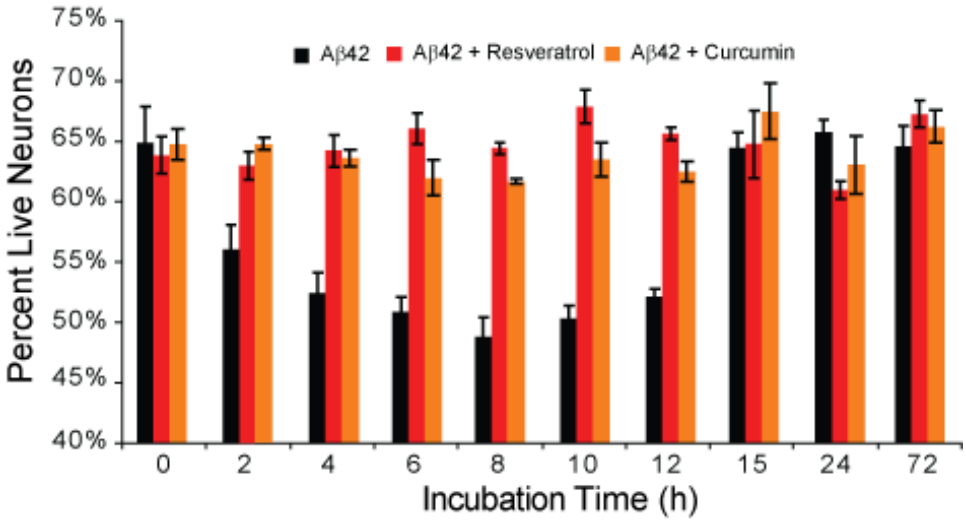

Figure 4.2 Neuronal toxicity of Aβ42 incubated in the presence of curcumin and resveratrol. 200 μM Aβ42 was incubated at 37 °C for 0 – 72 hours with or without inhibitors (Aβ: inhibitor ratio of 1:1). The Aβ42 peptides were diluted into neuronal cultures (12 μM final concentration) and incubated an additional 48 hours before viability was assayed. The samples incubated with curcumin or resveratrol exhibited lower toxicity than the Aβ42 peptides alone (p value for differences at 6, 8, and 10 hours was < 0.01).

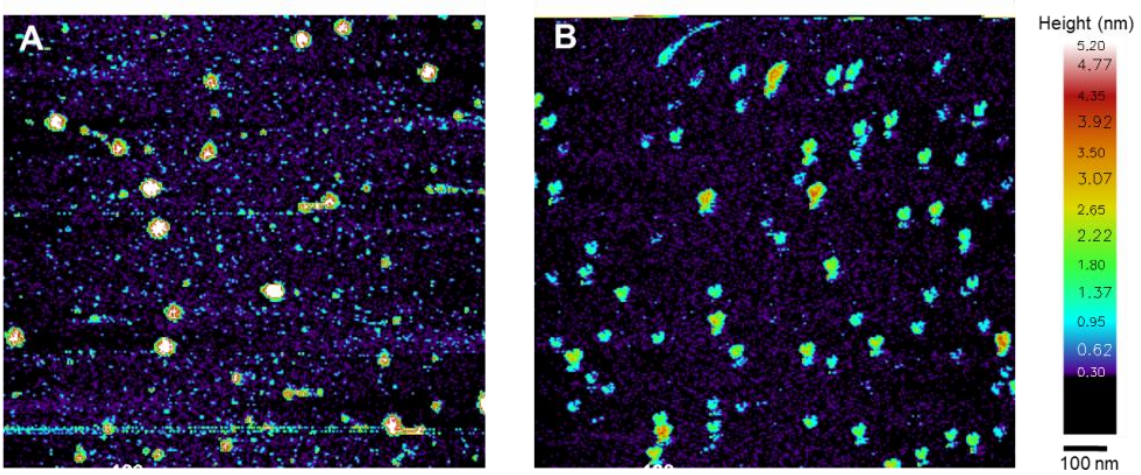

Figure 4.3 AFM images of Aβ42 + curcumin.
A) Aβ42 alone after 6 hours of incubation.
B) Aβ42 + curcumin after 6 hours of incubation.
200 μM Aβ42 was incubated at 37 °C for 6 hours with or without curcumin (Aβ: inhibitor ratio of 1:1). Samples were diluted to 1 μM for AFM imaging. The samples incubated with curcumin contained more of the short oligomers compared to the Aβ42 peptides alone.

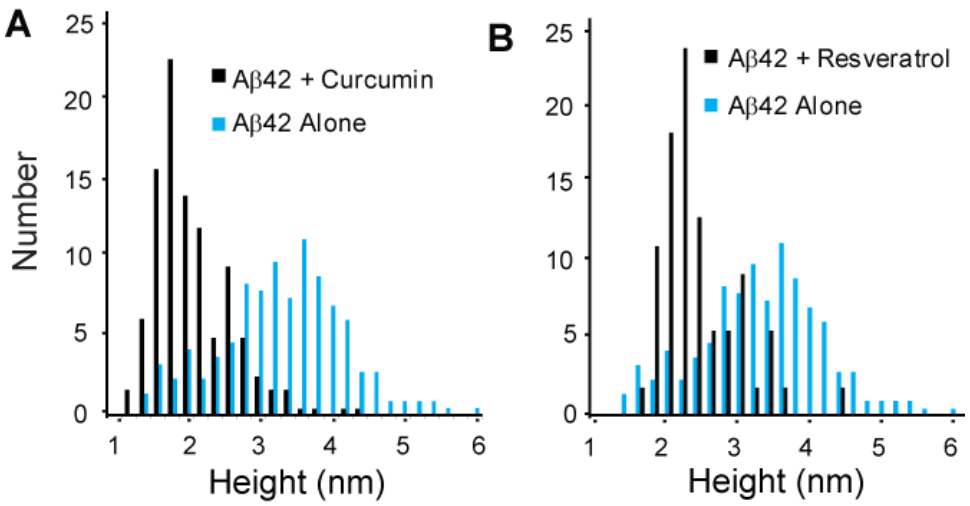

Figure 4.4 AFM histograms of Aβ42 with inhibitors.
A) Height histogram of Aβ42 with or without curcumin after 6 hours of incubation at 37°C.
B) Height histogram of Aβ42 with or without resveratrol after 6 hours of incubation at 37°C.
200 μM Aβ42 was incubated at 37 °C for 6 hours with or without curcumin (Aβ: inhibitor ratio of 1:1). Samples were diluted to 1 μM for AFM imaging. Histograms were generated from height analysis of the samples. The samples incubated with curcumin contained more of the shorter oligomers compared to the Aβ42 peptides alone (p value for differences at < 0.01).

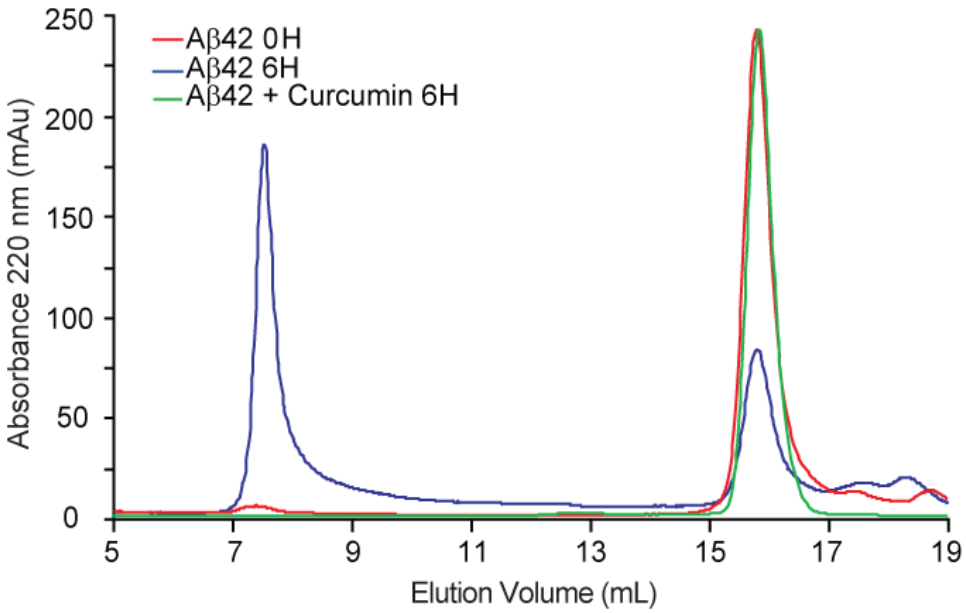

Figure 4.5 SEC profile of Aβ42 incubated 6 hours with and without curcumin.
200 μM Aβ42 was incubated at 37 °C for 0, 6 hours with or without curcumin (Aβ: inhibitor ratio of 1:1). The samples were injected into a Superdex 200 column for SEC analysis. When incubated for 6 hours, a large species eluting at 7 mL is observed only in the samples without curcumin (blue line). The curcumin containing samples (green line) have an elution profile similar to that of the freshly prepared sample (red line), indicating curcumin slows the formation of large aggregates.

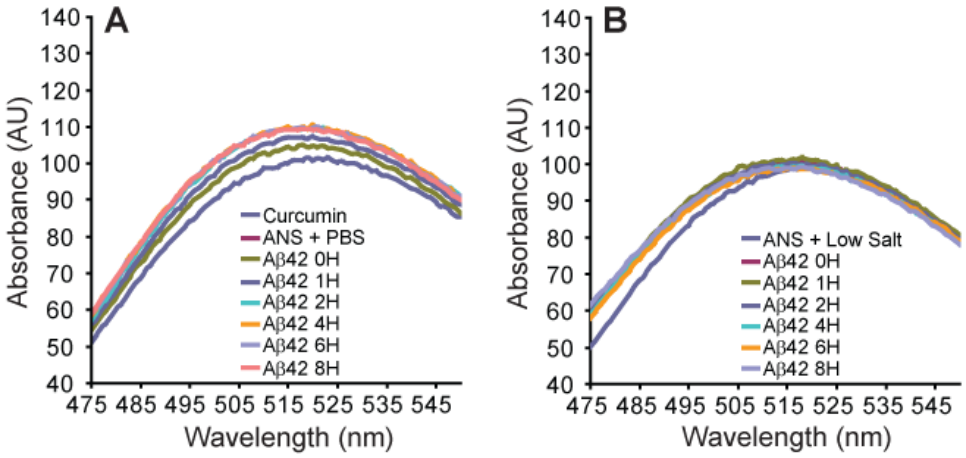

Figure 4.6 ANS fluorescence spectra of Aβ42 coincubated with curcumin.
A) ANS fluorescence spectra of Aβ42 coincubated with curcumin at 37 °C.
B) ANS fluorescence spectra of Aβ42 alone at 4 °C.
Fluorescence spectra of Aβ42 mixed with ANS. 200 μM Aβ42 was incubated at 37 °C for 0 – 8 hours with or without curcumin (Aβ: inhibitor ratio of 1:1), then mixed with ANS for a final ratio of 4.5 :1 ANS: peptide. The samples were excited at 349 nm and emisson spectra from 475 to 550 nm were collected. In both the presence of curcumin, or when maintained at 4 °C, there is no increase in flouerscene, indicating that curcumin prevents the formation of the Aβ42 species with increased hydrophobicity.

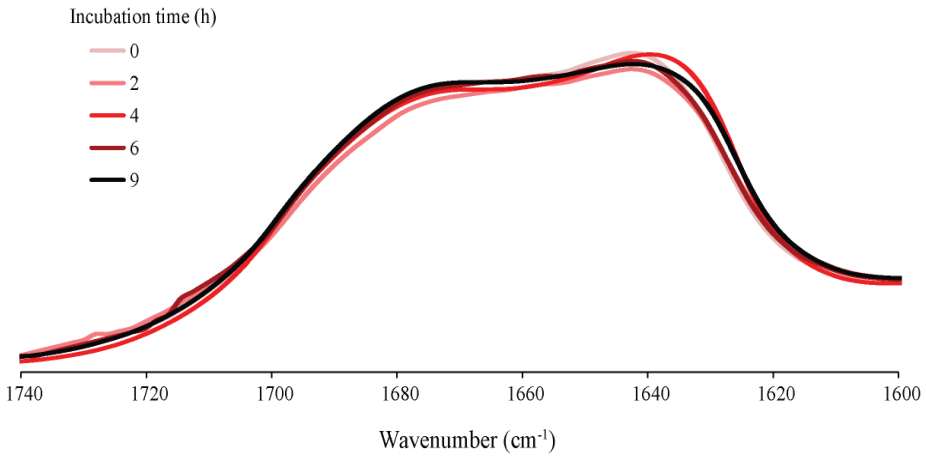

Figure 4.7 IR spectra of Aβ42 coincubated with curcumin.
FTIR spectra of a 200 µM Aβ42 + curcumin (1:1) solution prepared at 4 °C and then incubated at 37 °C for 9 hours. The region of the spectra spanning 1740 to 1600 cm^{-1} is shown. The spectra show little change over this time, and lack that increase in β – sheet character observed in samples without curcumin, indicating that curcumin prevents changes in structure associated with protofibril formation.

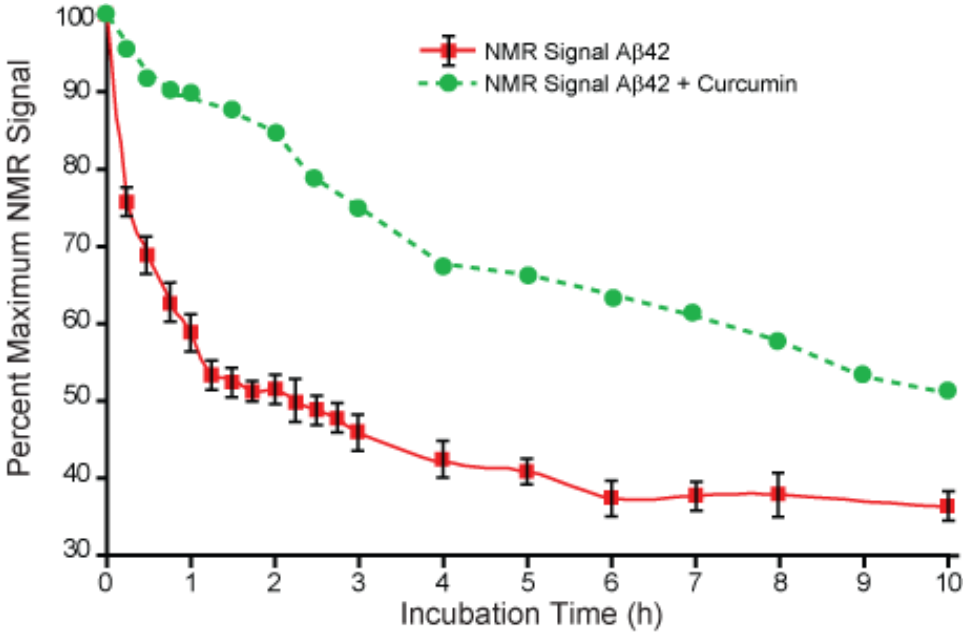

Figure 4.8 NMR signal decay of Aβ42 coincubated with curcumin.
Integrated signal intensity from the 0.15 to 1.15 ppm region of the ^{1}H NMR spectra of a 200 μM Aβ42 solution collected every 15 minutes at 37 °C. Samples with (green) and without (red) curcumin both show that a decrease in signal intensity occurs over time, however the sample without curcumin exibits a faster decay. The loss of NMR signal in the presence of curcumin indicates that curcmin does not prevent the assembly of monomers into oligomers.

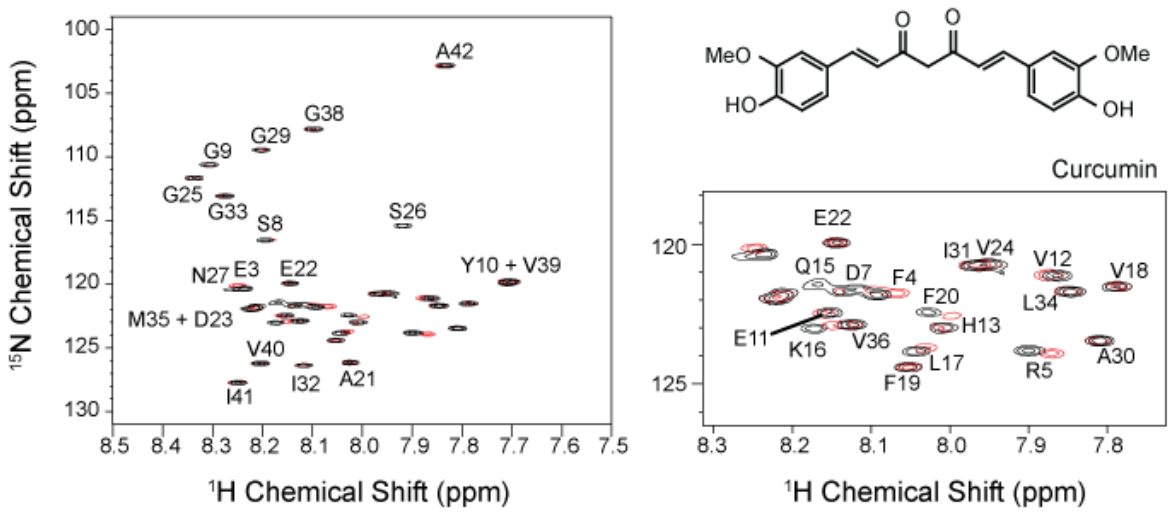

Figure 4.9 HSQC NMR spectra of Aβ42 coincubated with curcumin.
^{1}H – ^{15}N HSQC spectra of 200 µM ^{15}N labeled Aβ42 peptides alone (black) or with curcumin (1:1) (red). Samples were prepared and spectra were recorded at 4 °C. Large changes in chemical shift changes were observed at Arg5 and Phe20, indicating that curcumin is binding near these residues.

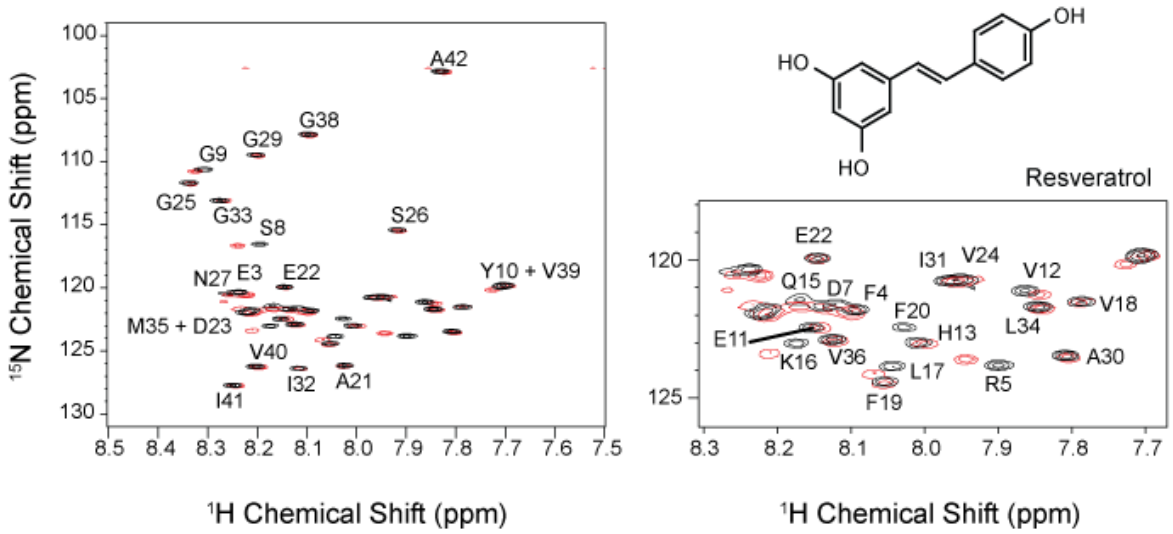

Figure 4.10 HSQC NMR spectra of Aβ42 coincubated with resveratrol.
^{1}H – ^{15}N HSQC spectra of 200 µM ^{15}N labeled Aβ42 peptides alone (black) or with resveratrol (1:1) (red). Samples were prepared and spectra were recorded at 4 °C. Large changes in chemical shift changes were observed at Arg5, Lys16 and Phe20, indicating that resveratrol binds near these residues.

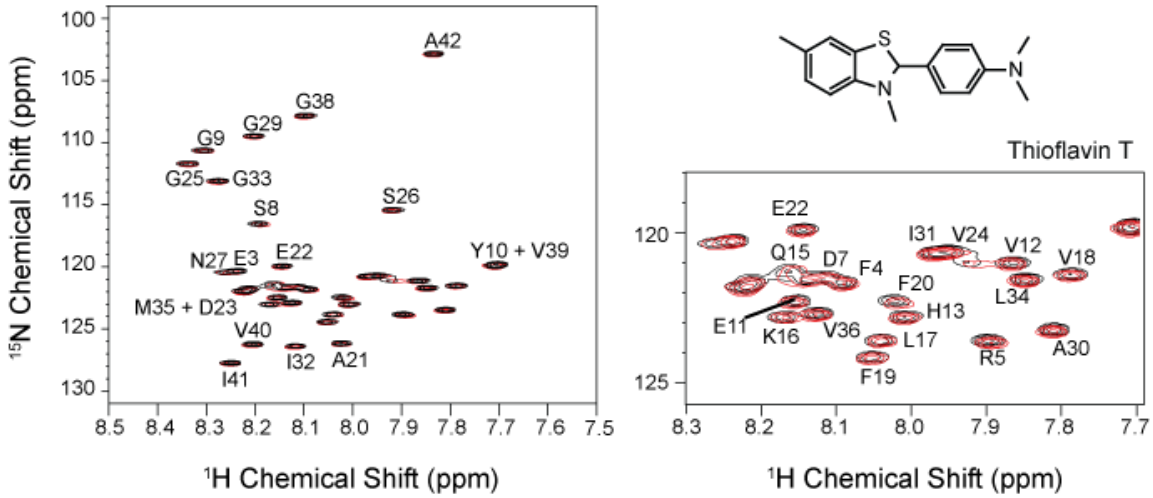

Figure 4.11 HSQC NMR spectra of Aβ42 coincubated with thioflavin T.
^{1}H – ^{15}N HSQC spectra of 200 µM ^{15}N labeled Aβ42 peptides alone (black) or with thioflavin T (1:1) (red). Samples were prepared and spectra were recorded at 4 °C. No changes were observed in the thioflavin T containing samples, consistent with no interaction between thioflavin T and monomeric Aβ42.

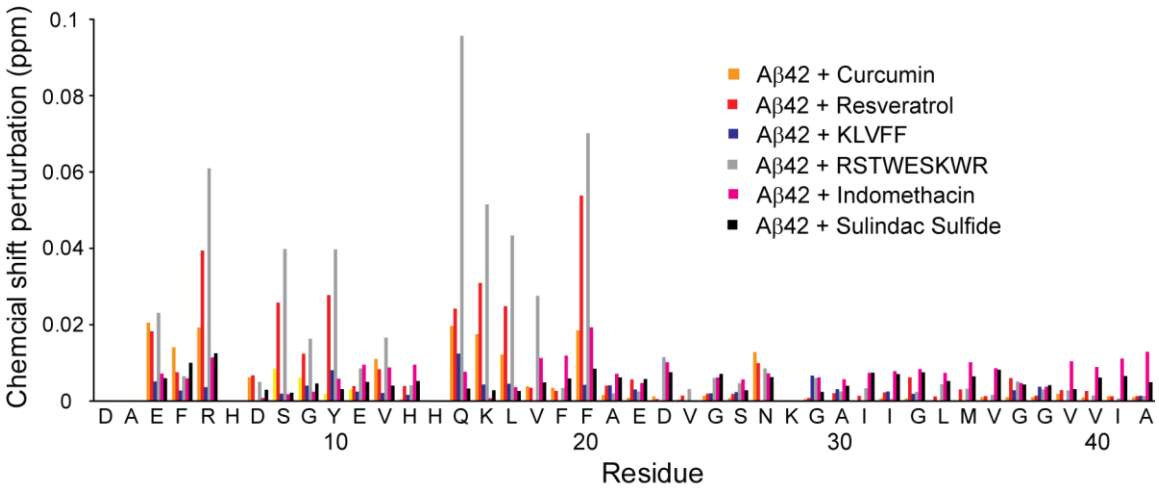

Figure 4.12 Histogram of peak shifts in HSQC NMR spectra for of Aβ42 coincubated with inhibitors.

Chemical shifts calculated using equation in (113). Both curcumin and resveratrol induce large changes in chemical shift at Arg5, Gln15 and Phe20. These similarities in binding to Aβ42 as well as similar height profiles by AFM implies that these two inhibitors share a common mechanism.

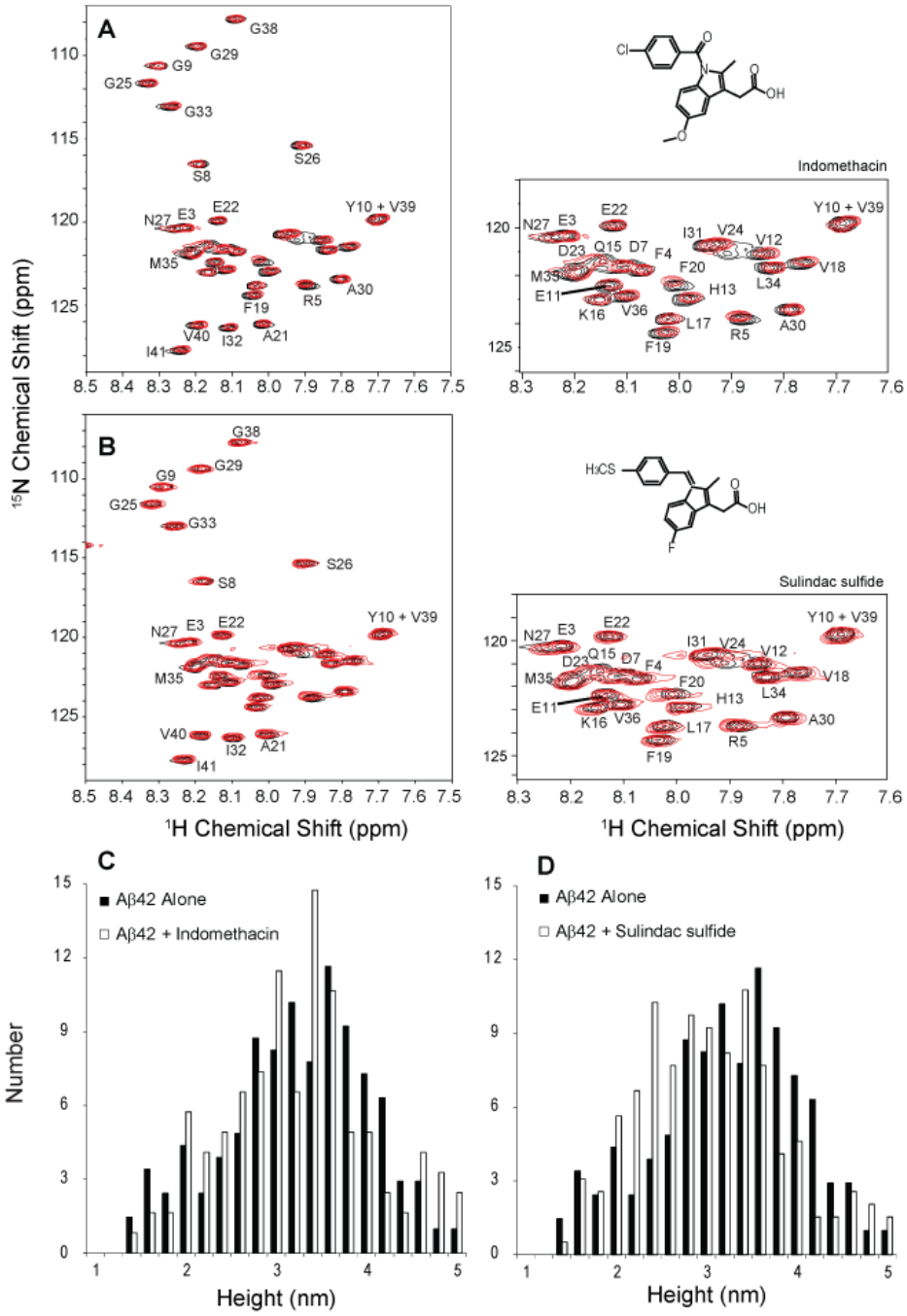

Figure 4.13 NMR of gamma secretase modulators and AFM histograms.
A) ^{1}H – ^{15}N HSQC spectra of 200 µM ^{15}N labeled Aβ42 peptides alone (black) or with indomethacin T (1:1) (red). Samples were prepared and spectra were recorded at 4 °C. Few changes were observed in the indomethacin containing samples, with only minor binding at the C-terminus.
B) ^{1}H – ^{15}N HSQC spectra of 200 µM ^{15}N labeled Aβ42 peptides alone (black) or with sulindac sulfide T (1:1) (red). Samples were prepared and spectra were recorded at 4 °C. Few changes were observed in the sulindac sulfide containing samples, with only minor binding at the C-terminus.

C) AFM histogram of Aβ42 incubated 6 hours with and without indomethacin.
D) AFM histogram of Aβ42 incubated 6 hours with and without sulindac sulfide.
Unlike the curcumin and resveratrol, $^{1}H - ^{15}N$ HSQC spectra of 200 μM ^{15}N labeled Aβ42 peptides alone (black) or indomethacin and sulindac sulfide (red) showed few changes. Additionally, these compounds were shown by AFM to have little effect on the heights of Aβ42 oligomers. Together these results indicate that GSMs influence Aβ42 by a different mechanism.

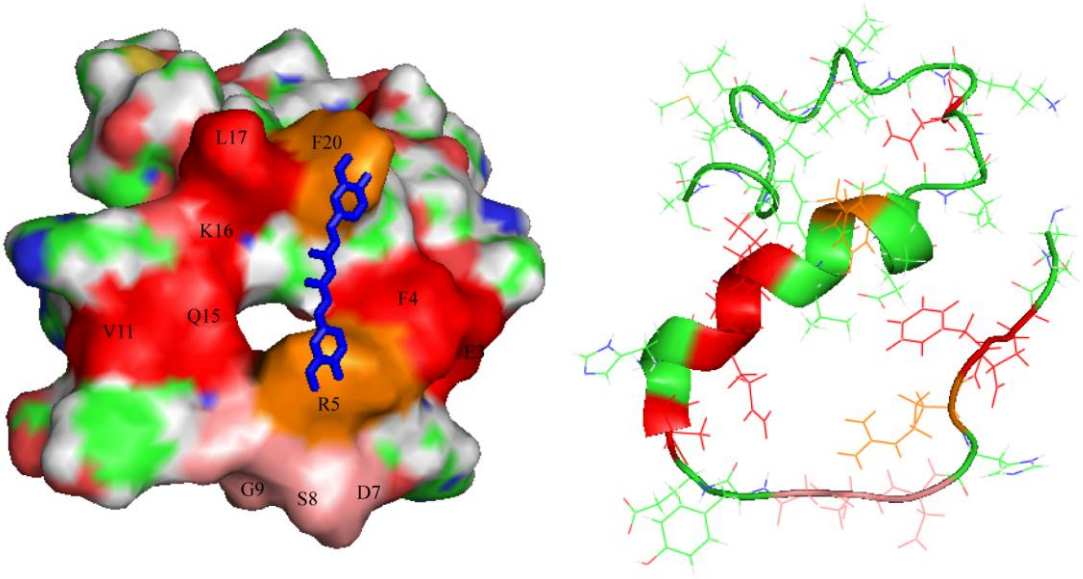

Figure 4.14 Solution NMR structure of Aβ40 monomer.
Coordinates taken from 2LFM PDB published in reference (112). Residues which exhibit chemical shift changes in the presence of curcumin are shown in pink (weak: Asp7, Ser8, Gly9), red (strong: Glu3, Phe5, Val12, Gln15, Lys16, Leu17) and orange (strongest: Arg5, Phe20). A curcumin molecule (blue) is overlaid to demonstrate that all of these residues are in a similar region, and thus this proposed structure is in agreement with our model for monomer folding.

Chapter 5 – Fibrils

While both Aβ40 and Aβ42 peptides are produced in the brain, plaques in AD patients are comprised mostly of Aβ42 (7), which is more toxic than Aβ40 and is considered to be the primary toxic species of AD (11, 114). While Aβ40 and Aβ42 only differ in length by two amino acids, recent studies on the structure of the oligomers of Aβ40 and Aβ42 show differences in both their structure and composition (31-34). Peptides of both Aβ40 and Aβ42, fold into a β-strand-turn-β-strand (β-turn-β) motif. A mixture of Aβ40 and Aβ42 may be the causative agent *in vivo*, since the ratio of Aβ40 to Aβ42 that is produced by processing by γ-secretase is roughly 9:1 (115), whereas the ratio of Aβ40 to Aβ42 in the plaques of AD patients is roughly 1:4 (7, 8). A mixture of these two species of Aβ peptide was shown by Kuperstein *et al.* (116) to be more toxic than Aβ42 alone. An increase in the Aβ42: Aβ40 ratio stabilizes toxic oligomeric species with a maximum toxicity at a 3:7 ratio (116) indicating that the two peptides may form mixed fibrils.

Since the two Aβ peptides differ in sequence only at the two C-terminal amino acids, it is most likely that this region is responsible for the differences in toxicity of the two Aβ peptides. Early studies on amyloid self-assembly found a binding site corresponding to the C-terminus of Aβ40 (117). Additionally, a recent clinical study has shown that a V40G mutation in Chinese/Taiwanese patients results in an early onset form of AD, which indicates the importance of the C-terminus in AD (118).

The length of the C-terminus has previously been shown to affect the rate of aggregation of Aβ peptides (10). The addition of two amino acids greatly increases the speed of Aβ42 aggregation compared to Aβ40. Additionally, Lim and coworkers found that NOE values

observed from ^{1}H-^{15}N Nuclear Overhauser Effect (NOE) experiments were more negative at the C-terminus of Aβ40 monomers than Aβ42 monomers indicating that Aβ42 is more structured and less flexible than Aβ40 (119). Many groups have looked at how mutations to the C-terminus affect the oligomer distribution of Aβ42 to determine how these last two residues affect aggregation.

It is thought that the hydrophobicity of the C-terminus is the driving factor in Aβ42 aggregation. This notion is supported by a mutational study by Kim and Hecht that demonstrated that the presence of hydrophobic residues, rather than a specific sequence, was the only requirement for Aβ42 aggregation, as hydrophobic-to-hydrophobic mutations maintain their aggregation rates (120). Bitan and Teplow used photo-induced cross-linking to look at oligomer distributions of various mutants and found that mutations I41G, I41A, I41V, I41L all shifted the oligomer distribution to one similar to Aβ40, with longer side chains causing a distribution more similar to Aβ42 (121). The conclusion can be drawn that the side chain size of residue 41 plays an important role in the early association and aggregation of the Aβ monomers (121). A similar effect was seen with substitutions of residue 42, leading to the conclusion that the hydrophobic interaction of the side chains is important for assembly into larger order oligomers because less hydrophobic substitutions remained small (121). Together these results emphasize the importance of the C-terminus and its role in toxicity of Aβ42 oligomers and fibrils.

Previous measurements of solvent exposure of Aβ42 fibrils using H/D exchange have revealed that the fibrils have two protected regions spanning residues 11-25 and 28-42 (122). These results also show a slight increase in solvent exposure at Gly38. This could be due to a turn at this region that would make the turn slightly more solvent exposed. Such a turn at Gly37,

Gly38 corresponds with scanning proline mutagenesis studies by Morimoto *et al.* (123). Proline substitutions favor turns over β-sheets, so the increase in aggregation rate of Aβ42 G38P indicates that there is a turn around Gly38 in Aβ42 fibrils (123). A mutation of Gly37 to leucine results in increased fibrillization rates but loss of toxicity (124). The C-terminus in fully formed Aβ42 fibrils was chosen for investigation based on its previously demonstrated importance in fibrillization.

There are two models of the Aβ42 C-terminus, one containing a bend at Gly37/38 which places Met35 in contact with Ala42 (123, 125) and a second where Met35 and Ala42 are part of a continuous β-sheet (34). An additional model has been proposed for Aβ40 where three peptides are arranged in a symmetric triangle with each Met35 in contact with the other Met35 residues (66). While all of these models include a β-turn-β structure, the position of Met35 is different in each model. Since Met35 is believed to play a role in Aβ42 toxicity, we wished to determine which model most closely matched our fibrils. To test these three models, Aβ42 peptides with ^{13}C labels at Ala42 ($^{13}C_1$), Met35 ($^{13}C_\varepsilon$), (Gly38 $^{13}C_\alpha$) and Phe19 ($^{13}C_r$) were synthesized. NMR spectra of this peptide (Figure 5.1A black line) showed splitting of the Met35 peak, which is indicative of two fibril conformations present in the sample. Conversely, the NMR spectra of oligomers do not show this splitting (Figure 5.1A red line), indicating that this phenomenon is exhibited only by fibrils.

Fibril structure of Aβ42 contains two conformations

Solid-state NMR studies of Aβ fibrils have previously looked at the disparity in the two fibril structures as seen by EM, which were believed to be due to two distinct fibril conformations (66). Other studies have proposed models with peptides in a β-turn-β structure

with fibrils comprised of one or two rows of these β-turn-β peptides (35, 126). The observed splitting in the NMR spectra (Figure 5.1A) indicates the presence of either one single homogenous fibril type with two conformations of Met35, or a heterogeneous mixture of two different types of fibrils. To investigate the possibility of a homogenous mixture, seeded fibrils were grown following the procedure devised by Tycko (65, 66). 12 generations were grown under sonicated conditions and used to seed fibrils that were grown stagnantly for 12 days. When directly compared, a sharpening of the peaks in the seeded fibrils was observed, corresponding to a more clearly resolved spectra in comparison to that of the unseeded fibrils (Figure 5.1B). The reduction in line width in the seeded fibrils indicates seeding produces samples that are more uniform in structure. The persistence of the splitting suggests two distinct conformations of Met35 in the seeded samples and the decrease in line width indicates that the splitting is due to a homogenous fibril.

Conformations are parallel and in-register

We had previously shown using $^{13}C - ^{13}C$ solid-state DARR NMR measurements of specifically labeled Aβ42 peptides that Aβ42 fibrils are arranged in a parallel and in-register orientation (36). In order to determine if the seeded peptides also are parallel and in-register we examined the crosspeaks between an equimolar mixture of two peptides, one labeled at Gly33 ($^{13}C_\alpha$), Ala21 ($^{13}C_1$) and a peptide labeled at Ala21 ($^{13}C_\alpha$), Gly33 ($^{13}C_1$). For seeded Aβ42 fibrils in a parallel and in-register orientation, neighboring Gly33 residues should be close enough (within 6 Å) that the Gly33 $^{13}C_\alpha$ of one peptide will be close enough to Gly33 $^{13}C_1$ of another peptide that a crosspeak is observed. These crosspeaks between Gly33 and Gly33 or Ala21 and Ala21 will only occur if the two residues are in a parallel and in-register orientation as we have previously shown (36). These crosspeaks were observed (Figure 5.2), indicating that despite the

two different conformations of Met35, the seeded fibrils adopt a parallel and in-register orientation. A second crosspeak was also observed between Gly33 and Ala21, indicating that these residues are in proximity in our fibrils. We have previously demonstrated a contact between Phe19 and Leu34 in fibrils (36), this contact between Gly33 and Ala21 would be possible based on this contact.

Side chain packing arrangement in the hydrophobic core

As we have previously shown that Aβ42 fibrils and oligomers adopt a β-turn-β structure with contacts between Phe19 and Leu34 (36), the presence of this contact was probed for in the seeded fibrils. As seen in Figure 5.3A, this contact was present in the seeded fibrils. Due to overlap between $^{13}C_{\beta}$ of Leu34 with $^{13}C_{\alpha}$ of Gly38 in samples containing uniformly labeled Leu34, we also investigated the Phe19-Leu34 contact in a peptide containing singly labeled ($^{13}C_{\alpha}$) Leu34 (Figure 5.3B) and the Phe19-Gly38 contact in a peptide lacking labels at Leu34 (Figure 5.3C). No crosspeak was seen between Phe19 and Gly38, indicating that the β-turn-β structure places Phe19 and Leu34 in contact, but not Phe19 and Gly38 (Figure 5.3C). The current model for Aβ42 fibrils based on mutational data by Riek and coauthors suggested that Phe19 and Gly38 are in contact, while the NMR structure proposed by Robert Tycko for Aβ40 fibrils suggested that Phe19 was instead in contact with Leu34. The NMR data presented in Figure 5.3C indicates that our fibrils more closely match the structure proposed for Aβ40.

A bend at Gly37 puts Met35 in contact with Gly38

One of the striking features about the NMR spectra of Met35 is the strong presence of a crosspeak between one of the Met35 components and Gly38 (Figure 5.4A). In contrast, the second Met35 component does not have this crosspeak (Figure 5.4A). The presence of a

crosspeak between Gly38 and Met35 is indicative that the C-terminus does not form a flat β-sheet, but rather there is a bend at Gly37/38 allowing Met35 to be in close proximity to Gly38. If residues Met35 through Gly38 are in a β-sheet, the distance between the Met35 side chain and Gly38 is too great for a crosspeak to be observable by NMR. The presence of a crosspeak indicates that there must be a turn to place these residues within the 6Å distance needed to be seen by NMR.

Further evidence of such a bend was observed by looking for an interaction between Gly38 and Gln15. If the two β-sheets of the peptide are parallel and unbent, it would be expected that Gly38 and Gln15 would be aligned on opposite faces of the β-turn-β structure, and a contact between Gly38 and Gln15 would be observed. If, however, there is a bend at Gly37/38, then a contact will not be seen. This contact was not observed, (note the Gly region of Figure 5.4A) further indicating that there is a bend at Gly37/38.

The bending of the peptide at Gly37/38 has been previously noted by Spencer and coworkers (127), where they observed a *cis* amide bond between residues 37-38 which may be involved in the early aggregation process. No contact is observed between Met35 and Ala42 or Gly38 and Ala42, indicating that while there is a bend in the peptide, the C-terminus does not completely loop back on itself.

Rows from the 2D DARR NMR spectra through Met35, Gly37 and Gly38 were compared in order to determine the relative orientation of these three residues in the β-sheet. Integral values of crosspeak areas were measured as a percentage of diagonal peak area, allowing comparison between different crosspeaks. Fibrillar Aβ42 showed a very strong crosspeak between Gly38 and Met35. The intensity of this crosspeak was stronger than that between Gly37

and Met35, which further supports the previous conclusion that the C-terminus does not form a flat β-sheet, and is instead bent at Gly37/38, allowing Met35 to be in closer proximity to Gly38 than to Gly37.

Molecular dynamics simulations by Roychaudhuri *et al.* have proposed that Aβ42 is capable of forming a bent structure at Val36 and Gly37 stabilized by backbone hydrogen bonds between Met35 and G38; Aβ40 is unable to form such a structure (128). While we observe this Met35 and Gly38 contact, we did not observe any contacts between Gly33 and Val39/40, indicating that a complete turn is not forming in our samples.

Since the splitting at Met35 was observed for fibrils but not in oligomers, it seemed that this conformation would be a good marker for fibril formation. Current monitors of fibrillization, such as thioflavin T fluorescence, are not able to distinguish between protofibrils and fibrils since both contain high β – sheet content. To determine if the protofibrils also contained a split conformation at Met35, Met35 + Gly38 labeled Aβ42 samples were incubated for 0 h (oligomers), 15 h (protofibrils) and 13 days (fibrils). The splitting at Met35 was measured, as was the crosspeak between Met35 and Gly38. These spectra are compared in Figure 5.5. 1D spectra of the oligomers, protofibrils and fibrils (Figure 5.5 A + B) all have a downfield Ala42 peak at 180 ppm, so they all likely have a negatively charged C-terminus. The rest of the peaks in the spectra overlap, with the exception that only the fibrils have a strong split at Met35. Rather than a split peak at Met35, only the 15 ppm component is observed, with a minor shoulder at 17 ppm in the oligomers and protofibrils. This shoulder may be what causes the small Met35-Gly38 crosspeak in these samples.

In the 2D spectra of the fibrils, the rows with the strongest Met35 - Gly38 crosspeak are the 17 ppm component of Met35 (Figure 5.5 C + D). This component is not seen to any significant amount in the oligomers and protofibrils (maybe a small shoulder), which would explain why the Met35-Gly38 crosspeak is only seen in the fibrils. In all of the samples, the Met35 row through 17 ppm has the largest Gly38 crosspeak, even when this is not the row corresponding to the Met35 diagonal (which is ~15 ppm in these spectra). The rest of the spectra line up at all of the peaks except for at Gly38 of the fibrils, which is at a slightly different frequency.

Both the oligomer and protofibril sample only exhibit a weak crosspeak between Met35 and Gly38, however when the sample is composed of mature fibrils, a strong crosspeak is observed. This indicates that the C-terminal bend is a structural feature unique to fibrils. Recent data in our lab indicate that the Aβ42 oligomers and protofibrils both contain an antiparallel β – sheet component that is not present in the mature fibrils. Since the Met35 splitting occurs on a similar timescale as the loss of the antiparallel β – sheet component, it may be that the transition from protofibril to fibril involves rearrangement of the antiparallel β – sheets into parallel β – sheets, which allows Met35 to come in contact with Gly38.

Orientation of the second Met35 component

Based on our previous model of Aβ42 fibrils, a contact between Gly38 and Gln15 was expected to be observed. While a contact between Gly38 and Gln15 was not observed, an unexpected crosspeak between the 15 ppm component of Met35 and Gln15 was observed (Figure 5.4A). This peak can only arise if Met35 is pointed toward the center of the fibrils instead of outward, as it is commonly believed to be in most fibril models. While this may

appear to be in conflict with the previous results that place Met35 pointed up and near Gly38, this explains the presence of the two Met35 peaks in the spectra (Figure 5.6). The crosspeak to Gly38 is only observed with the 17 ppm Met35 component while the 15 ppm Met35 component shows a crosspeak to Gln15, indicating that the two peaks arise from two distinct C-terminal conformations, one with Met35 bent up (in contact with Gly38) and one with Met35 bent down and extended (to contact Gln15) (Figure 5.6). The fact that the same results are seen in both seeded and unseeded fibrils seems to imply that it is one fibril with two conformations, possibly alternating up, down, up, down … along the length of the fibril. In both the bent and flipped conformations there is a turn at either Gly37-Gly38 or Gly38-Val39. These turn regions correspond well with scanning proline mutagenesis studies by Morimoto *et al.* (123).

A second contact in the fibrils was also observed between the 15 ppm component of Met35 and Phe19 (Figure 5.4C), which indicates that the downward facing Met35 component is in proximity to both Phe19 and Gln15.

Previous experiments measuring contacts between the two conformations of Met35 involved contacts between Met35 and two different peptides. In order to investigate the two conformations of Met35 within a single peptide, a peptide containing Gly37 ($^{13}C_{\alpha}$), Met35 ($^{13}C_{\varepsilon}$), Leu34 ($^{13}C_{\alpha}$), Gly33 ($^{13}C_{1}$) and Phe19 ($^{13}C_{r}$) was synthesized. It was expected that Phe19 would be in contact with Met35 and Gly33 in flipped peptide (Figure 5.4C), where Phe19 and Leu34 are not in contact.

Orientation of C-terminal β-strand segment after bend at Gly37/38 and interaction with the N-terminus

The strong crosspeak to Gly38 by one component and lack of crosspeak in the other component of Met35 indicates that there may be a conformation with Met35 and Gly38 in a parallel β-sheet (with Met35 pointed toward the center of the peptide) and a second conformation where Met35 and Gly38 are bent close together (Figure 5.6).

It has been proposed that there is an interaction between Ala42, Met35 and Tyr10, which is believed to be involved in the coordination of metal ions and the production of radicals (125). A contact between Tyr10 and Met35 or Ala42 has been proposed (125), as well as a Met35-Ala42 contact (which we do not see in our spectra). While this contact was not observed in either fibrils or oligomers under our conditions, it may be part of the mechanism by which Aβ42 oligomers are toxic in biological systems such as membranes (125). This contact may be transient, and only exist in the toxic dodecameric Aβ42 species, which have some β–sheet content but not the full β–sheet structure of fibrils. During the fibrillization process the charged C–terminus changes orientation and moves from being in contact with Tyr10 to a different residue. Since the C–terminal Ala42 residue is negatively charged, it is possible that there is an interaction with Arg5. Based on our model, the bend at Gly37/38 could allow the negatively charged C-terminus of one fibril to make contact with either Arg5 or Lys28 on the other fibril strand. This would provide a stabilizing force in the fibrils not present in the oligomers, and would explain the lack of a Met35-Ala42 contact in fibrils. It would also explain the increased fibrillization observed in peptides with His6Arg or Asp7Asn mutations (108, 109). By adding a second positive or removing a negative residue these mutations both make the N-terminus more positive, increasing the interaction with Ala42 and further stabilizing the fibrils.

In dodecamers, Phe20 may be in contact with Arg5 via a cation-π interaction (47, 104, 105). However, in mature fibrils, Arg5 shifts to be in contact with the negative C-terminus, disrupting the Tyr10 – Ala42 contact responsible for toxicity in the dodecamers and making fibrils less toxic. The Phe20 – Arg5 interaction can also be disrupted by inhibitors, preventing hexamer stacking and conversion into toxic dodecamers. Thus the differences in Met35 orientation in fibrils and oligomers may explain some of the differences in the toxicity of these two species.

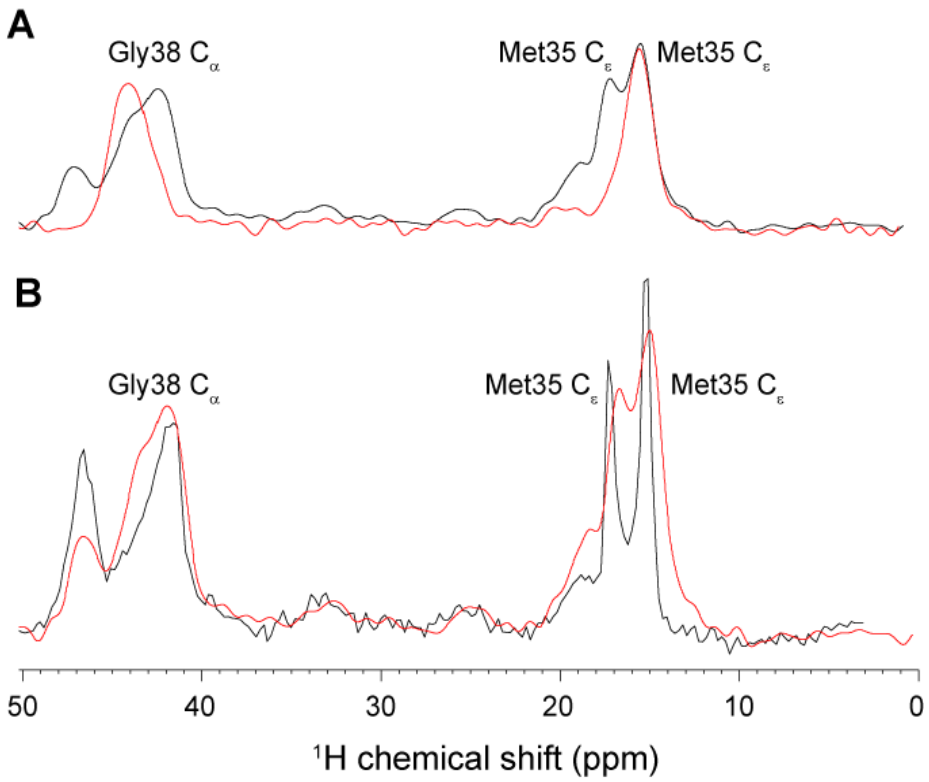

Figure 5.1 ^{1}H NMR spectra of Aβ42 peptide (Met35 ^{13}C label).
^{13}C labels at Ala42 ($^{13}C_1$), Gly38 ($^{13}C_\alpha$), Met35 ($^{13}C\varepsilon$) and Phe19 ($^{13}C_r$).
A) Region of the 1D spectra from 0 – 60 ppm of Aβ42 oligomers (red) and Aβ42 fibrils (black). The Met35 peak of the fibril sample is split, indicating that the fibrils have two conformations for this residue.
Spectra were collected at 600 MHz with 10 KHz spinning, ^{1}H field strength of 10.7 dB and 23 dB of decoupling.
B) Region of the 1D spectra from 0 – 60 ppm of Aβ42 fibrils (red) and seeded Aβ42 fibrils (black). The Met35 peak remains split in both samples but the peaks are more defined in the seeded samples.
Seeded fibril spectra were collected at 750 MHz with 11.5 KHz spinning, ^{1}H field strength of 10.7 dB and 19.6 dB of decoupling.

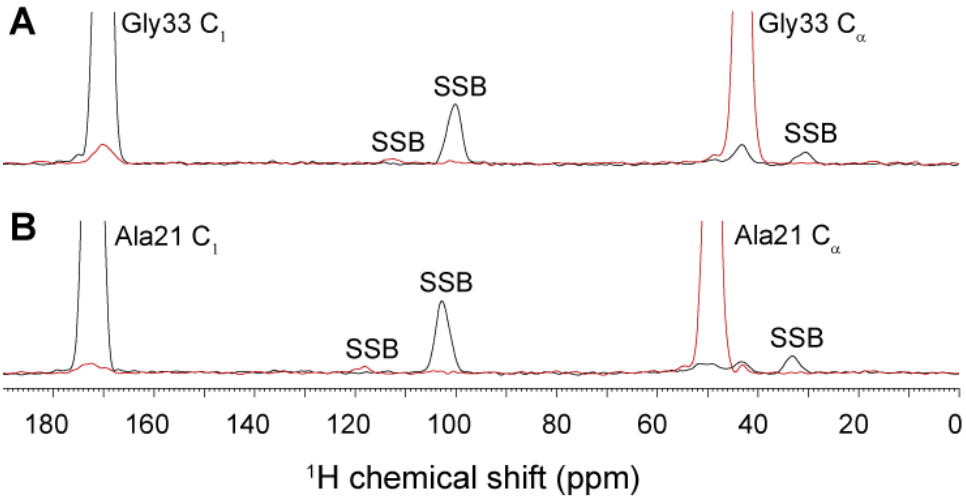

Figure 5.2 NMR spectra showing parallel-in-register orientation in seeded Aβ42 fibrils.
^{13}C labels in peptide 1: Gly33 ($^{13}C_1$) (black), Ala21 ($^{13}C_\alpha$) (red).
^{13}C labels in peptide 2: Ala21 ($^{13}C_1$) (black), Gly33 ($^{13}C_\alpha$) (red).
Seeded fibrils composed of a 1:1 mixture of the two peptides were grown by addition of a 5% volume of Ala42 ($^{13}C_1$), (Gly38 $^{13}C_\alpha$), Met35 ($^{13}C_\varepsilon$) Phe19 ($^{13}C_r$) peptide (seeded 12 generations). The small amount of additional labels in this 13th generation peptide does not contribute to the spectra.
Spectra were collected at 600 MHz with 10.5 KHz spinning, ^1H field strength of 10.7 dB and 23.55 dB of decoupling.
Spinning side bands are labeled SSB.
A) Full row from the 2D DARR NMR spectrum through Gly33 $^{13}C_1$ (black) and Gly33 $^{13}C_\alpha$ (red). A crosspeak between Gly33 $^{13}C_1$and Gly33 $^{13}C_\alpha$ is observed in these seeded fibrils, indicating that the β-strands in the fibrils associate in a parallel, in-register arrangement.
B) Full row from the 2D DARR NMR spectrum through Ala21 $^{13}C_1$ (black) and Ala21 $^{13}C_\alpha$ (red). A crosspeak between Ala21 $^{13}C_1$ and Ala21 $^{13}C_\alpha$ is observed in these seeded fibrils, indicating that the β-strands in the fibrils associate in a parallel, in-register arrangement.
Values for the integrated intensity of each peak relative to the diagonal peak are listed in Table 5.1.

Residue 1	Label	Chemical shift (ppm)	Residue 2	Label	Chemical shift (ppm)	Intensity (% diagonal)
Gly 33	$^{13}C_1$	170	Gly 33	$^{13}C_\alpha$	46	3.00%
Gly 33	$^{13}C_\alpha$	46	Gly 33	$^{13}C_1$	170	4.17%
Ala 21	$^{13}C_1$	173	Ala 21	$^{13}C_\alpha$	48	1.76%
Ala 21	$^{13}C_\alpha$	48	Ala 21	$^{13}C_1$	173	2.60%

Table 5.1 Integrated intensities of crosspeaks in Figure 5.2.

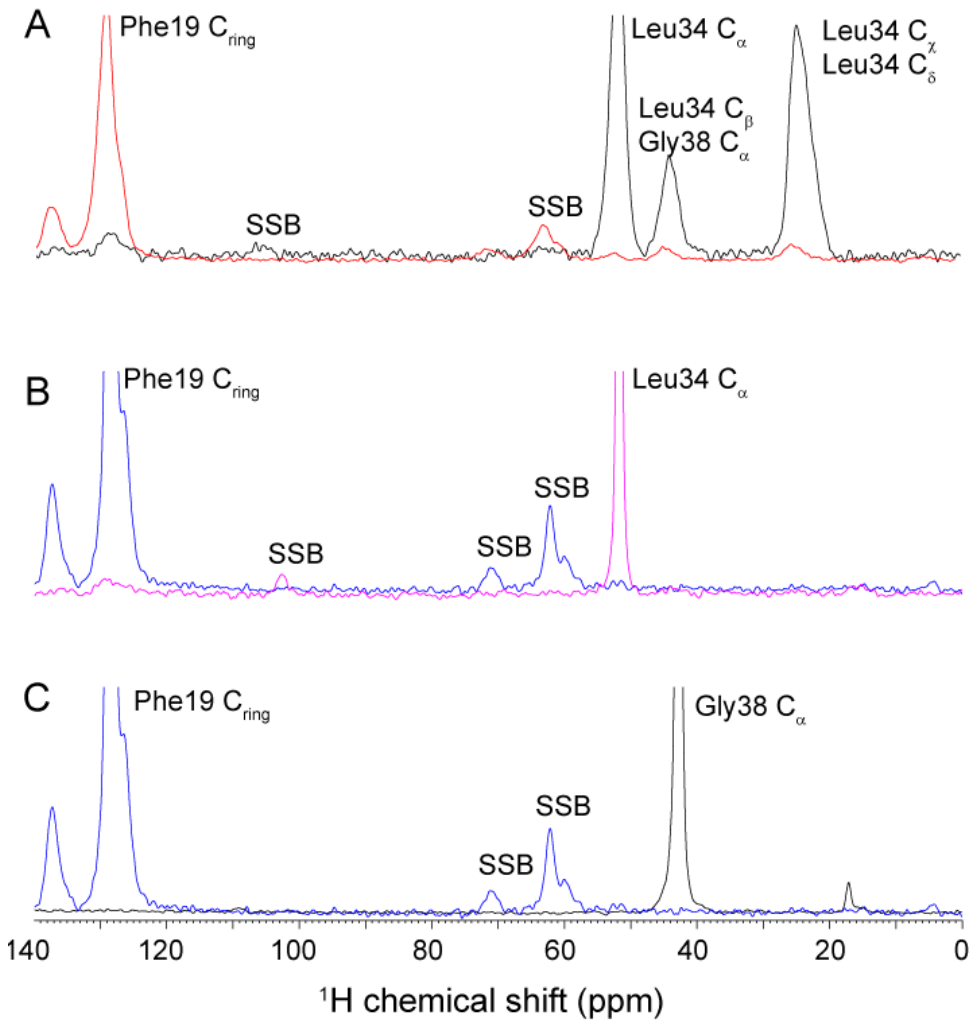

Figure 5.3 NMR spectra showing packing of β-turn-β structure in seeded Aβ42 fibrils. Spinning side bands are labeled SSB.

A) Expansion of the region spanning 0 – 140 ppm from the 2D DARR NMR spectrum through Phe19 $^{13}C_r$ (red) and Leu34 $^{13}C_\alpha$ (black). A crosspeak between Phe $^{13}C_r$ and Leu34 C1, C2, C3 is observed in seeded fibrils indicating that these residues are in proximity.

^{13}C labels at Gly38 ($^{13}C_\alpha$), Leu34 ($^{13}C_{uniform}$) and Phe19 ($^{13}C_r$). Seeded fibrils of this peptide were grown by addition of a 5% volume of Ala42 ($^{13}C_1$), (Gly38 $^{13}C_\alpha$), Met35 ($^{13}C_\varepsilon$) Phe19 ($^{13}C_r$) peptide (seeded 12 generations). The small amount of additional labels in this 13th generation peptide does not contribute to the spectra.

Spectra were collected at 600 MHz with 10 KHz spinning, ^1H field strength of 12.3 dB and 23.55 dB of decoupling.

B) Expansion of the region spanning 0 – 140 ppm from the 2D DARR NMR spectrum through Phe19 $^{13}C_r$ (blue) and Leu34 $^{13}C_\alpha$ (purple).

A crosspeak between Phe19 ring carbon and Leu34 C2, is observed in seeded fibrils indicating that these residues are in proximity.

^{13}C labels at Gly37 ($^{13}C_\alpha$), Met35 ($^{13}C_\varepsilon$), Leu34 ($^{13}C_\alpha$), Gly33 ($^{13}C_1$) and Phe19 ($^{13}C_r$). Seeded fibrils of this peptide were grown by addition of a 5% volume of Ala42 ($^{13}C_1$), (Gly38 $^{13}C_\alpha$), Met35 ($^{13}C_\varepsilon$) Phe19 ($^{13}C_r$) peptide (seeded 12 generations). The small amount of additional labels in this 13th generation peptide does not contribute to the spectra.

Spectra were collected at 600 MHz with 10 KHz spinning, ^{1}H field strength of 13.6 dB and 26.85 dB of decoupling.
C) Expansion of the region spanning 0 – 140 ppm from the 2D DARR NMR spectrum through Phe19 ($^{13}C_r$) (blue) and Gly38 ($^{13}C_\alpha$) (black). No Phe19 ring carbon crosspeak to Gly38 ($^{13}C_\alpha$) was observed in these seeded fibrils.
^{13}C labels at Ala42 ($^{13}C_1$), Gly38 ($^{13}C_\alpha$), Met35 ($^{13}C_\varepsilon$) Phe19 ($^{13}C_r$). Seeded fibrils of this peptide were grown for 12 generations.
Spectra were collected at 600 MHz with 10 KHz spinning, ^{1}H field strength of 12.3 dB and 23.55 dB of decoupling.
Values for the integrated intensity of each peak relative to the diagonal peak are listed in Table 5.2.

Residue 1	Label	Chemical shift (ppm)	Residue 2	Label	Chemical shift (ppm)	Intensity (% diagonal)
Leu 34	$^{13}C_\alpha$	52	Leu 34	$^{13}C_1$	171	28.02%
Leu 34	$^{13}C_\alpha$	52	Phe 19	$^{13}C_r$	128 138	8.20%
Leu 34	$^{13}C_\alpha$	52	Gly 38	$^{13}C_\alpha$	44	34.48%
Leu 34	$^{13}C_\alpha$	52	Leu 34	$^{13}C_\gamma$	25	100.75%
Phe 19	$^{13}C_r$	128 138	Leu 34	$^{13}C_1$	171	1.56 %
Phe 19	$^{13}C_r$	128 138	Leu 34	$^{13}C_\alpha$	52	1.09 %
Phe 19	$^{13}C_r$	128 138	Gly 38	$^{13}C_\alpha$	44	3.09 %
Phe 19	$^{13}C_r$	128 138	Leu 34	$^{13}C_\gamma$	25	4.59 %
Leu 34	$^{13}C_\alpha$	52	Phe 19	$^{13}C_r$	128 138	4.35 %
Phe 19	$^{13}C_r$	128 138	Leu 34	$^{13}C_\alpha$	52	1.05 %

Table 5.2 Integrated intensities of crosspeaks in Figure 5.3.

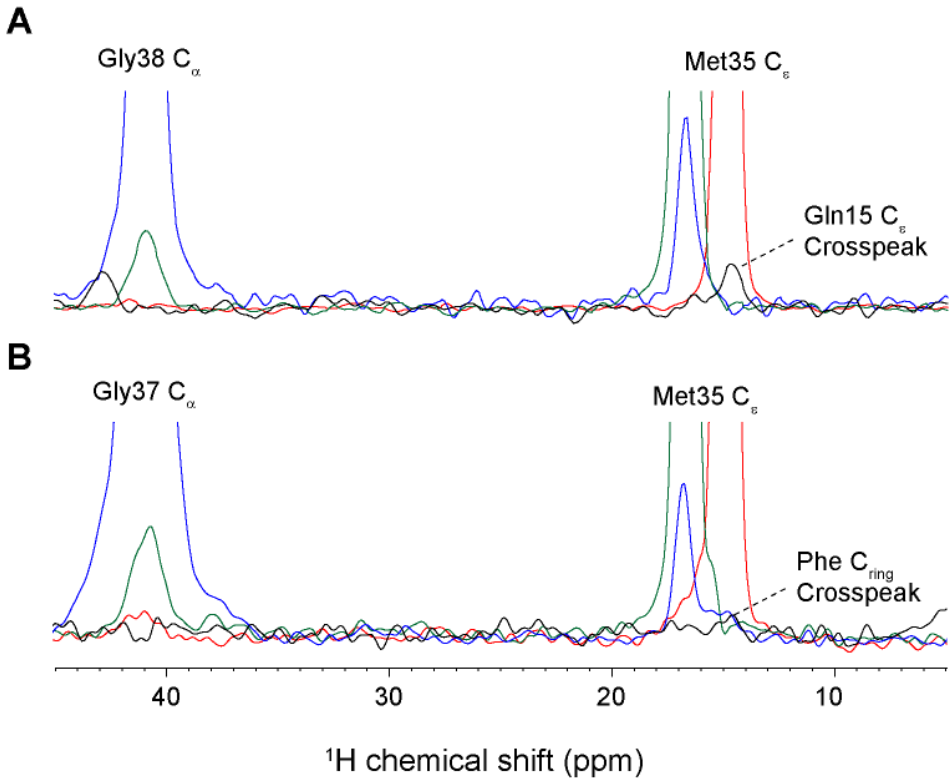

Figure 5.4 NMR spectra showing Met35 splitting and orientation in seeded Aβ42 fibrils.
A) Expansion of the region spanning 0 – 50 ppm from the 2D DARR NMR spectrum through Gly38 $^{13}C_{\alpha}$ (blue), Gln15 $^{13}C_{\varepsilon}$ (black) and Met35 $^{13}C_{\varepsilon}$ (green & red).
The 19 ppm component of Met35 (green) shows a strong crosspeak to Gly38 (blue) and not to Gln15 (black).
The 15 ppm Met35 peak (red) shows a strong crosspeak to Gln15 (black) and not to Gly38 (blue).
Together these rows show that the two Met35 conformations are in different directions.
Note the lack of a crosspeak between Gly38 and Gln15.
^{13}C labels in peptide 1: Ala42 ($^{13}C_1$), Gly38 ($^{13}C_{\alpha}$), Met35 ($^{13}C_{\varepsilon}$) and Phe19 ($^{13}C_r$).
^{13}C labels in peptide 2: Ala42 ($^{13}C_{\alpha}$), Gln15 ($^{13}C_{\varepsilon}$), His14 ($^{13}C_r$), His13 ($^{13}C_r$).
Seeded fibrils composed of a 1:1 mixture of the two peptides were grown by addition of a 5% volume of Ala42 ($^{13}C_1$), (Gly38 $^{13}C_{\alpha}$), Met35 ($^{13}C_{\varepsilon}$) Phe19 ($^{13}C_r$) peptide (seeded 12 generations).
Spectra were collected at 600 MHz with 10 KHz spinning, ^{1}H field strength of 12.3 dB and 23.55 dB of decoupling.
B) Expansion of the region spanning 0 – 50 ppm from the 2D DARR NMR spectrum through Gly37 $^{13}C_{\alpha}$ (blue), Phe19 $^{13}C_r$ (black) and Met35 $^{13}C_{\varepsilon}$ (green & red).
The 19 ppm component of Met35 (green) but not the 15 ppm peak (red) shows a strong crosspeak to Gly37 (blue).
Met35 15 ppm peak (red) but not 19 ppm peak (green) shows a crosspeak to Phe19 (black).
Together these rows show that the two Met35 conformations are in different directions.
^{13}C labels at Gly37 ($^{13}C_{\alpha}$), Met35 ($^{13}C_{\varepsilon}$), Leu34 ($^{13}C_{\alpha}$), Gly33 ($^{13}C_1$) and Phe19 ($^{13}C_r$). Seeded fibrils this peptide were grown by addition of a 5% volume of Ala42 ($^{13}C_1$), (Gly38 $^{13}C_{\alpha}$), Met35

($^{13}C_{\varepsilon}$) Phe19 ($^{13}C_{r}$) peptide (seeded 12 generations). The small amount of additional labels in this 13th generation peptide does not contribute to the spectra.
Spectra were collected at 600 MHz with 10 KHz spinning, ^{1}H field strength of 13.6 dB and 26.85 dB of decoupling.
Values for the integrated intensity of each peak relative to the diagonal peak are listed in Table 5.3.

Residue 1	Label	Chemical shift (ppm)	Residue 2	Label	Chemical shift (ppm)	Intensity (% diagonal)
Met 35 (down)	$^{13}C_{\varepsilon}$	15	Gln15	$^{13}C_{\varepsilon}$	176	2.02%
Gln 15	$^{13}C_{\varepsilon}$	176	Met 35 (down)	$^{13}C_{\varepsilon}$	15	2.87%
Gly 38	$^{13}C_{\alpha}$	44	Met 35 (up)	$^{13}C_{\varepsilon}$	17	11.87%
Met 35 (up)	$^{13}C_{\varepsilon}$	17	Gly 38	$^{13}C_{\alpha}$	44	9.39%
Met 35 (down)	$^{13}C_{\varepsilon}$	15	Gly 38	$^{13}C_{\alpha}$	44	0.97%
Gly 37	$^{13}C_{\alpha}$	44	Met 35 (up)	$^{13}C_{\varepsilon}$	17	2.59%
Met 35 (up)	$^{13}C_{\varepsilon}$	17	Gly 37	$^{13}C_{\alpha}$	44	5.92%
Met 35 (down)	$^{13}C_{\varepsilon}$	15	Gly 37	$^{13}C_{\alpha}$	44	0.14%

Table 5.3 Integrated intensities of crosspeaks in Figure 5.4.

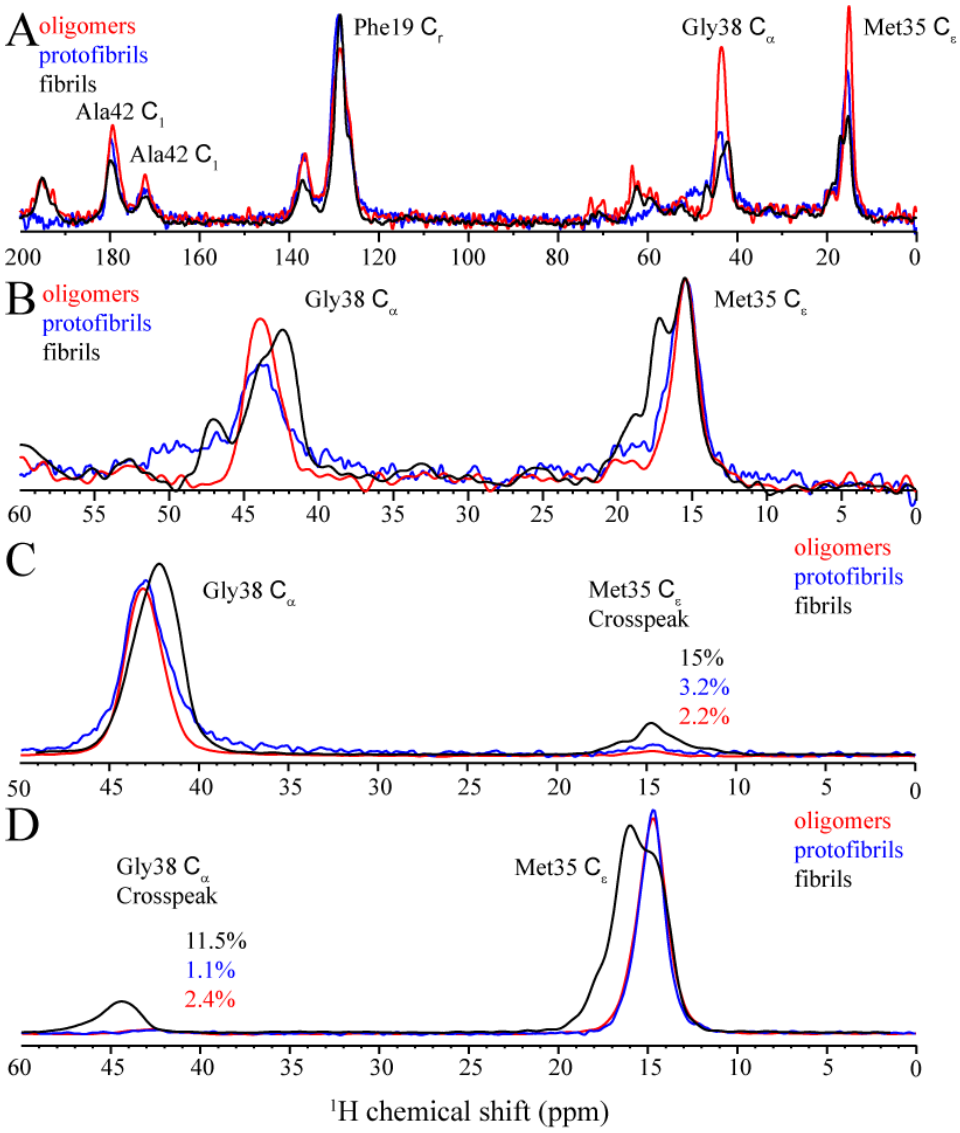

Figure 5.5 ^{1}H NMR spectra of Aβ42 peptides over time.
^{13}C labels at Ala42 (1-^{13}C), (Gly38 2-^{13}C), Met35 (5-^{13}C) and Phe19 (ring carbons).
A) Full 1D spectra of Aβ42 oligomers (red), protofibrils (blue) and fibrils (black). All three samples contain a downfield Ala42 peak at 180 ppm, indicating that the C-terminus is negatively charged in these samples.
B) Expansion of the region of the 1D spectra from 0 – 60 ppm of Aβ42 oligomers (red), protofibrils (blue) and fibrils (black). This splitting at Met35 is only observed in the fibril sample.
C) Row from the 2D DARR NMR spectrum through Gly38 C2 of Aβ42 oligomers (red), protofibrils (blue) and fibrils (black). The strong crosspeak between Gly38 and Met35 is only observed for the fibril sample.
D) Row from the 2D DARR NMR spectrum through Met35 C5 of Aβ42 oligomers (red), protofibrils (blue) and fibrils (black). The strong crosspeak between Gly38 and Met35 is only observed for the fibril sample.

Values for the integrated intensity of each peak relative to the diagonal peak are listed in Table 5.4.

Residue 1	Label	Chemical shift (ppm)	Residue 2	Label	Chemical shift (ppm)	Intensity (% diagonal)
O Gly 38	$^{13}C_{\alpha}$	44	Met 35 (up)	$^{13}C_{\varepsilon}$	17	2.2%
P Gly 38	$^{13}C_{\alpha}$	44	Met 35 (up)	$^{13}C_{\varepsilon}$	17	3.2%
F Gly 38	$^{13}C_{\alpha}$	44	Met 35 (up)	$^{13}C_{\varepsilon}$	17	15%
O Met 35 (up)	$^{13}C_{\varepsilon}$	17	Gly 38	$^{13}C_{\alpha}$	44	2.4%
P Met 35 (up)	$^{13}C_{\varepsilon}$	17	Gly 38	$^{13}C_{\alpha}$	44	1.1%
F Met 35 (up)	$^{13}C_{\varepsilon}$	17	Gly 38	$^{13}C_{\alpha}$	44	11.5%

Table 5.4 Integrated intensities of crosspeaks in Figure 5.5.

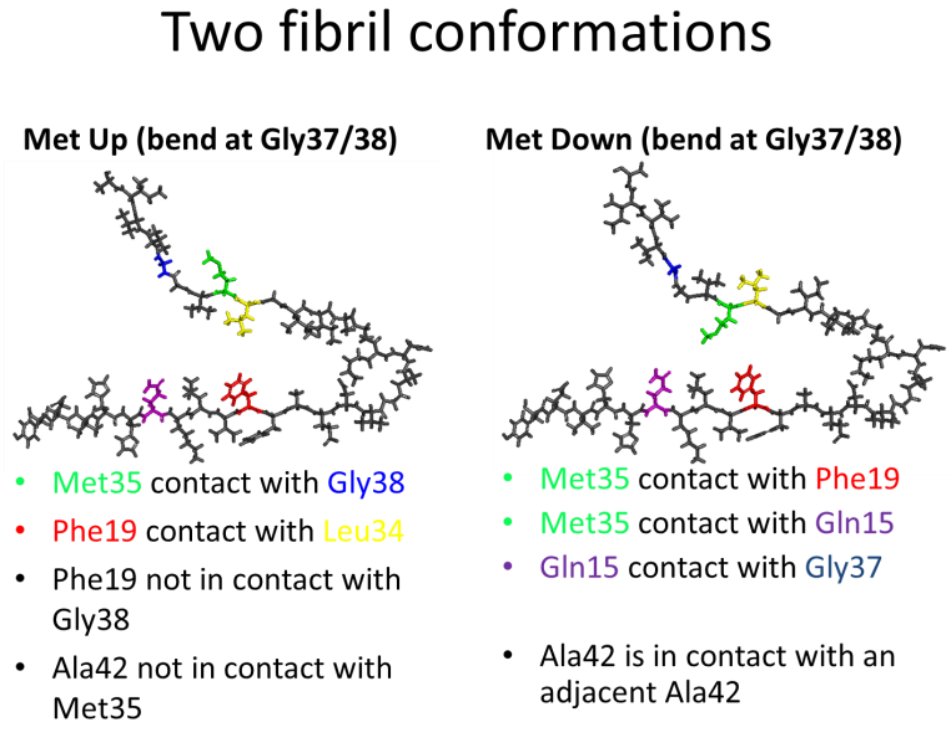

Figure 5.6 Cartoon representation of both Met35 orientations.

Conclusions and future directions

In attempting to characterize the process by which Aβ42 peptides convert from monomers into oligomers and into fibrils, numerous insights into the aggregation pathway were discovered.

Aβ42 peptides remain monomeric at low temperature

NMR experiments indicated that the Aβ42 peptides remain mostly monomeric at 4 °C at the concentrations used in our experiments. This stabilization of monomeric Aβ42 is the reason for the lack of secondary structure changes by IR or fluorescence when the peptide is left at 4 °C. However, when the monomeric Aβ42 samples are heated to 37 °C, the monomers quickly assemble into larger hexameric oligomers. Over time these hexamers stack to form a taller, dodecameric species, and the appearance of this species correlates with an increase in toxicity to neuronal cells. The appearance of this species precedes conversion into β – sheet rich protofibrils observable by thioflavin T fluorescence or FTIR spectroscopy. When the Aβ42 peptides are incubated with small molecule inhibitors such as curcumin or resveratrol, the toxicity is abolished. Based on NMR experiments, these inhibitors are binding to the central and N–terminal regions of the peptide, with strong binding at Arg5 and Phe19. Inhibitor binding does not interfere with hexamer formation, but does prevent stacking of the hexamers into the toxic dodecamers. This prevention of stacking also inhibits further progression along the fibril formation pathway into β – sheet rich protofibrils. In contrast to curcumin and resveratrol, other inhibitors such as the gamma secretase modulator indomethacin bind to the C–terminus of Aβ42 and do not cap the hexamers. This emphasizes the different methods by which Aβ42 inhibitors

act, and that the region where they bind to Aβ42 may play a role in their mechanism of inhibition.

The NMR data indicates that in the dodecamers, Phe20 may be in contact with Arg5, possibly by a cation-π interaction, and that when the inhibitors bind to this region, dodecamer formation is disrupted. In mature fibrils Arg5 may be in contact with Ala42, so the conversion of dodecamers into fibrils may require a shift in the position of Arg5 from contact with Phe20 to Ala42. This shift would disrupt contacts between Ala42, Met35 and Tyr10 present in the dodecamers, which may be required for toxicity, explaining why dodecamers are the most toxic Aβ42 species. As the dodecamers convert into fibrils, a bend at Gly37/38 forms, allowing Ala42 to come in contact with Arg5 on a neighboring fibril strand, stabilizing the growing fibril. This bend at Gly37/38 causes two conformations for Met35 to arise. These interactions are all unique to fibrils, and would provide a unique NMR marker for fibril formation.

Aβ42 monomers are partially structured

The NMR experiments provide evidence that the Aβ42 monomers stabilized at 4 °C are structured. The increase in diffusion speed at pH 7 verses at pH 10 indicates that a larger or less structured species is present at high pH, where peptides become denatured and unstructured. This indicates that the monomeric Aβ42 peptides have a structure at pH 7 which can unfold at high pH.

Additional evidence of a structured monomer comes from the solvent accessibility data which reveals that certain regions of the monomer are more accessible than others. Residues 10-12 and 17-19 were both shown to have little exchange with water while neighboring residues 15 and 16 were greatly exposed. This could indicate a turn in the N-terminus at residues 15/16

making a small hydrophobic region of the monomer. Residues 1-9 are mostly exposed to solvent and may fold back to shield the protected regions. The three C-terminal hydrophobic residues are also protected from solvent exchange. This region may interact with the other hydrophobic regions.

Additionally, NMR experiments produced reproducible spectra where specific residues shifted upon addition of inhibitors. These changes in chemical shift indicated that certain residues were experiencing a change in environment in the presence of inhibitors, while the rest of the peptide remained the same. Such local changes could only occur if the Aβ42 monomers had a defined secondary structure. Many of the regions that showed changes in chemical shift upon inhibitor binding were also shown to be solvent exposed, this is consistent with a structured monomer where some residues are exposed to solvent and able to bind inhibitors, while other residues are buried.

Our model for a structured oligomer with buried hydrophobic regions and exposed areas is consistent with a recent NMR solution structure for Aβ40 monomers proposed by Ramamoorthy and coworkers (112). While this model contains an α – helix, our secondary structure data from IR data is inconclusive. The initial low temperature CD spectra may contain an α – helix component, which is lost as the sample converts into β – sheet containing oligomers. The region to which the inhibitors curcumin and resveratrol bind are all clustered in this model, so it is consistent with our NMR data for Aβ42 monomers in the presence of these inhibitors.

Hydrophobic interactions drive Aβ42 monomers association into low molecular weight oligomers

Aβ42 peptides remain monomeric at low temperature but quickly assemble into larger oligomer species when the temperature is increased. This temperature dependence for oligomer assembly suggests that the process is entropy driven and most likely due to the removal of water from hydrophobic surfaces. As the water is released from these surfaces, they associate, stabilizing the oligomers. The solvent accessibility data shows that residues 10-12, 17-19 and 39-42 are all isolated from solvent. These residues may all come together to form the hydrophobic core of the oligomers. The C-terminus has been shown to drive oligomer formation, with increases in hydrophobicity increasing the rate of aggregation (120, 121). The hydrophobic association of the C-terminus probably is the driving force for oligomer formation.

SEC and NMR both show that the low molecular weight oligomers associate to form larger aggregates. This association is likely due to hydrophobic interactions between oligomers. When the samples are diluted these interactions become less favorable and the sample is reduced to containing only hexameric oligomers.

High molecular weight oligomers form due to β – sheet stacking of low molecular weight oligomers

The IR and CD data both indicate a transition from random coil β – sheet with a further increase in β – sheet content over time. The increases in β – sheet content occurs before the formation of protofibrils as observed by thioflavin T fluorescence. These increases in β – sheet are likely due to the formation of small β – sheet regions in the C-terminus of the peptide. The solvent accessibility data indicates that this region is structured, and once these protected

structures form, β – sheets between the hydrophobic regions begin to form. These β – sheets form in an antiparallel orientation not observed in the fibrils. These findings are in agreement with reported antiparallel β – sheets in oligomers by other labs (129).

Antiparallel β – sheet formation in pre-fibrillar oligomers creates toxic species

There have been numerous experiments conducted by many labs measuring the toxicity of Aβ42 peptides, however most of these studies look at a single time point. The results presented in this thesis are unique in that they have been conducted over a variety of times, which allows a full comparison of the toxicity of various species ranging from monomers to fibrils. Another problem with the previous experiments is that different labs use different peptide concentrations, temperature and buffer conditions, so a full comparison between the structural data or toxicity was not possible. By conducting all of our experiments under similar conditions, a full comparison of the structural changes in the Aβ42 peptide as they convert from monomers to fibrils is possible.

The mechanism by which Aβ42 oligomers kill neuronal cells is not fully understood. Numerous mechanisms including pore formation, membrane thinning and activation of signaling pathways have been suggested. Our time course data indicate that the large oligomers are more toxic than the shorter oligomers. The key difference between these two oligomeric species is their heights. The height of a dodecamer is about 4 nm, which is large enough to span a membrane bilayer, while a 2 nm hexamer will be too short. This ability to span membranes may be the reason for the increased toxicity of the dodecamers.

Eisenberg and co-workers have recently proposed toxic Aβ42 oligomer structures which contain a cross-β structure (130). This β – barrel structure would be capable of forming a pore in

the membrane, which could explain the toxic nature of Aβ42 oligomers. While both oligomers contain β – sheets, the differences between the Eisenberg structure and that of the oligomers observed in this study could be that this barrel pore only forms in the presence of membranes.

High molecular weight oligomers and protofibrils contain antiparallel β – sheets

IR data in our lab show that the antiparallel β – sheets which form in low molecular weight oligomers persist in both the high molecular weight oligomers and in the protofibrils. IR spectra obtained over time show that the peaks corresponding to antiparallel β – sheets do not reduce in intensity until the samples have been incubated for over 24 hours, indicating that it is only when fibrils form that the antiparallel β – sheets are lost.

Fibril formation involves a transition to parallel-in-register β – sheets

While fibrils and protofibrils both contain high β – sheet content, the β – sheets in both species appear to be distinct. Protofibrils (and oligomers) contain an antiparallel β – sheet, while fibrils contain a parallel- in-register β – sheet. The conversion from protofibril to fibril must therefore involve a transition from antiparallel to parallel β – sheet. This difference in β – sheet orientation may explain the differences in shape between protofibrils and fibrils. EM images of protofibrils show that the protofibrils are relatively short (~100 nm) and curled, while fibrils are longer and straight. As the high molecular weight oligomers associate, they do so in a random, lateral fashion, resulting in the beads on a string morphology which converts into curled protofibrils, containing a high amount of antiparallel β – sheets. However, parallel β – sheets appear to be a lower energy conformation, and form as the protofibrils mature into fibrils. This transition to parallel-in-register β – sheets results in the formation of long straight fibrils. This alignment of the β – sheets also results in the dual conformation of Met35, which shows a split

NMR peak only in the fibril samples lacking antiparallel IR structure. This difference in β – sheet morphology allows for a method to use thioflavin T and NMR to distinguish oligomer, protofibrils and fibrils. An antiparallel species with low thioflavin T fluorescence is oligomeric, a thioflavin T positive antiparallel species is due to protofibrils, and thioflavin T positive parallel species are fibrils. This method provides a novel way to distinguish protofibrils and fibrils, which both contain high β – sheet content and thus have similar thioflavin T fluorescence.

References

1. Stefani M & Dobson CM (2003) Protein aggregation and aggregate toxicity: new insights into protein folding, misfolding diseases and biological evolution. *J. Mol. Med.* 81(11):678-699.
2. Heron M (2012) Deaths: leading causes for 2008. *National vital statistics reports: from the Centers for Disease Control and Prevention, National Center for Health Statistics, National Vital Statistics System* 60(6):1-94.
3. Molsa PK, Marttila RJ, & Rinne UK (1986) Survival and cause of death in Alzheimer's disease and multi-infarct dementia. *Acta Neurol. Scand.* 74(2):103-107.
4. Masters CL, *et al.* (1985) Amyloid plaque core protein in Alzheimer disease and Down syndrome. *Proc. Natl. Acad. Sci. U. S. A.* 82(12):4245-4249.
5. Zhang YW, Thompson R, Zhang H, & Xu H (2011) APP processing in Alzheimer's disease. *Mol. Brain* 4:3.
6. Haass C & Selkoe DJ (2007) Soluble protein oligomers in neurodegeneration: lessons from the Alzheimer's amyloid β-peptide. *Nature Reviews Molecular Cell Biology* 8(2):101-112.
7. Portelius E, *et al.* (2010) Mass spectrometric characterization of brain amyloid beta isoform signatures in familial and sporadic Alzheimer's disease. *Acta Neuropathologica* 120(2):185-193.
8. Iwatsubo T, *et al.* (1994) Visualization of Aβ42(43) and Aβ40 in senile plaques with end-specific A beta monoclonals: Evidence that an initially deposited species is Aβ42(43). *Neuron* 13(1):45-53.
9. Fukumoto H, *et al.* (2010) High-molecular-weight β-amyloid oligomers are elevated in cerebrospinal fluid of Alzheimer patients. *FASEB J.* 24(8):2716-2726.
10. Jarrett JT, Berger EP, & Lansbury PT (1993) The carboxy terminus of the β-amyloid protein is critical for the seeding of amyloid formation - Implications for the pathogenesis of Alzheimer's disease. *Biochemistry* 32(18):4693-4697.
11. Dahlgren KN, *et al.* (2002) Oligomeric and fibrillar species of amyloid-β peptides differentially affect neuronal viability. *J. Biol. Chem.* 277(35):32046-32053.
12. McLean CA, *et al.* (1999) Soluble pool of Aβ amyloid as a determinant of severity of neurodegeneration in Alzheimer's disease. *Ann. Neurol.* 46(6):860-866.
13. Lue LF, *et al.* (1999) Soluble amyloid β peptide concentration as a predictor of synaptic change in Alzheimer's disease. *Am. J. Path.* 155(3):853-862.
14. Hsia AY, *et al.* (1999) Plaque-independent disruption of neural circuits in Alzheimer's disease mouse models. *Proc. Natl. Acad. Sci. U. S. A.* 96(6):3228-3233.
15. Lambert MP, *et al.* (1998) Diffusible, nonfibrillar ligands derived from $A\beta_{1-42}$ are potent central nervous system neurotoxins. *Proc. Natl. Acad. Sci. U. S. A.* 95(11):6448-6453.
16. Walsh DM, *et al.* (2002) Naturally secreted oligomers of amyloid β protein potently inhibit hippocampal long-term potentiation in vivo. *Nature* 416(6880):535-539.
17. Kayed R, *et al.* (2003) Common structure of soluble amyloid oligomers implies common mechanism of pathogenesis. *Science* 300(5618):486-489.
18. Barghorn S, *et al.* (2005) Globular amyloid β-peptide$_{1-42}$ oligomer - a homogenous and stable neuropathological protein in Alzheimer's disease. *J. Neurochem.* 95(3):834-847.
19. Cleary JP, *et al.* (2005) Natural oligomers of the amyloid-protein specifically disrupt cognitive function. *Nat. Neurosci.* 8(1):79-84.

20. Ferreira ST, Vieira MNN, & De Felice FG (2007) Soluble protein oligomers as emerging toxins in Alzheimer's and other amyloid diseases. *IUBMB Life* 59(4-5):332-345.
21. Bernstein SL, *et al.* (2009) Amyloid-β protein oligomerization and the importance of tetramers and dodecamers in the aetiology of Alzheimer's disease. *Nat. Chem.* 1:326-331.
22. Bitan G, *et al.* (2003) Amyloid β-protein (Aβ) assembly: Aβ40 and Aβ42 oligomerize through distinct pathways. *Proc. Natl. Acad. Sci. U. S. A.* 100(1):330-335.
23. Yamamoto N, *et al.* (2007) A ganglioside-induced toxic soluble Aβ assembly - Its enhanced formation from Aβ bearing the Arctic mutation. *J. Biol. Chem.* 282(4):2646-2655.
24. Yanagisawa K (2007) Role of gangliosides in Alzheimer's disease. *Biochim. Biophys. Acta* 1768(8):1943-1951.
25. Magdesian MH, *et al.* (2008) Amyloid-beta binds to the extracellular cysteine-rich domain of frizzled and inhibits wnt/beta-catenin signaling. *J. Biol. Chem.* 283(14):9359-9368.
26. De Felice FG, *et al.* (2007) A beta oligomers induce neuronal oxidative stress through an N-methyl-D-aspartate receptor-dependent mechanism that is blocked by the Alzheimer drug memantine. *J. Biol. Chem.* 282(15):11590-11601.
27. Shankar GM, *et al.* (2007) Natural oligomers of the Alzheimer amyloid-beta protein induce reversible synapse loss by modulating an NMDA-type glutamate receptor-dependent signaling pathway. *J. Neurosci.* 27(11):2866-2875.
28. Valincius G, *et al.* (2008) Soluble amyloid β-oligomers affect dielectric membrane properties by bilayer insertion and domain formation: Implications for cell toxicity. *Biophys. J.* 95(10):4845-4861.
29. Kawahara M & Kuroda Y (2000) Molecular mechanism of neurodegeneration induced by Alzheimer's beta-amyloid protein: Channel formation and disruption of calcium homeostasis. *Brain Res. Bull.* 53(4):389-397.
30. Soto C (2003) Unfolding the role of protein misfolding in neurodegenerative diseases. *Nature Reviews Neuroscience* 4(1):49-60.
31. Petkova AT, *et al.* (2002) A structural model for Alzheimer's β-amyloid fibrils based on experimental constraints from solid state NMR. *Proc. Natl. Acad. Sci. U. S. A.* 99(26):16742-16747.
32. Antzutkin ON, Balbach JJ, & Tycko R (2003) Site-specific identification of non-β-strand conformations in Alzheimer's β-amyloid fibrils by solid-state NMR. *Biophys. J.* 84(5):3326-3335.
33. Petkova AT, Yau WM, & Tycko R (2006) Experimental constraints on quaternary structure in Alzheimer's β-amyloid fibrils. *Biochemistry* 45(2):498-512.
34. Lührs T, *et al.* (2005) 3D structure of Alzheimer's amyloid-β (1-42) fibrils. *Proc. Natl. Acad. Sci. U. S. A.* 102(48):17342-17347.
35. Tycko R (2011) Solid-State NMR sudies of amyloid fibril structure. *Annu. Rev. Phys. Chem.* 62:279-299.
36. Ahmed M, *et al.* (2010) Structural conversion of neurotoxic amyloid-β_{1-42} oligomers to fibrils. *Nat. Struct. Mol. Biol.* 17(5):561–567.
37. Siemers ER, *et al.* (2006) Effects of a γ-secretase inhibitor in a randomized study of patients with Alzheimer disease. *Neurology* 66(4):602-604.

38. Czirr E & Weggen S (2006) γ-secretase modulation with Aβ42-lowering nonsteroidal anti-inflammatory drugs and derived compounds. *Neurodegenerative Diseases* 3(4-5):298-304.
39. van Es JH, *et al.* (2005) Notch/γ-secretase inhibition turns proliferative cells in intestinal crypts and adenomas into goblet cells. *Nature* 435(7044):959-963.
40. Geling A, Steiner H, Willem M, Bally-Cuif L, & Haass C (2002) A γ-secretase inhibitor blocks Notch signaling in vivo and causes a severe neurogenic phenotype in zebrafish. *EMBO Rep.* 3(7):688-694.
41. Augelli-Szafran CE, *et al.* (2010) Discovery of Notch-sparing γ-secretase inhibitors. *Current Alzheimer Research* 7(3):207-209.
42. Ono K, Hasegawa K, Naiki H, & Yamada M (2004) Curcumin has potent anti-amyloidogenic effects for Alzheimer's β-amyloid fibrils in vitro. *J. Neurosci. Res.* 75(6):742-750.
43. Yang FS, *et al.* (2005) Curcumin inhibits formation of amyloid β oligomers and fibrils, binds plaques, and reduces amyloid *in vivo*. *J. Biol. Chem.* 280(7):5892-5901.
44. Mishra R, Sellin D, Radovan D, Gohlke A, & Winter R (2009) Inhibiting islet amyloid polypeptide fibril formation by the red wine compound resveratrol. *ChemBioChem* 10(3):445-449.
45. Jang JH & Surh YJ (2003) Protective effect of resveratrol on β-amyloid-induced oxidative PC12 cell death. *Free Radical Biol. Med.* 34(8):1100-1110.
46. Rivière C, *et al.* (2007) Inhibitory activity of stilbenes on Alzheimer's β-amyloid fibrils in vitro. *Bioorg. Med. Chem.* 15(2):1160-1167.
47. Porat Y, Abramowitz A, & Gazit E (2006) Inhibition of amyloid fibril formation by polyphenols: Structural similarity and aromatic interactions as a common inhibition mechanism. *Chemical Biology & Drug Design* 67(1):27-37.
48. Wang J, *et al.* (2006) Moderate consumption of Cabernet Sauvignon attenuates Aβ neuropathology in a mouse model of Alzheimer's disease. *FASEB J.* 20(13):2313-2320.
49. Hilbich C, *et al.* (1990) Amyloid of Alzheimers-disease - structure-function- relationships and peptide inhibitors of fibril formation. *Neurobiol. Aging* 11(3):302-302.
50. Sato T, *et al.* (2006) Inhibitors of amyloid toxicity based on β-sheet packing of Aβ40 and Aβ42. *Biochemistry* 45(17):5503-5516.
51. Austen BM, *et al.* (2008) Designing peptide inhibitors for oligomerization and toxicity of Alzheimer's β-amyloid peptide. *Biochemistry* 47(7):1984-1992.
52. Findeis MA, *et al.* (1999) Modified-peptide inhibitors of amyloid β-peptide polymerization. *Biochemistry* 38(21):6791-6800.
53. Wiesehan K, *et al.* (2008) Inhibition of cytotoxicity and amyloid fibril formation by a D-amino acid peptide that specifically binds to Alzheimer's diseaseamyloid peptide. *Protein Engineering Design & Selection* 21(4):241-246.
54. Gilead S & Gazit E (2004) Inhibition of amyloid fibril formation by peptide analogues modified with α-aminoisobutyric acid. *Angew. Chem.-Int. Edit.* 43(31):4041-4044.
55. Madine J, Doig AJ, & Middleton DA (2008) Design of an N-methylated peptide inhibitor of α-synuclein aggregation guided by solid-state NMR. *J. Am. Chem. Soc.* 130(25):7873-7881.
56. Gordon DJ, Tappe R, & Meredith SC (2002) Design and characterization of a membrane permeable N-methyl amino acid-containing peptide that inhibits $A\beta_{1-40}$ fibrillogenesis. *J. Peptide Res.* 60(1):37-55.

57. Necula M, Kayed R, Milton S, & Glabe CG (2007) Small molecule inhibitors of aggregation indicate that amyloid β oligomerization and fibrillization pathways are independent and distinct. *J. Biol. Chem.* 282(14):10311-10324.
58. Taylor M, *et al.* (2010) Development of a proteolytically stable retro-inverso peptide inhibitor of β-amyloid oligomerization as a potential novel treatment for Alzheimer's Disease. *Biochemistry* 49(15):3261-3272.
59. Lin SJ, Shiao YJ, Chi CW, & Yang LM (2004) Aβ Aggregation inhibitors. Part 1: Synthesis and biological activity of phenylazo benzenesulfonamides. *Bioorg. Med. Chem. Lett.* 14(5):1173-1176.
60. Mastrangelo IA, *et al.* (2006) High-resolution atomic force microscopy of soluble Aβ42 oligomers *J. Mol. Biol.* 358(1):106-119
61. Kay LE, Torchia DA, & Bax A (1989) Backbone dynamics of proteins as studied by ^{15}N inverse detected heteronuclear NMR-spectroscopy: Application to staphylococcal nuclease. *Biochemistry* 28(23):8972-8979.
62. Yan YL & Wang CY (2006) Aβ42 is more rigid than Aβ40 at the C terminus: Implications for Aβ aggregation and toxicity. *J. Mol. Biol.* 364(5):853-862.
63. Mosmann T (1983) Rapid Colorimetric Assay For Cellular Growth and Survival - Application to Prolferation and Cyto-toxicity Assays. *J. Immunol. Methods* 65(1-2):55-63.
64. Papadopoulos NG, *et al.* (1994) An Improved Fluorescence Assay for the Determination of Lymphocyte-mediated Cytotoxicity Using Flow Cytometry. *J. Immunol. Methods* 177(1-2):101-111.
65. Paravastu AK, Qahwash I, Leapman RD, Meredith SC, & Tycko R (2009) Seeded growth of β-amyloid fibrils from Alzheimer's brain-derived fibrils produces a distinct fibril structure. *Proc. Natl. Acad. Sci. U. S. A.* 106(18):7443-7448.
66. Paravastua AK, Leapman RD, Yau WM, & Tycko R (2008) Molecular structural basis for polymorphism in Alzheimer's β-amyloid fibrils. *Proc. Natl. Acad. Sci. U. S. A.* 105(47):18349-18354.
67. Crocker E, *et al.* (2004) Dipolar assisted rotational resonance NMR of tryptophan and tyrosine in rhodopsin. *J. Biomol. NMR* 29(1):11-20.
68. Bennett AE, Rienstra CM, Auger M, Lakshmi KV, & Griffin RG (1995) Heteronuclear decoupling in rotating solids. *J. Chem. Phys.* 103(16):6951-6958.
69. Takegoshi K, Nakamura S, & Terao T (2001) ^{13}C-^{1}H dipolar-assisted rotational resonance in magic-angle spinning NMR. *Chemical Physics Letters* 344(5-6):631-637.
70. Fawzi NL, Ying J, Ghirlando R, Torchia DA, & Clore GM (2011) Atomic-resolution dynamics on the surface of amyloid-β protofibrils probed by solution NMR. *Nature* 480(7376):268–272.
71. Nag S, *et al.* (2011) Nature of the amyloid-β monomer and the monomer-oligomer equilibrium. *J. Biol. Chem.* 286(16):13827-13833.
72. Hou LM, *et al.* (2004) Solution NMR studies of the A beta(1-40) and A beta(1-42) peptides establish that the met35 oxidation state affects the mechanism of amyloid formation. *J. Am. Chem. Soc.* 126(7):1992-2005.
73. Bernstein SL, *et al.* (2005) Amyloid β-protein: Monomer structure and early aggregation states of Aβ42 and its Pro(19) alloform. *J. Am. Chem. Soc.* 127(7):2075-2084.
74. Chromy BA, *et al.* (2003) Self-assembly of $A\beta_{1-42}$ into globular neurotoxins. *Biochemistry* 42(44):12749-12760.

75. LeVine H (1999) Quantification of β-sheet amyloid fibril structures with thioflavin T. *Methods Enzymol.* 309:274-284.
76. Krebs MRH, Bromley EHC, & Donald AM (2005) The binding of thioflavin-T to amyloid fibrils: localisation and implications. *J. Struct. Biol.* 149(1):30-37.
77. Khurana R, *et al.* (2005) Mechanism of thioflavin T binding to amyloid fibrils. *J. Struct. Biol.* 151(3):229-238.
78. Hong HS, *et al.* (2009) Inhibition of Alzheimer's amyloid toxicity with a tricyclic pyrone molecule in vitro and in vivo. *J. Neurochem.* 108(4):1097-1108.
79. Fawzi NL, Ying JF, Torchia DA, & Clore GM (2010) Kinetics of amyloid β monomer-to-oligomer exchange by NMR relaxation. *J. Am. Chem. Soc.* 132(29):9948-9951.
80. Danielsson J, Jarvet J, Damberg P, & Graslund A (2002) Translational diffusion measured by PFG-NMR on full length and fragments of the Alzheimer A beta(1-40) peptide. Determination of hydrodynamic radii of random coil peptides of varying length. *Magn. Reson. Chem.* 40:S89-S97.
81. Yamaguchi T, Matsuzaki K, & Hoshino M (2011) Transient formation of intermediate conformational states of amyloid-beta peptide revealed by heteronuclear magnetic resonance spectroscopy. *FEBS Lett.* 585(7):1097-1102.
82. Walsh DM, Lomakin A, Benedek GB, Condron MM, & Teplow DB (1997) Amyloid β-protein fibrillogenesis - Detection of a protofibrillar intermediate. *J. Biol. Chem.* 272(35):22364-22372.
83. Bitan G & Teplow DB (2005) Preparation of aggregate-free, low molecular weight amyloid-β for assembly and toxicity assays. *Methods Mol. Biol.* 299:3-9.
84. Bolognesi B, *et al.* (2010) ANS binding reveals common features of cytotoxic amyloid species. *ACS Chem. Biol.* 5(8):735–740.
85. Lesne S, *et al.* (2006) A specific amyloid-β protein assembly in the brain impairs memory. *Nature* 440(7082):352-357.
86. Giuffrida ML, *et al.* (2009) β-amyloid monomers are neuroprotective. *J. Neurosci.* 29(34):10582-10587.
87. Bliss TVP & Collingridge GL (1993) A synaptic model of memory: long-term potentiation in the hippocampus. *Nature* 361(6407):31-39.
88. Larson ME & Lesne SE (2012) Soluble Aβ oligomer production and toxicity. *J. Neurochem.* 120:125-139.
89. Feng Y, *et al.* (2009) Resveratrol inhibits beta-amyloid oligomeric cytotoxicity but does not prevent oligomer formation. *Neurotoxicology* 30(6):986-995.
90. Ono K, Condron MM, & Teplow DB (2009) Structure-neurotoxicity relationships of amyloid β-protein oligomers. *Proc. Natl. Acad. Sci. U. S. A.* 106(35):14745-14750.
91. Hamaguchi T, Ono K, & Yamada M (2010) Curcumin and Alzheimer's Disease. *Cns Neuroscience & Therapeutics* 16(5):285-297.
92. Lim GP, *et al.* (2001) The curry spice curcumin reduces oxidative damage and amyloid pathology in an Alzheimer transgenic mouse. *J. Neurosci.* 21(21):8370-8377.
93. Garcia-Alloza M, Borrelli LA, Rozkalne A, Hyman BT, & Bacskai BJ (2007) Curcumin labels amyloid pathology in vivo, disrupts existing plaques, and partially restores distorted neurites in an Alzheimer mouse model. *J. Neurochem.* 102(4):1095-1104.
94. Reinke AA & Gestwicki JE (2007) Structure-activity relationships of amyloid beta-aggregation inhibitors based on curcumin: Influence of linker length and flexibility. *Chemical Biology & Drug Design* 70(3):206-215.

95. Yanagisawa D, *et al.* (2010) Relationship between the tautomeric structures of curcumin derivatives and their Aβ-binding activities in the context of therapies for Alzheimer's disease. *Biomaterials* 31(14):4179-4185.
96. Ryu EK, Choe YS, Lee KH, Choi Y, & Kim BT (2006) Curcumin and dehydrozingerone derivatives: Synthesis, radiolabeling, and evaluation for β-amyloid plaque imaging. *J. Med. Chem.* 49(20):6111-6119.
97. Ladiwala ARA, *et al.* (2010) Resveratrol selectively remodels soluble oligomers and fibrils of amyloid Aβ into off-pathway conformers. *J. Biol. Chem.* 285(31):24228-24237.
98. Savaskan E, *et al.* (2003) Red wine ingredient resveratrol protects from β-amyloid neurotoxicity. *Gerontology* 49(6):380-383.
99. Marambaud P, Zhao HT, & Davies P (2005) Resveratrol promotes clearance of Alzheimer's disease amyloid-beta peptides. *J. Biol. Chem.* 280(45):37377-37382.
100. Harmeier A, *et al.* (2009) Role of amyloid-β glycine 33 in oligomerization, toxicity, and neuronal plasticity. *J. Neurosci.* 29(23):7582-7590.
101. Li H, *et al.* (2010) Mechanistic Investigation of the Inhibition of Aβ42 Assembly and Neurotoxicity by Aβ42 C-terminal Fragments. *Biochemistry* 49(30):6358-6364.
102. Frydman-Marom A, *et al.* (2009) Cognitive-performance recovery of Alzheimer's disease model mice by modulation of early soluble amyloidal assemblies. *Angew. Chem.-Int. Edit.* 48(11):1981-1986.
103. Galanakis PA, *et al.* (2011) Study of the interaction between the amyloid beta peptide (1-40) and antioxidant compounds by NMR spectroscopy. *Peptide Science* 96(3):316-327.
104. Gazit E (2002) A possible role for pi-stacking in the self-assembly of amyloid fibrils. *FASEB J.* 16(1):77-83.
105. Jean L, Lee CF, Shaw M, & Vaux DJ (2008) Structural elements regulating amyloidogenesis: A cholinesterase model system. *PLoS One* 3(3):e1834.
106. Hirohata M, Ono K, Naiki H, & Yamada M (2005) Non-steroidal anti-inflammatory drugs have anti-amyloidogenic effects for Alzheimer's beta-amyloid fibrils in vitro. *Neuropharmacology* 49(7):1088-1099.
107. Richter L, *et al.* (2010) Amyloid beta 42 peptide (Aβ42)-lowering compounds directly bind to Aβ and interfere with amyloid precursor protein (APP) transmembrane dimerization. *Proc. Natl. Acad. Sci. U. S. A.* 107(33):14597-14602.
108. Hori Y, *et al.* (2007) The Tottori (D7N) and English (H6R) familial Alzheimer disease mutations accelerate A beta fibril formation without increasing protofibril formation. *J. Biol. Chem.* 282(7):4916-4923.
109. Ono K, Condron MM, & Teplow DB (2010) Effects of the english (H6R) and tottori (D7N) familial Alzheimer disease mutations on amyloid β protein assembly and toxicity. *J. Biol. Chem.* 285(30):23186-23197.
110. Boyd-Kimball D, Abdul HM, Reed T, Sultana R, & Butterfield DA (2004) Role of phenylalanine 20 in Alzheimer's amyloid,beta-peptide (1-42)-induced oxidative stress and neurotoxicity. *Chem. Res. Toxicol.* 17(12):1743-1749.
111. Williams AD, Shivaprasad S, & Wetzel R (2006) Alanine scanning mutagenesis of Aβ(1-40) amyloid fibril stability. *J. Mol. Biol.* 357(4):1283-1294.
112. Vivekanandan S, Brender JR, Lee SY, & Ramamoorthy A (2011) A partially folded structure of amyloid-beta(1-40) in an aqueous environment. *Biochem. Biophys. Res. Commun.* 411(2):312-316.

113. Kim MJ, *et al.* (2007) NMR structural studies of interactions of a small, nonpeptidyl Tpo mimic with the thrombopoietin receptor extracellular juxtamembrane and transmembrane domains. *J. Biol. Chem.* 282(19):14253-14261.
114. Roher AE, *et al.* (1993) β-amyloid-(1-42) is a major component of cerebrovascular amyloid deposits - Implications for the pathology of Alzheimer-disease. *Proc. Natl. Acad. Sci. U. S. A.* 90(22):10836-10840.
115. Naslund J, *et al.* (1994) Relative abundance of Alzheimer Aβ amyloid peptide variants in Alzheimer-disease and normal aging. *Proc. Natl. Acad. Sci. U. S. A.* 91(18):8378-8382.
116. Kuperstein I, *et al.* (2010) Neurotoxicity of Alzheimer's disease Aβ peptides is induced by small changes in the $A\beta_{42}$ to $A\beta_{40}$ ratio. *EMBO J.* 29(19):3408-3420.
117. Tjernberg LO, *et al.* (1996) Arrest of β-amyloid fibril formation by a pentapeptide ligand. *J. Biol. Chem.* 271(15):8545-8548.
118. Thajeb P, Wang P, Chien CL, & Harrigan R (2009) Novel polymorphisms of the amyloid precursor protein (APP) gene in Chinese/Taiwanese patients with Alzheimer's disease. *Journal of Clinical Neuroscience* 16(2):259-263.
119. Lim KH, Collver HH, Le YTH, Nagchowdhuri P, & Kenney JM (2007) Characterizations of distinct amyloidogenic conformations of the Aβ(1-40) and (1-42) peptides. *Biochem. Biophys. Res. Commun.* 353(2):443-449.
120. Kim W & Hecht MH (2006) Generic hydrophobic residues are sufficient to promote aggregation of the Alzheimer's Aβ42 peptide. *Proc. Natl. Acad. Sci. U. S. A.* 103(43):15824-15829.
121. Bitan G, Vollers SS, & Teplow DB (2003) Elucidation of primary structure elements controlling early amyloid β-protein oligomerization. *J. Biol. Chem.* 278(37):34882-34889.
122. Olofsson A, Sauer-Eriksson AE, & Ohman A (2006) The solvent protection of Alzheimer amyloid-β-(1-42) fibrils as determined by solution NMR spectroscopy. *J. Biol. Chem.* 281(1):477-483.
123. Morimoto A, *et al.* (2004) Analysis of the secondary structure of β-amyloid (Aβ 42) fibrils by systematic proline replacement. *J. Biol. Chem.* 279(50):52781-52788.
124. Hung LW, *et al.* (2008) Amyloid-β Peptide (Aβ) neurotoxicity is modulated by the rate of peptide aggregation: Aβ dimers and trimers correlate with neurotoxicity. *J. Neurosci.* 28(46):11950-11958.
125. Murakami K, *et al.* (2005) Formation and stabilization model of the 42-mer Aβ radical: Implications for the long-lasting oxidative stress in Alzheimer's disease. *J. Am. Chem. Soc.* 127(43):15168-15174.
126. Tycko R (2006) Molecular structure of amyloid fibrils: Insights from solid-state NMR. *Q. Rev. Biophys.* 39(1):1-55.
127. Spencer RG, *et al.* (1991) An unusual peptide conformation may precipitate amyloid formation in Alzheimer's disease: Application of solid-state NMR to the determination of protein secondary structure. *Biochemistry* 30(43):10382-10387.
128. Roychaudhuri R, *et al.* (2013) C-terminal turn stability determines assembly differences between Aβ40 and Aβ42. *J. Mol. Biol.* 425(2):292-308.
129. Cerf E, *et al.* (2009) Antiparallel β-sheet: a signature structure of the oligomeric amyloid β-peptide. *Biochem. J.* 421(3):415-423.
130. Stroud JC, Liu C, Teng PK, & Eisenberg D (2012) Toxic fibrillar oligomers of amyloid-β have cross-β structure. *Proc. Natl. Acad. Sci. U. S. A.* 109(20):7717-7722.